The roles of integrin-linked kinase at the centrosome and its regulation of microtubule dynamics

by

Simin Lim

B.Sc., National University of Singapore, 2005

A THESIS SUBMITTED IN PARTIAL FULFILMENT OF THE REQUIREMENTS FOR

THE DEGREE OF

MASTER OF SCIENCE

in

THE FACULTY OF GRADUATE STUDIES
(Interdisciplinary Oncology)

THE UNIVERSITY OF BRITISH COLUMBIA
(Vancouver)

March 2012

© Simin Lim, 2012

Abstract

Integrin-linked kinase (ILK) is both a scaffolding protein and a serine/threonine kinase that localizes to the focal adhesions. It interacts with the cytoplasmic domain of the β1-integrin subunit and acts as a hub for the localization of several actin cytoskeletal and signaling proteins resulting in the transduction of signals from cell-matrix interactions and growth factors into the cell interior. These signaling cascades go on to regulate important cellular processes such as cell migration, survival and proliferation. ILK has a second cellular localization at the centrosomes, where it regulates mitotic spindle organization and the interaction between ch-TOG, TACC3 and Aurora A, which is important for their function in regulating microtubule dynamics and spindle organization. However, the specific role of ILK's kinase activity, separate from a possible scaffolding role, in spindle organization is unclear.

For this study, I attempted to characterize the spindle defect caused by QLT-0267, a small molecule inhibitor that is highly selective for ILK kinase activity. Treatment of HeLa cells with 10 μM QLT-0267 is known to result in a disorganized mitotic spindle that appeared arrested in a prometaphase-like phenotype. Here, I show that QLT-0267 exposure resulted in an increase in tension across sister centromeres aligned between two poles, suggesting a possible effect on spindle microtubule dynamics. Treatment with QLT-0267 was also associated with slower microtubule regrowth after depolymerization and the presence of a more stable population of microtubules in the mitotic spindle as evidenced by higher levels of acetylated α-tubulin. To further assess the role of ILK in regulating microtubule dynamics, the parameters of microtubule

dynamic instability were measured in both QLT-0267-treated HeLa cells and ILK overexpressing HeLa cells. QLT-0267 appeared to dampen microtubule dynamic instability, while ILK overexpression enhanced it. ILK overexpression was also associated with decreased sensitivity to paclitaxel, a chemotherapeutic agent that stabilizes microtubule dynamics.

Taken together, the results suggest a role for ILK's kinase activity in regulating microtubule dynamics. Finally, this study reports a novel mechanism of action for the small molecule inhibitor QLT-0267, which dampens microtubule dynamics and should be taken into consideration when designing future uses for the compound.

Preface

All the work presented in this thesis was performed by me, with the following exceptions:

(1) For the work in Chapter 3.5, the original Flag-tagged ILK plasmid in the pIRES-hrGFP vector was constructed by Dr. Mykola Maydan. This plasmid was then used as a template by Dr. Hongbing Yu to construct a lentiviral vector containing Flag-ILK. Dr. Hongbing Yu also performed the lentiviral transduction to introduce Flag-ILK into HeLa cells before I took over the cells for selection of single clones and subsequent experiments.

(2) The original venus-tubulin construct was made by Ms. Kathleen Lisaingo, and used as a template by Dr. Hongbing Yu to construct a lentiviral vector containing venus-tubulin. The introduction of venus-tubulin into cells by lentiviral transduction was performed by Dr. Hongbing Yu as well.

(3) In Chapter 3.6, the independent, repeat blind scoring of mitosis duration was performed by Dr. Eiko Kawamura to confirm my initial analysis and measurement of mitosis duration.

Table of contents

Abstract ii
Preface iv
Table of contents v
List of tables vii
List of figures viii
List of abbreviations ix
Acknowledgements x
Chapter 1. Introduction 1
1.1 Mitosis 1
1.2 Microtubule structure and dynamics 2
1.3 Mitotic spindle assembly 4
1.4 Spindle assembly checkpoint 9
1.5 Paclitaxel: mechanism of action and resistance 11
1.6 Integrin-linked kinase structure and function 15
1.7 Integrin-linked kinase and cancer signaling 17
1.8 Integrin-linked kinase at the centrosome 20
1.9 Objectives 23
Chapter 2. Materials and methods 25
2.1 Antibodies, drugs and small molecule inhibitor 25
2.2 Cell lines, culture and treatment 25
2.3 Generation of stable cell lines 26
2.4 Cell lysis and western blot 27
2.5 Cell viability assay 28
2.6 Cell cycle analysis 28
2.7 Immunofluorescence, image acquisition and analysis 29
2.8 Live cell time-lapse imaging 31
2.9 Microtubule dynamics measurement 32
Chapter 3. Results 34
3.1. Inhibition of ILK with QLT-0267 results in an aberrant spindle phenotype 34

3.2. Inhibition of ILK's kinase activity does not affect kinetochore architecture or kinetochore-microtubule attachment 36
3.3. Inhibition of ILK's kinase activity results in higher than normal centromere tension 40
3.4. Inhibition of ILK's kinase activity is associated with slower microtubule regrowth and turnover 43
3.5. Generation of stable ILK-overexpressing HeLa cell clones 48
3.6. Overexpression of ILK is associated with faster mitotic progression 52
3.7. Overexpression of ILK is associated with increased aneuploidy 56
3.8. ILK regulates microtubule dynamics in living interphase HeLa cells 59
3.9. ILK overexpression is associated with paclitaxel resistance in HeLa cells 65
Chapter 4. Discussion 69
Chapter 5. Conclusions and future research directions 75
References 79
Appendix A 92

List of tables

Table 3.1: Parameters of dynamic instability in HeLa cells with DMSO or QLT-0267 treatment 62

Table 3.2: Parameters of dynamic instability in control and ILK overexpressing HeLa cells 62

Table 3.3: Summary of the effects of QLT-0267 treatment or ILK overexpression on parameters of dynamic instability in HeLa cells 63

List of figures

Figure 1.1 Schematic diagram of microtubule structure and microtubule dynamic instability. 2

Figure 1.2 Schematic diagram of the components of the mitotic spindle..... 5

Figure 1.3 Schematic diagram of kinetochore-microtubule interaction in prometaphase and metaphase. 6

Figure 1.4 Schematic diagram of the modes of kinetochore-microtubule interactions. ... 8

Figure 1.5 Schematic diagram of ILK structure and binding partners at the focal adhesion..... 16

Figure 1.6 Overview of the intracellular signaling pathways regulated by ILK. 18

Figure 3.1 HeLa cells express ILK at the centrosome and are sensitive to QLT-0267-induced spindle defects. 35

Figure 3.2 (A-B) Inhibition of ILK's kinase activity does not affect kinetochore stability. 37

Figure 3.2 (C) Inhibition of ILK's kinase activity does not affect kinetochore-microtubule attachment. 39

Figure 3.3 Centromere tension is higher than normal in cells treated with QLT-0267... 41

Figure 3.4 (A-B) Microtubule regrowth after depolymerization is slower in QLT-0267-treated cells. 45

Figure 3.4 (C-D) ILK inhibition increases microtubule stability during mitosis. 47

Figure 3.5 Generation of HeLa cell clones that stably overexpress Flag-ILK. 51

Figure 3.6 Time lapse imaging of control Vector 8 and ILK-overexpressing ILK 10 cell undergoing mitosis. 54

Figure 3.7 ILK overexpression is associated with increased polyploidy. 58

Figure 3.8 ILK regulates microtubule dynamics in living interphase HeLa cells. 61

Figure 3.9 ILK overexpression is associated with paclitaxel resistance in HeLa cells... 66

Figure A.1 Positive control for calcium-induced depolymerization of non-kinetochore microtubules 92

Figure A.2 Quantification of the integrated density of acetylated α-tubulin immunofluorescence signal relative to that of total α-tubulin 93

Figure A.3 Western blot to check expression levels stable HeLa clones expressing Flag-ILK..... 93

Figure A.4 Spectrophotometric absorbance readings of Vector 8 cells 94

List of abbreviations

AML: acute myeloid leukemia

APC/C: anaphase-promoting complex/cyclosome

BUB: budding uninhibited by benzimidazole

CASK: calcium/calmodulin (CaM)–activated serine-threonine kinase

Ch-TOG: colonic and hepatic tumor over-expressed gene

DMSO: dimethyl sulfoxide

ECM: extracellular matrix

FACS: fluorescence-activated cell sorting

FLT3: FMS-like tyrosine kinase 3

ILK: integrin-linked kinase

ILKAP: integrin-linked kinase associated protein

IQGAP1: IQ motif containing GTPase activating protein 1

MAD: mitotic-arrest deficient

MAP: microtubule associated protein

MCAK: mitotic centromere-associated kinesin

NEBD: nuclear envelope breakdown

P-gp: P-glycoprotein

PINCH: particularly interesting new cysteine-histidine-rich protein

RUVBL1: RuvB-like 1

SAC: spindle assembly checkpoint

siRNA: small interfering RNA

TACC: transforming, acidic coiled-coil containing

TPX2: targeting protein for Xklp2

Acknowledgements

I would like to express my deepest gratitude to my research supervisor, Dr. Shoukat Dedhar, firstly for the opportunity to pursue graduate studies at his laboratory and for the chance to work on a fascinating project. I also thank him for the patience and support that he has shown in guiding my research training. I am greatly thankful to the members of my supervisory committee, Dr. Robert Kay and Dr. Michel Roberge for their time and effort, and for providing valuable insights, discussions and suggestions for my thesis project.

My heartfelt thanks also go out to past and present members of the Dedhar laboratory, who have been so generous with sharing their knowledge, suggestions and moral support, especially Daiana Becker, Andrew Fielding, Iveta Dobreva, Eiko Kawamura, Paul McDonald, Frances Lock, Isabel Serrano, Yuanmei Lou and Mykola Maydan. Special appreciation is extended to the staff at the BC Cancer Research Center Terry Fox Laboratory Flow Cytometry Core facility, especially David Ko, Wen Bo and Gayle Thornbury for their technical assistance.

Finally, I am forever thankful to my friends and family: To my closest childhood friends Shireen, Angeline and Hwee Cheng, for standing by me through good and especially the bad times. To my mother, for her unconditional love and support in every possible way. To Hongbing, for his unwavering love, patience and companionship. And to little Cara, for giving me a new purpose in life.

This work was supported by funds from the Canadian Institutes of Health Research and by a University Graduate Fellowship from the University of British Columbia.

Chapter 1. Introduction

1.1 Mitosis

Mitosis is arguably the most dramatic event to occur in a cell's life and is marked by a series of major structural changes - reorganization of the cytoskeleton, chromosome condensation, breakdown of the nuclear envelope, formation of the mitotic spindle, and segregation of the sister chromatids. The goal of mitosis is to faithfully segregate the duplicated chromosomes. This has to be performed with complete fidelity because the completion of mitosis is irreversible and missegregation of whole chromosomes leads to aneuploidy - a characteristic of malignant cells (Hanahan and Weinberg, 2011).

Mitotic progression had traditionally been divided into stages based on gross changes seen under the microscope over 100 years ago in the behaviour and structure of the chromosomes and mitotic spindle. The first stage of mitosis occurs with prophase, during which the replicated chromosomes undergo extensive condensation, adherent cells start to round up and nuclear envelope breakdown (NEBD) is initiated. The completion of NEBD marks the end of prophase and the beginning of prometaphase. During prometaphase, the absence of the nuclear envelope allows the spindle microtubules to interact with and attach to the chromosomes. Cells are considered to be at metaphase once all chromosomes have aligned at the spindle equator to form a metaphase plate. The two sister chromatids then separate at anaphase and move towards the opposing spindle poles. In the last stage of mitosis, termed telophase, the chromosomes start forming two daughter nuclei while

microtubules at the original spindle equator form a midbody and a cleavage furrow to take part in cytokinesis.

1.2 Microtubule structure and dynamics

Microtubules and their inherent dynamic instability are the main workhorses of the mitotic spindle machinery. These long, fairly rigid filaments provide physical strength as a key component of the cell's cytoskeleton while serving as tracks for the intracellular transport network. They also guide axonal growth and direction of cell migration. Performing such diverse functions in response to extra- and intracellular cues requires delicate regulation of both microtubule dynamics and the interactions with subcellular structures like kinetochores and the cell cortex.

Microtubules are hollow, cylindrical polymers made up of α-tubulin and β-tubulin heterodimers that associate linearly to form protofilaments (Figure 1.1A). Thirteen such parallel protofilaments then associate laterally to form the hollow microtubule lattice (Desai and Mitchison, 1997). The linear arrangement of the α and β tubulin subunits results in the structural polarity of microtubules, with the β-tubulin subunits exposed at the "plus" end (polymerizes faster), and α-tubulin subunits exposed at the "minus" end (polymerizes slower) (Figure 1.1A). Both tubulin subunits are highly homologous, each binding a guanine nucleotide (GTP), but the GTP is only exchangeable in β-tubulin and not α-tubulin. The GTP bound to β-tubulin is hydrolysed to GDP shortly after heterodimer addition to the microtubule lattice, resulting in a microtubule polymer that contains mainly GDP-bound tubulin, with newly added heterodimers remaining bound to GTP (known as a GTP "cap") (Figure 1.1B). GDP-bound heterodimers have a slightly

altered conformation compared to GTP-bound heterodimers and adopt a curved protofilament conformation. Therefore, it is thought that the GTP "cap" constrains the polymer and maintains the straight conformation necessary for microtubule assembly, or growth. Conversely, the loss of the GTP "cap" results in outward curling of the protofilaments and rapid microtubule disassembly (Figure 1.1B) (Hyman et al., 1995; Mandelkow et al., 1991; Muller-Reichert et al., 1998). This transition between states of growing and shortening is sudden and unpredictable, and is termed "dynamic instability" (Billger et al., 1996; Joshi, 1998; Panda et al., 1994).

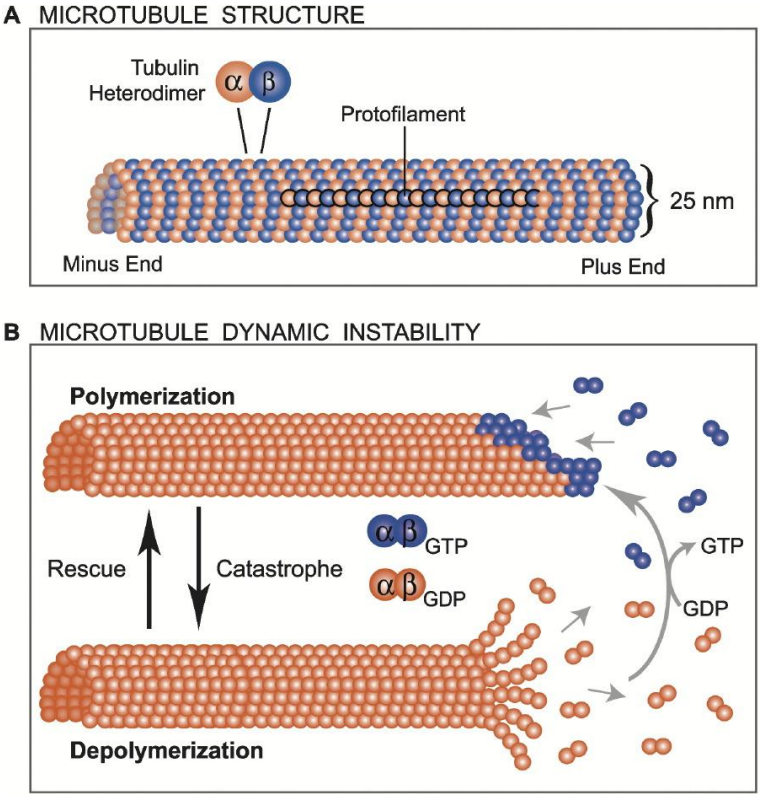

Figure 1.1 Schematic diagram of microtubule structure and microtubule dynamic instability.

Reprinted from Molecular Cell, 15, Susan L Kline-Smith, Claire E Walczak, Mitotic spindle assembly and chromosome segregation: Refocusing on microtubule dynamics, 317-327, 2004, with permission from Elsevier.

A number of parameters are typically used to describe microtubule dynamic instability. These include the rates of growth and shortening, the frequency of catastrophe (transition from growth or pause to shortening), the frequency of rescue (transition from shortening or pause to growth), periods of pause in which changes in microtubule length have stopped, and "dynamicity", which describes the overall rate of tubulin exchange (Toso et al., 1993). It should be noted that microtubules that appear to "pause" under the microscope may actually still be growing or shortening at a very slow rate, but these changes in length (<0.5 μm) cannot be accurately detected due to the limits of resolution imposed by microscopy (Kamath et al., 2010).

The diverse functions of microtubules are achieved through similarly diverse ways of regulation. These include interactions with various microtubule associated proteins (MAPs) such as the dynein and kinesin motor proteins, and many microtubule-regulatory proteins like colonic and hepatic tumor over-expressed gene (ch-TOG) (Spittle et al., 2000), mitotic centromere-associated kinesin (MCAK) (Maney et al., 2001) and end binding 1 (EB1) (Ligon et al., 2003). In addition, different tubulin isotypes (6 forms of α-tubulin and 7 forms of β-tubulin in human) are expressed for different functions at varying levels in different cells and tissues (Luduena, 1998). Further post-translational modifications are also applied to these tubulins such as phosphorylation, acetylation and detyrosination (Luduena, 1998).

Changes to microtubule dynamics are cell cycle dependent, as the interphase microtubule network is dismantled at the onset of mitosis and replaced by spindle microtubules that exhibit a 4-100 fold increase in dynamicity (Rusan et al., 2001; Zhai et al., 1996). This dramatic change in dynamic instability can be attributed to modification

and regulation by cell cycle-dependent phosphorylation of most microtubule regulatory proteins (Cassimeris, 1999). In addition, the unique properties of microtubules make them sensitive to depolymerization at low temperatures (Brinkley and Cartwright, 1975; Wallin and Stromberg, 1995) and high calcium concentrations (Weisenberg and Deery, 1981). Again, the level of sensitivity depends on the factors that interact with the microtubules, such as binding of microtubules to kinetochores, and certain tubulin isotypes and post-translational modifications (Wallin and Stromberg, 1995).

1.3 Mitotic spindle assembly

The mitotic spindle is made up of microtubules, motors and other regulatory proteins. It assembles around the chromosomes and is capable of capturing duplicated chromosomes and segregating them to daughter nuclei in mitosis with stunning precision. Highly dynamic microtubules are essential to all stages of mitosis, including their timely and accurate attachment to kinetochores at prometaphase, the congression of chromosomes to the metaphase plate, the synchronous separation of sister chromatids at anaphase and the completion of telophase (Kline-Smith et al., 2005).

In the spindle, the microtubule minus ends are anchored at the duplicated centrosomes that separate and move to opposite poles during prophase, while the plus ends become attached to kinetochores as kinetochore-microtubules (kMT) or K-fibers (Figure 1.2). The kinetochores are huge multiprotein complexes that assemble on a particular locus of each DNA molecule called centromeres, and facilitate attachment of chromosomes to spindle microtubules.

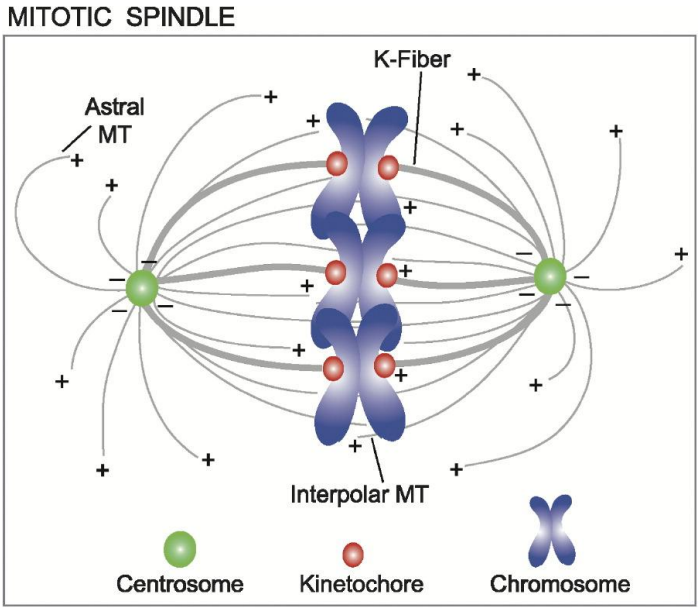

Figure 1.2 Schematic diagram of the components of the mitotic spindle.

Reprinted from Molecular Cell, 15, Susan L Kline-Smith, Claire E Walczak, Mitotic spindle assembly and chromosome segregation: Refocusing on microtubule dynamics, 317-327, 2004, with permission from Elsevier.

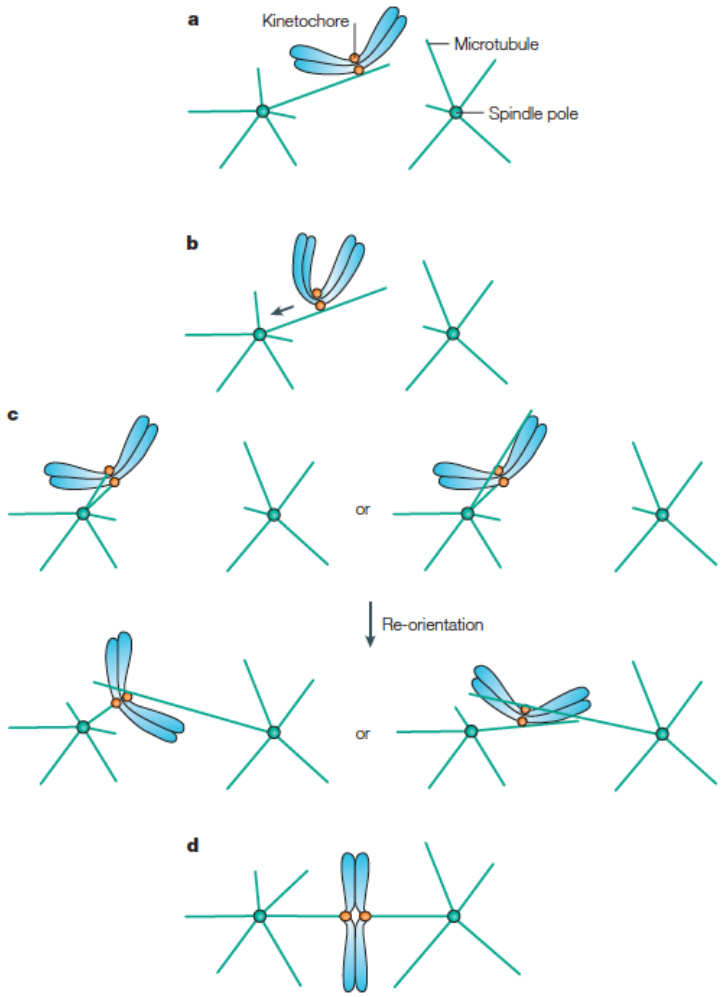

Figure 1.3 Schematic diagram of kinetochore-microtubule interaction in prometaphase and metaphase.

(a) The kinetochore is first captured by the lateral surface of a single microtubule extending from one of the spindle poles. (b) After being captured, the kinetochore is transported along the microtubule towards the spindle pole. (c) During transport to the spindle pole, both sister kinetochores become attached to microtubules emanating from the same (upper panel) or opposite (lower panel) spindle poles. If both kinetochores attach to microtubules from the same pole, re-orientation occurs until bi-orientation is established. (d) Tension from microtubule pulling forces applied on sister kinetochores from opposite poles result in alignment of chromosome at the metaphase plate.

Reprinted by permission from Macmillan Publishers Ltd: Nature Reviews Molecular Cell Biology, 6(12):929-942, 2005

How exactly do spindle microtublues become attached to kinetochores? The earliest proposed model was the "search and capture" model, in which microtubules randomly probe the three-dimensional space after nuclear envelope breakdown, and become stabilized upon capture by kinetochores (Kirschner and Mitchison, 1986). This model has since been verified using imaging experiments that observed the capturing of chromosomes by elongating microtubules (Hayden et al., 1990; Tanaka et al., 2005).

The kinetochore is first captured by the lateral surface of a microtubule (rather than at the tip) (Figure 1.3a), and is transported along the microtubule toward the spindle pole by ATP-driven motor proteins such as Kar3 (a kinesin-14 family member) (Figure 1.3b) (Tanaka et al., 2005). Unfortunately, the mechanism by which this lateral attachment is converted to end-on attachment to the microtubule tip is currently unclear. During transportation, the other sister kinetochore gets attached to microtubules emanating from the same or opposite spindle poles (Figure 1.3c). Attachment of both sister kinetochores to microtubules from the same spindle pole is known as a syntelic attachment (Figure 1.4b), and requires Aurora B to correct it to an amphitelic attachment (Figure 1.4c) (Hauf et al., 2003; Lampson et al., 2004). Bi-orientation of the chromosome is achieved as tension generated from the opposing microtubules pulling forces brings the chromosome in between both spindle poles. (Figure 1.3d).

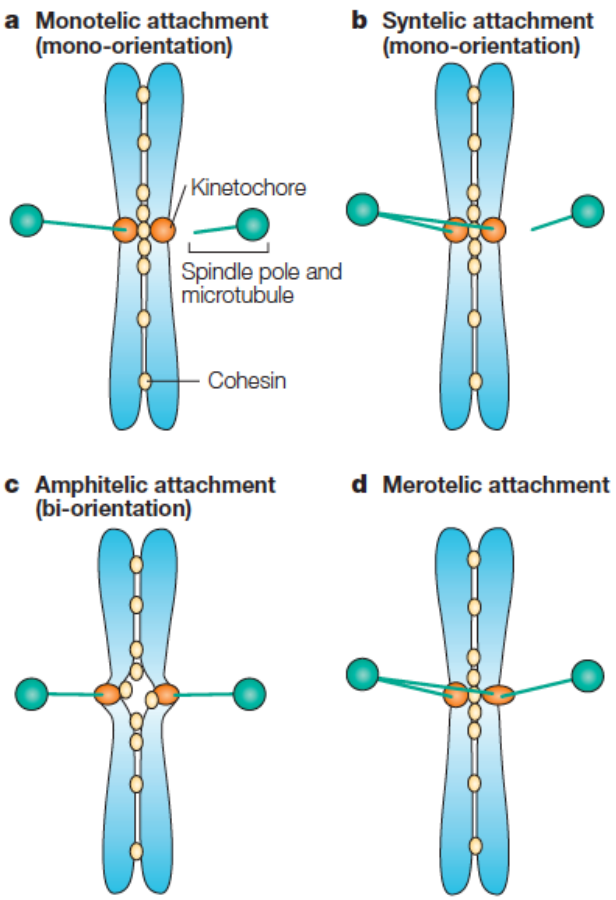

Figure 1.4 Schematic diagram of the modes of kinetochore-microtubule interactions.
Reprinted by permission from Macmillan Publishers Ltd: Nature Reviews Molecular Cell Biology, 6(12):929-942, 2005

However, it is now believed that the process of chromosome capture may not be entirely random. Rather, microtubule dynamics in the vicinity of chromosomes is altered by a RanGTP gradient and other associated proteins around chromosomes, leading to more efficient kinetochore capture by microtubules (Wollman et al., 2005). Therefore, a complementary model has been proposed that includes the centrosome-independent pathway for spindle assembly. Chromosomes have been observed to capture short microtubules that form in their vicinity (Witt et al., 1980), and the nucleation of these

microtubules is hypothesized to be promoted by the RanGTP gradient (Karsenti et al., 1984). One of the proteins targeted by RanGTP is targeting protein for Xklp2 (TPX2). During mitosis, TPX2 is bound to α and β importins, but RanGTP causes dissociation of this complex and releases TPX2, which then plays a role in microtubule nucleation around chromsomes(Gruss and Vernos, 2004). The short microtubules begin by growing away from the kinetochore, and the distal end of the growing fiber subsequently encounters and attaches to an astral microtubule that then directs it to the centrosome (Maiato 2004).

1.4 Spindle assembly checkpoint

The accuracy with which the mitotic spindle segregates chromosomes is guarded by the mitotic checkpoint, also known as the spindle assembly checkpoint (SAC). This is an indispensable component of mammalian cells as the complete inactivation of SAC in mammals leads to severe chromosome missegregation, cell death and embryonic lethality (Dobles et al., 2000; Kalitsis et al., 2000; Kops et al., 2004; Michel et al., 2001). However, it is interesting to note that the SAC is not essential for viability in some organisms, such as yeast and flies (Buffin et al., 2007; Hoyt et al., 1991; Li and Murray, 1991). The SAC pathway is active in prometaphase and prevents premature sister chromatid separation by monitoring kinetochore occupancy by microtubules (Musacchio and Hardwick, 2002; Musacchio and Salmon, 2007; Taylor et al., 2004).

There has been a long-standing debate in the literature over whether tension or occupancy is the signal that SAC responds to. It is now thought that attachment is the *only* signal required by the SAC, as mounting evidence suggests that the SAC

allows exit from mitosis whether the chromosome attachments are correct or erroneous (Khodjakov and Pines, 2010; Musacchio and Salmon, 2007). Instead, cells rely on the Aurora B pathway to correct erroneous monotelic, syntelic and merotelic attachments (Liu and Lampson, 2009; Nezi and Musacchio, 2009).

Components of the SAC were first identified in 1991 when two independent screens found various genes whose mutations caused *Saccharomyces cerevisiae* cells to bypass their ability to arrest in mitosis in the presence of spindle poisons (Hoyt et al., 1991; Li and Murray, 1991). The genes include 3 *MAD (mitotic-arrest deficient*) genes, *MAD1, MAD2* and *MAD3* (also known as *BUBR1* in humans), and the *BUB* (budding uninhibited by benzimidazole) gene *BUB1*. Functionally, the SAC targets CDC20, a co-factor of the ubiquitin ligase anaphase-promoting complex/cyclosome (APC/C) (Hwang et al., 1998) and negatively regulates the ability of CDC20 to activate further downstream effectors that lead to cleavage of the cohesin, a complex that holds sister chromatids together (Figure 1.4). Mad1 and Mad2, two of the SAC effectors (Sudakin et al., 2001), accumulate at unattached kinetochores and are removed upon kinetochore occupancy for SAC inactivation. Interestingly, studies have shown that a single unattached kinetochore is sufficient to provide negative feedback and delay anaphase (Rieder et al., 1994).

In 1914, it was postulated by Boveri that chromosome missegregation might cause tumor development (Boveri, 1914). Since then, most solid tumor cells have been found to be aneuploidy (Heim, 1995). Chromosomal instability (CIN), the frequent gain and or loss of whole chromosomes during mitosis, has also been found in various cancer cell lines (Lengauer et al., 1997). One of the causes of the observed aneuploidy

is likely to be a weakened or defective SAC (Kops et al., 2005), which has been associated with the transformation process in tumors. For example, in one mouse study, heterozygous loss of Mad2 resulted in a 27% increase in the frequency of spontaneous tumour development (Michel et al., 2001), while in another, mice heterozygous for BubR1 exhibited higher rates of tumorigenesis after carcinogen treatment (Dai et al., 2004). Cahill *et al.* also demonstrated the presence of defective spindle checkpoints in a large number of colorectal cancer cell lines (Cahill et al., 1998).

The inability to sustain SAC signaling, assayed by a reduced mitotic index after long-term drug-mediated spindle disruption (Cahill et al., 1998; Ouyang et al., 2002; Tighe et al., 2001; Wang et al., 2000), is a frequent feature of human tumor cells and cell lines (Wang et al., 2000). While somatic mutations of checkpoint proteins have been identified (Kops et al., 2005), they do not appear to be a common mechanism for aneuploidization. Rather, it is more likely that various oncogenes and tumor suppressors reduce the levels of checkpoint components to produce a weakened SAC. Indeed, many tumour suppressor proteins have been shown to regulate the expression levels of SAC genes (Kops et al., 2005). One such example is the regulation of the *MAD1L1* promoter by the p53 tumour suppressor, although the findings are currently contradictory as to whether p53 activation increases or decreases *MAD1L1* expression (Chun and Jin, 2003; Iwanaga and Jeang, 2002).

1.5 Paclitaxel: mechanism of action and resistance

The importance of microtubules to the process of mitosis makes them very attractive targets for anticancer drugs. Among the most successful of these drugs is

paclitaxel, a complex molecule that was first isolated in 1967 from the bark of the Pacific yew tree (Wani et al., 1971). The compound underwent slow development until the surprising discovery, in 1979, that paclitaxel stimulated microtubule polymerization (Schiff et al., 1979). Even then, clinical development was held back due to limited supplies of the natural compound, until a method for its semi-synthesis was devised and made production feasible (Horwitz, 1994). The drug was finally approved for clinical use in 1995 and is now widely used to treat a range of epithelial cancers (Rowinsky, 1997).

Paclitaxel does not bind soluble tubulin, but binds directly and reversibly to β-tubulin on the inside surface of the microtubule lattice (Diaz et al., 1998; Nogales et al., 1995; Parness and Horwitz, 1981). This binding induces a conformational change in tubulin and increases its affinity for neighboring tubulin subunits through an unknown mechanism, thereby stabilizing the microtubule and increasing polymerization (Nogales, 2001). The microtubule stabilization by paclitaxel results in suppression of microtubule dynamics and causes mitotic arrest (Yvon et al., 1999). In particular, cancer cells are prevented from progressing from metaphase into anaphase, eventually leading to cell death by apoptosis (Jordan et al., 1996; Kelling et al., 2003; Yvon et al., 1999).

However, as with many cancer therapeutic agents, the development of resistance to paclitaxel remains a significant problem. The two main mechanisms are the expression of multidrug resistance (MDR) phenotypes and alterations to the tubulin/microtubule system (Krishna and Mayer, 2000; Orr et al., 2003). Drug resistant tumors often exhibit simultaneous resistance to a diverse range of drugs, and are typically mediated by the overexpression of drug efflux transporters such as P-glycoprotein (P-gp). Increased expressions of the P-gp protein, and its

corresponding *mdr1* gene, have been associated with paclitaxel resistance in many tumor types and cell lines (Alvarez et al., 1995; Haber et al., 1995; Schondorf et al., 1999).

Several alterations to the tubulin/microtubule system have been identified as well, one of which is the existence of point mutations in beta-tubulin that either directly affect paclitaxel binding, or enhance microtubule dynamics by altering the interactions between tubulin heterodimers and their regulatory proteins (Galletti et al., 2007). Another mechanism for paclitaxel resistance is a change in expression levels of the β-tubulin isotype. Overexpression of βIII-tubulin has been reported in various paclitaxel-resistant cell lines, including lung, prostate, breast and ovarian cancer (Banerjee, 2002; Ferlini et al., 2005; Goncalves et al., 2001), and also in clinical ovarian tumor cells (Goncalves et al., 2001). It has been proposed that the observed reduction in paclitaxel sensitivity is due to reduced binding affinity for the βIII isotype as a result of a different amino acid residue present at β275, which is located at the paclitaxel binding site (Galletti et al., 2007; Lowe et al., 2001). In addition, increased βIII expression has been shown *in vitro* and in cells to impair microtubule stability (Derry et al., 1997; Hari et al., 2003), and this destabilization is thought to counteract paclitaxel-induced stabilization and induce drug resistance (Orr et al., 2003).

Besides the microtubules themselves, altered expression or post-translational modifications of microtubule regulatory proteins also contribute to paclitaxel resistance. For example, stathmin sequesters soluble tubulin dimers and destabilizes microtubules (Andersen, 2000) and has been reported to inhibit paclitaxel-induced microtubule polymerization *in vitro* (Larsson et al., 1999). Increased stathmin activity is thus likely to

hinder paclitaxel's stabilizing action on microtubules and confer resistance. In fact, increased stathmin expression has been detected in paclitaxel-resistant ovarian cancer cells (Balachandran et al., 2003).

Other less studied putative mechanisms of paclitaxel resistance include altered regulation of the cell cycle, apoptosis and cell death signal (Luqmani, 2005). In particular, a weakened spindle assembly checkpoint (SAC) has been associated with reduced paclitaxel sensitivity (Sudo et al., 2004). An interesting observation with the chronic activation of SAC by paclitaxel treatment is the occurrence of mitotic slippage (also known as mitotic checkpoint adaptation). This is a process in which cells arrested in mitosis re-enter interphase without chromosome segregation or cell division, and is an observation made in cells exposed to microtubule-targeting agents (Andreassen and Margolis, 1991; Rudner and Murray, 1996; Weaver and Cleveland, 2005), including paclitaxel (Long and Fairchild, 1994). The highly condensed state of mitotic chromosomes halts the production of new RNA by blocking transcriptional access to the DNA (Blagosklonny, 2007; Prescott, 1964), As a result, cells arrested in mitosis cannot remain viable for an indefinite amount of time due to the progressive loss of essential proteins through natural degradation (Bhalla, 2003; Blagosklonny, 2007; Jordan et al., 1996), and the loss of SAC proteins is thought to be a trigger for mitotic slippage. The rate of mitotic slippage after paclitaxel treatment had recently been studied and appears to be dependent on cell type and paclitaxel concentration (Riffell et al., 2009).

1.6 Integrin-linked kinase structure and function

Integrin-linked kinase (ILK) was originally discovered in a yeast two-hybrid screen as a binding partner of the β1-integrin subunit cytoplasmic domain (Hannigan et al., 1996). Only one *ILK* gene exists in humans and it was mapped to the distal tip of chromosome 11 (band 11p15.4/15.5) (Hannigan et al., 1997). Subsequent genetic studies in *Drosophila*, *Caenorhabditis elegans*, Xenopus laevis, and zebrafish and mice have shown ILK to be required for embryonic development (Hannigan et al., 2005). The translated ILK protein contains 3 evolutionarily conserved domains: four ankyrin repeats near the N-terminus, a pleckstrin homology-like domain in the central region that binds phosphoinositide lipids (Delcommenne et al., 1998; Persad et al., 2000), and a kinase catalytic domain near the C-terminus. The ankyrin repeats of ILK bind to an adaptor protein called PINCH (particularly interesting new cysteine-histidine-rich protein), which is involved in recruiting ILK to the focal adhesions (Zhang et al., 2002). The ankyrin repeats also bind to ILKAP (ILK-associated protein), which is a phosphatase that negatively regulates ILK (Kumar et al., 2004; Leung-Hagesteijn et al., 2001).

The C-terminus catalytic domain of ILK binds to integrins (Hannigan et al., 2005), and functions both as an adaptor and a kinase. As an adaptor, it interacts with the focal adhesion proteins paxillin (Nikolopoulos and Turner, 2001; Nikolopoulos and Turner, 2002) and parvins (Hannigan et al., 2005; Hannigan et al., 2007; Legate et al., 2006), both of which link ILK, and hence integrins, to the actin cytoskeleton. ILK's interaction with the parvins also regulate actin cytoskeletal dynamics (Hannigan et al., 2005).

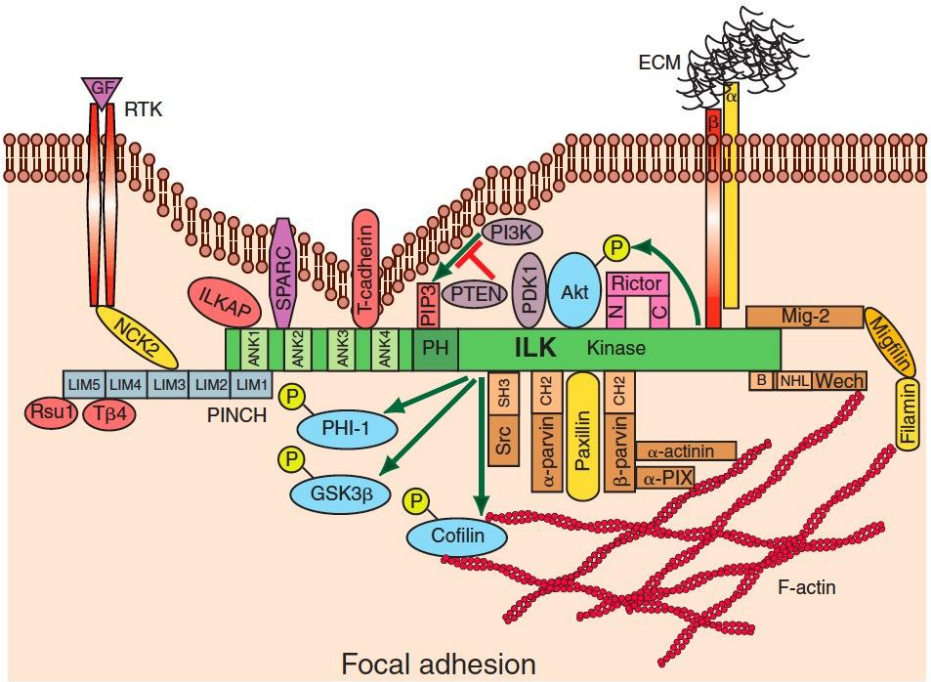

Figure 1.5 Schematic diagram of ILK structure and binding partners at the focal adhesion.

Reproduced with permission from the Journal of Cell Science, 121(19):3121-3132, Integrin-linked kinase - essential roles in physiology and cancer biology, 2008.

As a kinase, ILK has been shown to be a serine/threonine kinase (Hannigan et al., 2005; Hannigan et al., 2011). The ILK kinase domain is considered atypical because it lacks the highly conserved amino acid triplet Asp-Phe-Gly (DFG) and His-Arg-Asp (HRD) motifs found in most kinases, but retains the ATP-binding Lys residue at K220, as well as the third highly conserved Ala-Pro-Glu (APE) motif (Boudeau et al., 2006; Hannigan et al., 2005; Wickstrom et al., 2010b). As a result, ILK is considered to be a pseudokinase (Boudeau et al., 2006; Wickstrom et al., 2010b). However, it has been argued that catalytically functional kinases such as CASK and haspin do not have all 3 amino acid triplet motifs, and that there is considerable sequence flexibility within a kinase catalytic domain (Hannigan et al., 2011). Recently, Maydan *et al.* showed that

highly purified ILK is a functional Mn^{2+}-dependent kinase that could phosphorylate Ser-9 of GSK3-β *in vitro*, with enzyme kinetics comparable to other active protein kinases (Maydan et al., 2010). Specifically, they established the importance of Lys-220, as a mutation to alanine resulted in a significant reduction in ILK's catalytic activity. In addition, ILK has repeatedly been shown to phosphorylate Ser-473 on AKT and Ser-9 on GSK3-β (McDonald et al., 2008).

Functionally, at the focal adhesions, ILK acts as a hub through which signals from cell-matrix interactions and growth factors transduce into the cell interior. Many of these signaling pathways regulate cellular processes that are often implicated in cancer.

1.7 Integrin-linked kinase and cancer signaling

After the discovery of ILK, it quickly became apparent that overexpression of active ILK could transform cells by promoting anchorage-independent growth, motility, invasion, proliferation and angiogenesis (Hannigan et al., 2005). Figure 1.2 shows an overview of the signaling cascades regulated by ILK, which ultimately control a diverse array of cellular processes involved in normal tissue homeostasis as well as cellular transformation / malignancy. The majority of work that studied ILK's role in cell signaling made use of transformed and/or tumorigenic cells. This is of note because ILK-controlled pathways may differ in their regulation and function between non-transformed and cancer cells. Several studies have demonstrated a role for ILK in regulating the phosphorylation of Akt at Ser473 and of glycogen synthase kinase 3 (GSK3) (McDonald et al., 2008). In particular, the phosphorylation of Akt at Ser473 leads to full activation of this protein and activates important pathways that control cell survival.

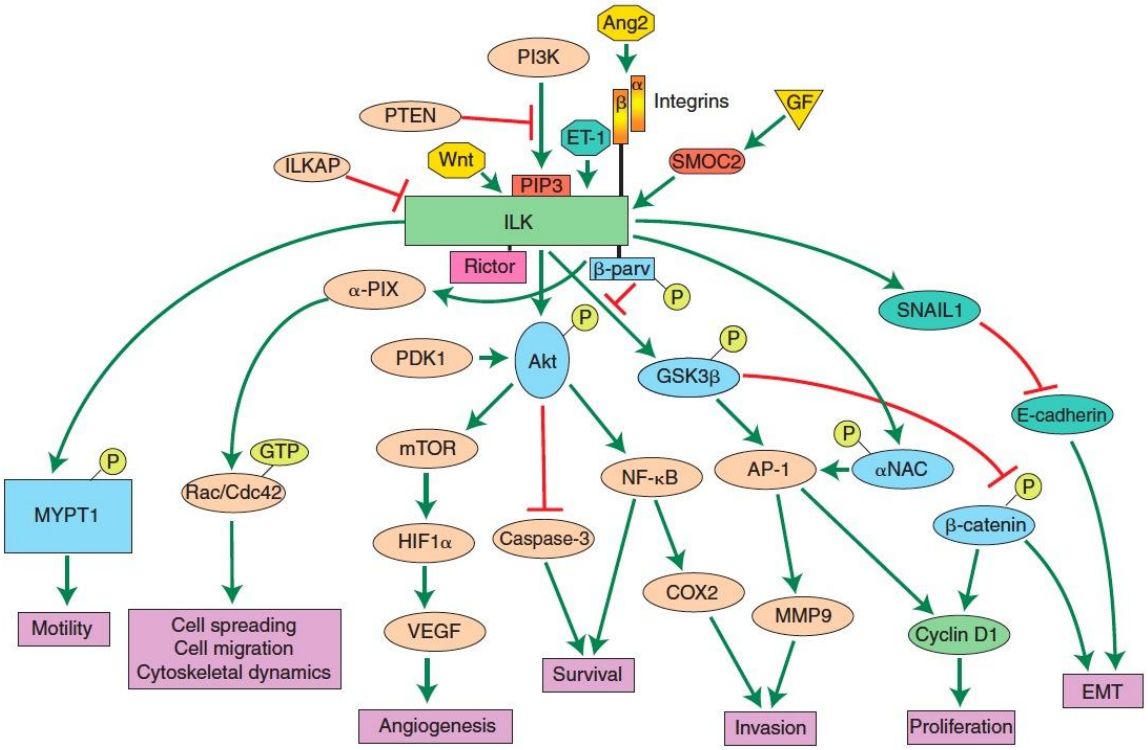

Figure 1.6 Overview of the intracellular signaling pathways regulated by ILK.
Reproduced with permission from the Journal of Cell Science, 121(19):3121-3132, Integrin-linked kinase - essential roles in physiology and cancer biology, 2008.

ILK expression is often found to be elevated in clinical tumor samples and correlates with aggressive tumor phenotype and poor prognosis (McDonald et al., 2008). However, the exact mechanisms behind the elevated expression are currently unclear. Certain signaling pathways controlling cell survival, proliferation and invasion become more dependent on ILK activity in cancer cells compared to untransformed cells (Troussard et al., 2006). This dependency, coupled with the constitutively high levels of ILK expression and activity in cancer cells, provide an attractive therapeutic opportunity to bring the level of ILK activity down to that of normal cells.

The pharmacological inhibition of ILK activity has been pursued with the development of small-molecule inhibitors against ILK's kinase activity. These inhibitors are ATP analogs that compete with endogenous ATP for the ILK kinase domain ATP-binding site. Derivatives of the KP15792 class of inhibitor, KP-392 and the more potent QLT-0267, have been widely used (Jin et al., 2008; Kalra et al., 2011; Kalra et al., 2009; Koul et al., 2005; Liu et al., 2006; Mills et al., 2003; Troussard et al., 2006; Younes et al., 2005; Younes et al., 2007). QLT-0267 has previously been described to be highly selective against ILK phosphotransferase activity (Younes et al., 2005). *In vitro,* QLT-0267 inhibited the kinase activity of purified ILK in an ATP-competitive manner and showed the most potent inhibition when compared with several other kinase inhibitors (Maydan et al., 2010). This compound inhibited ILK kinase activity with a half maximal inhibitory concentration (IC50) of between 2-5 μM, depending on cell type (Troussard et al., 2006).

However, as with most small molecule kinase inhibitors that target a highly conserved target (the kinase domain), it should be noted that absolute specificity against any one kinase could never be achieved (Bantscheff et al., 2007), and some effects of QLT-0267 could be “off target”. Although the compound had shown 10-1000-fold selectivity against other kinases tested under similar conditions, including DNA-PK, PKB/AKT and GSK3β (Younes et al., 2005), Muranyi *et al.* had shown that QLT-0267 could inhibit FMS-like tyrosine kinase 3 (FLT3) with equivalent potency to that seen against ILK (Muranyi et al., 2009). Nevertheless, preclinical studies have begun to assess the use of QLT-0267 for cancer therapy. In two studies utilizing acute myeloid leukemia (AML) cell lines, QLT-0267 exhibited selective toxicity against AML progenitor

cells while sparing normal hematopoietic counterparts (Fukuda et al., 2011; Muranyi et al., 2009). In addition, the use of QLT-267 in combination with docetaxel demonstrated drug synergism in an orthotopic cancer mouse model (Kalra et al., 2009) but not in a resistant metastatic disease mouse model (Kalra et al., 2011), suggesting that the use of QLT-0267 could provide good clinical benefits in an adjuvant or neoadjuvant setting.

1.8 Integrin-linked kinase at the centrosome

The discovery of ILK's localization to the centrosomes was made serendipitously in a recent proteomics study to identify ILK binding partners (Dobreva et al., 2008). Using SILAC (stable isotope labeling with amino acids in cell culture)-based quantitative mass spectrometry, a ratio of specific to non-specific binding to ILK was obtained for every protein identified (Foster et al., 2006; Ong et al., 2002). While the known ILK binding partners, PINCH and α-parvin were identified with high specificity ratios, α and β-tubulin, and a number of centrosomal/mitotic spindle proteins were also identified with equally high ratios, including RuvBl1 and ch-TOG (Dobreva et al., 2008). In fact, about half the proteins on the list of ILK binding partners were known centrosomal and/or spindle proteins.

ILK was subsequently shown by biochemical fractionation and immunofluorescence microscopy to localize to interphase and mitotic centrosomes, where it exists as part of a second multiprotein complex distinct from the focal adhesions (Fielding et al., 2008b). Specifically, ILK was present in purified mitotic spindle extracts, along with α-tubulin and ch-TOG, but the known focal adhesion ILK interactors PINCH and α-parvin were absent. ILK was also shown by

immunofluorescence to co-localize with α-parvin at the focal adhesions but only ILK was present at the centrosomes, and not α-parvin. Conversely, ch-TOG was absent from the soluble cell extract, where ILK, PINCH and α-parvin were found. Additionally, immunofluorescence analysis revealed co-localization of ILK and RUVBL1 at the cnetrosome, but only ILK was seen at the focal adhesions. Therefore, the association with distinct protein complexes allows ILK to partition between the actin and tubulin cytoskeletal networks.

At the centrosomes, ILK depletion or inhibition of its kinase activity has been shown to cause mitotic spindle defect, with highly disorganized spindles that were unable to properly align all chromosomes (Fielding et al., 2008b). Cells contained condensed chromosomes and separated centrosomes, but microtubules from one, and in some cases both, centrosomes would radiate in all directions.

One potential mechanism of ILK action at the centrosome is through its interaction with RuvB-like protein 1 (RuvBl1), a DNA helicase essential for homologous recombination and DNA double-strand break repair. RuvBl1 and RuvBl2 are two human homologues of the bacterial protein RuvB, and are able to form homo or hetero complexes (Bauer et al., 2000). RuvBl1 has been reported to regulate microtubule dynamics and mitotic spindle organization (Ducat et al., 2008; Gartner et al., 2003). In addition, ILK and RuvBl1 are mutually dependent for their localization to the centrosome (Fielding et al., 2008b). Interestingly, β-catenin, a known ILK effector (Novak et al., 1998; Oloumi et al., 2006) that localizes to the centrosomes and regulates mitotic spindle organization (Kaplan et al., 2004), has also been shown to bind to RuvBl1 (Bauer et al., 2000; Bauer et al., 1998). It is therefore possible that ILK, RuvBl1/2 and β-

catenin form a complex at the centrosome that is essential for mitotic spindle organization.

In another mechanism of action, ILK depletion or inhibition of its kinase activity disrupts formation of the Aurora A/ch-TOG/TACC3 complex (Fielding et al., 2008b) (Figure 1.7), although the direct downstream target of ILK that regulates this complex formation has yet to be identified. Aurora A kinase is an important organizer of the spindle poles (Marumoto et al., 2005) and its mechanism of action depends partly on two downstream effectors, TACC3 and ch-TOG. Transforming, acidic coiled-coil containing (TACC) proteins exist as 3 isoforms in humans, all of which bind to ch-TOG and are required for the localization of ch-TOG to the centrosome (Cullen and Ohkura, 2001; Gergely et al., 2000; Lee et al., 2001). Furthermore, the phosphorylation of TACC3 at Ser558 is regulated by ILK in an Aurora A-dependent manner (Fielding et al., 2011). This is significant because Ser558 phosphorylation is required for TACC3's microtubule-regulating functions at the centrosome (Barros et al., 2005; Giet et al., 2002; Kinoshita et al., 2005; LeRoy et al., 2007; Peset et al., 2005).

Ch-TOG (XMAP215 in *Xenopus laevis*, Msps in *Drosophila melanogaster*, Stu2p in *Saccharomyces cerevisiae*) is a processive polymerase (Brouhard et al., 2008) and microtubule binding protein that stabilizes microtubules *in vitro* (Gard and Kirschner, 1987; Spittle et al., 2000), by promoting plus end polymerization and by counteracting the activity of the microtubule catastrophe-promoting protein MCAK (XKCM1 in *Xenopus*) (Tournebize et al., 2000; Vasquez et al., 1994). Despite controlling plus end dynamics, ch-TOG is strongly localized to the spindle poles / centrosomes during mitosis.

It is thought that Aurora A-mediated phosphorylation of TACC3 targets it to the centrosome (Barr and Gergely, 2007), where the same phosphorylation serves to target ch-TOG to the centrosomes (Barros et al., 2005). This allows ch-TOG to be "loaded" onto microtubule plus ends as they initially grow out of the centrosome (Lee et al., 2001), and also protects ch-TOG against MCAK activity (Barros et al., 2005). As a result, centrosome-nucleated microtubules are stabilized and allowed to form an organized bipolar spindle.

Finally, recent work on centrosome clustering revealed that ILK is required for the clustering of supernumerary centrosomes (Fielding et al., 2011). This particular function of ILK does not depend on the focal adhesions and is mediated through Aurora A's phosphorylation of Ser558 on TACC3. The presence of more than 2 centrosomes is a common characteristic of cancer cells (Pihan et al., 2003; Zyss and Gergely, 2009). Through a poorly understood mechanism of centrosome clustering, these cancer cells are able to cluster their centrosomes to form bipolar spindles, thus ensuring bipolar mitosis and cell survival (Kwon et al., 2008). Therefore, targeting ILK-mediated centrosome clustering may be a very effective and promising cancer-specific therapy.

1.9 Objectives

It was previously demonstrated that pharmacological inhibition or depletion of ILK resulted in a disorganized mitotic spindle phenotype (Fielding et al., 2008b). Because of ILK's dual role as a kinase and a scaffolding protein, I am now interested specifically in how ILK's kinase activity regulates mitotic spindle organization. In this study, I set out to characterize the spindle defect caused specifically by inhibiting ILK's kinase activity

using the ILK-specific small molecule inhibitor, QLT-0267, and to address the centrosomal functions of ILK's kinase activity.

Chapter 2. Materials and methods

2.1 Antibodies, drugs and small molecule inhibitor

The following primary antibodies were used for immunofluorescence and western blot staining: mouse anti-α-tubulin (Sigma-Aldrich), rabbit anti-α-tubulin (GeneTex), mouse anti-acetylated-α-tubulin (acetylated Lys40) (Sigma-Aldrich), rabbit anti-ILK (Abcam), human anti-centromere (Antibodies Inc.), mouse anti-hec1 (Abcam), rabbit anti-pericentrin (Abcam), mouse anti-ILK (BD Biosciences), rabbit anti-flag (Cell Signaling Technology), mouse anti-paxillin (BD Biosciences). AlexaFluor 488 anti-mouse and AlexaFluor 594 anti-rabbit were used as secondary antibodies for immunofluorescence staining, while IR-Dye 680-conjugated anti-rabbit and IRDye 800-conjugated anti-mouse antibodies (Rockland Immunochemicals, Inc.) were used for western blotting.

The small molecule inhibitor, QLT-0267, was a kind gift from Quadra Logic Technologies Inc., and was dissolved in dimethyl sulfoxide (DMSO). Paclitaxel (Sigma-Aldrich) and nocodazole (Sigma-Aldrich) were also dissolved in DMSO prior to usage in experiments.

2.2 Cell lines, culture and treatment

HeLa cells were grown in DMEM, supplemented with 10% fetal bovine serum, at 37°C in 5% CO_2 atmosphere. Subsequent stable cell lines derived from the parental HeLa cells were cultured in the same manner and maintained with 0.5μg/ml puromycin. Unless otherwise stated, treatment with QLT-0267 was carried out at 10 μM for 6 hours

under regular cell culture conditions. Nocodazole treatment was performed at 1 μM for 16 hours. Cells were treated with varying concentrations of paclitaxel dissolved in DMSO under regular culture conditions for 20 or 48 hours.

2.3 Generation of stable cell lines

Using pIRES-hrGFP-ILK (obtained from Dr. Mykola Maydan at the Dedhar laboratory) as template, Flag-ILK was amplified by PCR with primers that added an XhoI site plus a kozak sequence at the 5' end (ILK-XhoI-For: 5'-GGACTCTCGAGGCCATGGACGACATTTTCACTCAGT-3') and an XbaI site at the 3' end (ILK-XbaI-Rev: 5'-GACTTCTAGATGCAGTCGTCGAGGAATTGCTAT-3'). The resulting PCR product was cloned into XhoI- and XbaI-digested lentivirus pLVX-puro vector (Clontech) to generate lentiviral construct pLVX-puro-ILK. This construct, together with pLVX-puro (empty vector, EV), was individually packaged into lentivirus particles in 293T cells (American Type Culture Collection) using a lentiviral packaging mix (Sigma). HeLa cells were infected with these lentivirus particles and selected in culture media containing 3 μg/mL puromycin for two weeks. Single cell-derived stable cell lines were further obtained by culturing cells in a 96-well plate using a cell sorter. The stable cell lines were designated as Vector 6, Vector 8, ILK 7 and ILK 10.

Using CAG_Tubulin5_VEN (kind gift from Dr. Peter Lansdorp) as a template, the N-terminus and C-terminus of Tubulin-Venus were amplified by PCR with primer pairs N-Terminus (N-EcoRI-For: GCCTGAATTCACCATGTTCATGCCTTCTTCTTTTTCCT; N-BamHI-Rev: GAGCTTGTTGGGGATCCATTCCACGAAGTAGCTGCT) and C-terminus (C-BamHI-For: GCAGCTACTTCGTGGAATGGATCCCCAACAATGTCAA; C-

BamHI-Rev: GACAGGATCCTTACTTGTACAGCTCGTCCATGCCGAGA). The N-terminus of Tubulin-Venus was cloned into EcoRI- and BamHI-digested pLVX-IRES-Neo (Clontech), generating the construct pLVX-Neo-N-terminus. The C-terminus of Tubulin-Venus was then cloned into BamHI-digested pLVX-Neo-N-terminus, resulting in a construct (pLVX-Neo-Tubulin-Venus) that contains the full length Tubulin-Venus fusion protein. As described above, lentivirus particles prepared with pLVX-Neo-Tubulin-Venus was used to infect Vector 8 and ILK 10. These infected cell lines were then selected in culture media containing 600 µg/mL G418 for two weeks, and populations of cells from both cell lines showing similar levels of fluorescence at 488 nm were selected through fluorescence-activated cell sorting (FACS).

2.4 Cell lysis and western blot

To obtain whole cell lysates, cells were lysed with an NP-40 buffer containing 50mM Tris (pH7.6), 150mM NaCl, 1% NP-40, and 1mM ethylenediaminetetraacetic acid (EDTA), supplemented with 1x Protease Inhibitor (Roche), 1mM Na_3VO_4, 1mM NaF and 20mM β-glycerophosphate. Mitotic spindles were purified as previously described (Fielding et al., 2008b). Protein concentration was determined using the bicinchoninic acid (BCA) assay.

Western blot analysis was performed on equal amounts of whole cell lysates or spindle fractions. The proteins were resolved on SDS-PAGE gels, and electrophoretically transferred onto nitrocellulose membranes. The Odyssey blocking buffer (LI-COR Biosciences) was used for blocking the membranes and incubation of primary antibodies (diluted in 5% nonfat milk) occurred overnight at 4°C. Secondary

antibodies diluted in 5% nonfat milk were used to detect the primary antibodies and the membrane was visualized with the Odyssey IR imaging system (LI-COR Biosciences).

2.5 Cell viability assay

Cell viability was determined using the cell proliferation kit from Roche (Catalogue no.: 11465007001) that utilizes the MTT (3-(4,5-dimethythiazol-. 2-yl)-2,5-diphenyl tetrazolium bromide) assay. 5000 cells per well were initially seeded in the wells of a 96-well plate and allowed to recover overnight under standard culture conditions. DMSO or paclitaxel was then added for 48 hours before the MTT assay was performed. The level of intensity of the resulting formazan crystals in the wells were measured using a spectrophotometer at 570 nm, and the absorbance values within each cell line was converted to a percentage, with the values of the untreated sample set at 100%.

2.6 Cell cycle analysis

Asynchronous Vector 8 and ILK 10 cells were collected, washed in PBS, fixed overnight in 70% ethanol at 4°C, and then washed again in PBS. DNA was labeled with 40µg/ml propidium iodide in PBS containing 500µg/ml RNase for 30 minutes at 37°C, in the dark. Cells were then kept in the dark, on ice, until fluorescence-activated cell sorting (FACS) using a Becton Dickinson (BD) FACSort analyzer. FACS data was acquired using the BD CellQuest™ Pro (Version 5.2) software, and the appropriate gate across the FL-2W vs. FL-2A plot was applied to acquire data from 5,000 or 10,000 cells that were single cells, and not clumps of 2 or more cells. The data was then analyzed

using the FlowJo software, and the same gate was applied in FlowJo before using the Dean-Jett-Fox cell cycle analysis algorithm to estimate the proportion of cells in each cell cycle stage.

2.7 Immunofluorescence, image acquisition and analysis

Unless otherwise stated, cells were grown on glass coverslips and fixed with ice-cold methanol for 20 minutes at -20°C then washed 3 times with phosphate-buffered saline (PBS). The coverslips were either left overnight at 4°C, or blocked immediately with 1% BSA in PBS at room temperature for 30 minutes. Primary and secondary antibodies were diluted in a blocking buffer containing 0.2% fish skin gelatin and 0.1% goat serum in PBS. Immunostaining of primary antibodies took place either for 2 hours at room temperature, or overnight at 4°C. After washing 3 times with PBS, secondary antibodies were added for 1 hour at room temperature, in the dark, followed by another 3 PBS washes. Finally, DNA was stained using Hoechst 33342 for 10 minutes at room temperature, in the dark, and coverslips were washed 3 times with PBS and mounted onto glass slides with VECTASHIELD® mounting medium. Slides were kept at 4°C in the dark before viewing.

In order to visualize ILK at the centrosomes, cells were partially lysed with 100mM piperazine-N,N′-bis(2-ethanesulfonic acid) (PIPES), 5mM $MgCl_2$, 1mM ethylene glycol tetraacetic acid (EGTA) and 0.5% Triton-X100 for 1 minute at 37°C, before fixation.

For the calcium microtubule depolymerization experiments, cells were incubated with a calcium buffer (100mM PIPES pH6.8, 1mM $MgCl_2$, 1mM $CaCl_2$ and 0.1% Triton-X100) for 2 minutes at room temperature before fixation.

For the microtubule regrowth experiments, cells were treated with DMSO or 10 μM QLT-0267 for 6 hours, with the first 5 hours at 37°C and the last hour at 4°C, on ice, to completely depolymerize all microtubules. Fresh, pre-warmed media (containing either DMSO or 10 μM QLT-0267) was then added to the cells before they were returned to 37°C for varying timepoints before fixation.

Cells were viewed under a Zeiss Colibri fluorescence microscope and images acquired with an AxioCamMRm camera using the AxioVision Rel. 4.7/4.8 software. Z-stacks of 0.25 μm were acquired for images visualizing kinetochores/centromeres and mitotic spindle bundles (Figures 3.1A, 3.1B, 3.2A, 3.2B, 3.2C, 3.3A and 3.4A). The number of stacks varied to accommodate different cells and to ensure that the depth of the entire mitotic cell and all centromeres were captured in the images. In order to more clearly visualize centromeres and mitotic spindle bundles, the z-stacks were deconvolved using AutoQuant X2 (MediaCybernetics). For qualitative analyses, images were exported as TIFF images at maximum intensity projection. For the measurement of mitotic spindle bundle length in the microtubule regrowth experiments, images were viewed at maximum intensity projection, and the length measurement tool in AutoQuant X2 was used to measure the length of the 4 longest mitotic spindle bundles in each cell. For the measurement of intercentromere distance, individual z stacks of the deconvolved images were visually analyzed to pick out identifiable pairs of centromeres for distance measurement.

For quantification of acetylated α-tubulin signal intensity, 13 z-stacks at 1 μm spacings were obtained. The images were not deconvolved to minimize alteration to signal intensities. The stacks were viewed in ImageJ at maximum intensity, and background subtracted using a rolling ball radius of 50 without "light background", before measuring the integrated density within a fixed round area drawn around the spindle.

Phase contrast images of cells in Figure 3.5B were viewed using the same microscope, camera and software as above. Cells were not imaged under controlled environment as the imaging took place over a very short period of time.

For the estimation of mitotic index, cells were imaged for Hoechst 33342 and anti-α-tubulin stains at 10X or 20X, before manual counting of the number of mitotic cells on the screen, and estimating the total number of cells based on the DNA stain using Image J. The mitotic index was then presented as a percentage of mitotic cells over the total number of cells in the image.

2.8 Live cell time-lapse imaging

Live Vector 8 and ILK 10 cells were grown in 6-well plates at low confluency. While HeLa cells do not exhibit contact inhibition, having cells at low confluency would allow easy visualization of mitotic cells. Overlapping cells tended to obscure proper viewing of the condensed chromosomes. The same microscope set-up previously described in Section 2.7 was used for visualization and image acquisition. Additionally, the plate was maintained at 37°C and 5% CO_2 by placing it on a heating insert with a CO_2 cover. Image sequences were acquired every 2 minutes for 10 hours and viewed

in AxioVision 2.7. The brightness and contrast were adjusted for better visualization of chromosomes.

The combined duration of prophase and prometaphase were estimated from the time when the cell was first seen to be rounding up to the time when a metaphase plate was first observed. Metaphase to anaphase duration was estimated from the first appearance of a metaphase plate to when the chromosomes were first seen to separate. The end of mitosis was estimated to occur when the first cleavage furrow was first observed in the elongated cell after anaphase.

2.9 Microtubule dynamics measurement

One day before imaging, 1.5 $\times 10^5$ cells were seeded onto a 35 mm glass bottom dish (MatTek). Immediately before imaging, cells were washed with PBS +/+ (PBS containing Ca^{2+} and Mg^{2+}) twice and replaced with 3 ml of Leibovitz's L-15 media (Invitrogen) containing 10% FBS and oxyrase (1:100) (Oxyrase). The appropriate concentration of DMSO or QLT-0267 was also included and maintained in the L-15 media. Imaging was performed with a high speed spinning disc confocal microscope (Perkin-Elmer) every 3 seconds over 3-5 minutes, and acquired using the software Volocity (Improvision).

A series of time-lapse images were exported from Volocity and analyzed using ImageJ (http://rsb.info.nih.gov/ij/). The images were adjusted for brightness and contrast in ImageJ to achieve optimum visualization of microtubule tips. The positions of the tips at every image frame were then marked with a mouse-controlled cursor using the Manual Tracking plugin. Due to the resolution limit of a confocal microscope

(Kamath et al., 2010), only changes in length >0.5 μm were called growth or shortening events. Phases of undetectable changes in length (≦0.5 μm) were considered pauses. The calculations for transition frequencies and dynamicity were as described previously (Goncalves et al., 2001; Yvon et al., 1999). The rescue frequency was calculated by dividing the number of transitions from shortening to pause and shortening to growing by the time spent shortening or total distance shortened. The catastrophe frequency was calculated by dividing the number of transitions from pause to shortening or growing to shortening by the sum of the time spent growing and pausing or by the total distance grown. Dynamicity was calculated as the total length grown and shortened divided by the life span of the microtubule.

Chapter 3. Results

3.1. Inhibition of ILK with QLT-0267 results in an aberrant spindle phenotype

For this study, I chose to use HeLa cells for their fast doubling time of about 24 hours (based on observations of cells in culture). This ensured a relatively high number of mitotic cells available for analysis in an asynchronous culture. The expression and localization of ILK at the centrosome was also confirmed in this cell line (Figure 1A), as evidenced by the immunostaining of ILK at the two mitotic spindle poles.

Inhibition of ILK's kinase activity in HeLa cells using QLT-0267 resulted in a disorganized mitotic spindle that failed to align all chromosomes to the metaphase plate between both spindle poles, and cells appeared to be arrested in a prometaphase-like stage (Figure 1, lower panel). This is consistent with the abnormal spindle phenotype seen previously in HeLa and Hek293 cells when ILK activity was inhibited by QLT-0267 (Fielding et al., 2008b).

(A)

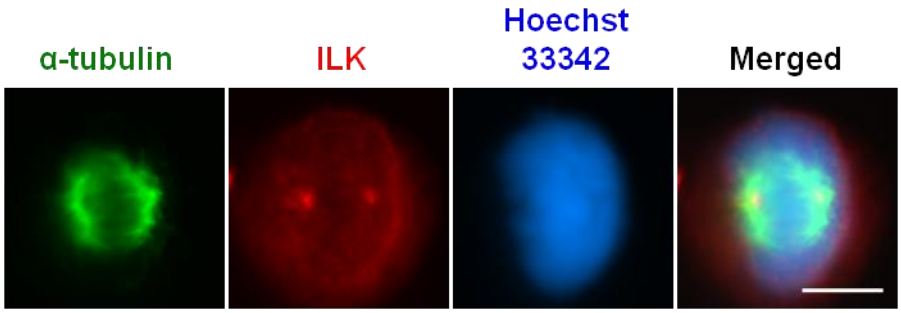

(B)

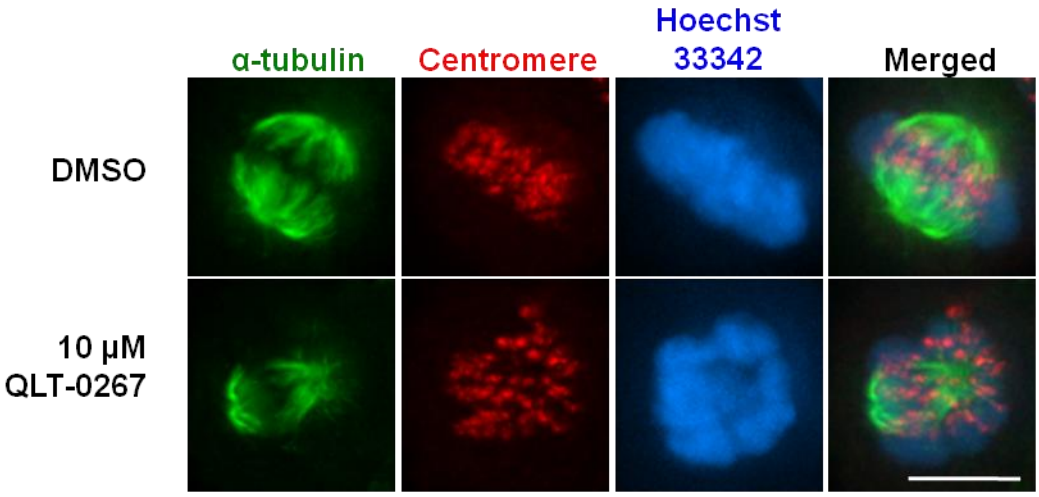

Figure 3.1 HeLa cells express ILK at the centrosome and are sensitive to QLT-0267-induced spindle defects.

(A) ILK is expressed in HeLa cells and localized to the centrosome. The figure shows a representative image of a HeLa mitotic cell fixed from an asynchronous culture and immunostained with anti-α-tubulin (green) and anti-ILK (red). Bar = 10 μm. **(B)** Inhibition of ILK results in an aberrant spindle phenotype in which chromosomes were unable to properly align at the metaphase plate. Asynchronous HeLa cells were treated with DMSO or 10 μM QLT-0267 for 6 hours before being fixed and immunostained with anti-α-tubulin (green) and anti-centromere antibody (red). Bar = 10 μm.

3.2. Inhibition of ILK's kinase activity does not affect kinetochore architecture or kinetochore-microtubule attachment

To characterize the abnormal spindle phenotype, I first assessed the integrity of the kinetochore architecture. Hec1 (also known as Ndc80) resides on the outer kinetochore and is 1 of 4 subunits in the Ndc80 complex, which is a key structural component of the kinetochore (Ciferri et al., 2007; Kline-Smith et al., 2005). Together with the KNL-1/Mis12 complex, the Ndc80 complex constitutes the core microtubule-binding site on the kinetochore (Cheeseman et al., 2006). The localization of Hec1 to the kinetochores had been reported by Schneider *et al.* to be reduced during TACC3 depletion (Schneider et al., 2007) and I wanted to see if inhibition of ILK's kinase activity with QLT-0267 would have any effect on Hec1 localization. HeLa cells were treated with DMSO or 10 μM QLT-0267 for 6 hours and the localization of Hec1 was assessed by immunofluorescence (Figure 3.2A). Treatment of HeLa cells with QLT-0267 did not appear to alter Hec1's localization to the kinetochores as Hec1 was clearly seen next to the centromeres. It should be noted that the signals for Hec1 and centromeres did not colocalize completely as Hec1 is a component of the outer kinetochore, and would not be found directly on the centromeres.

(A)

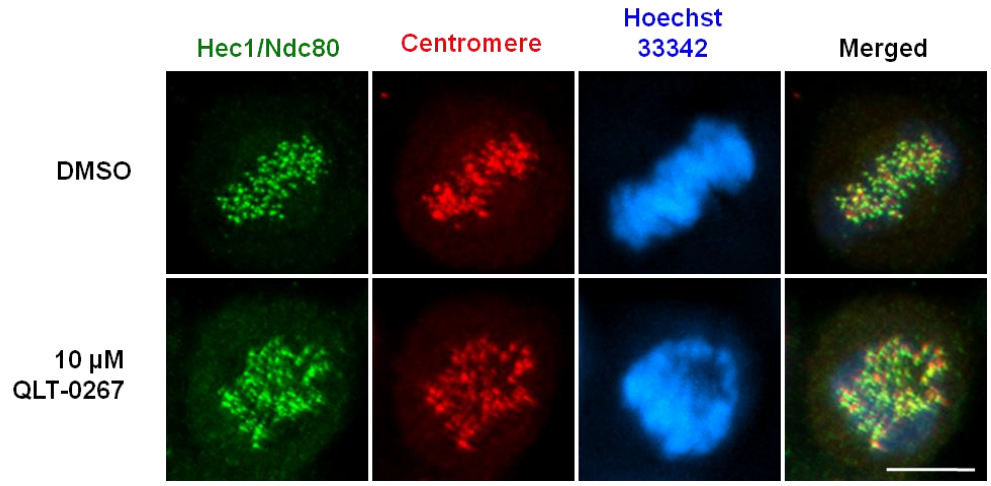

(B)

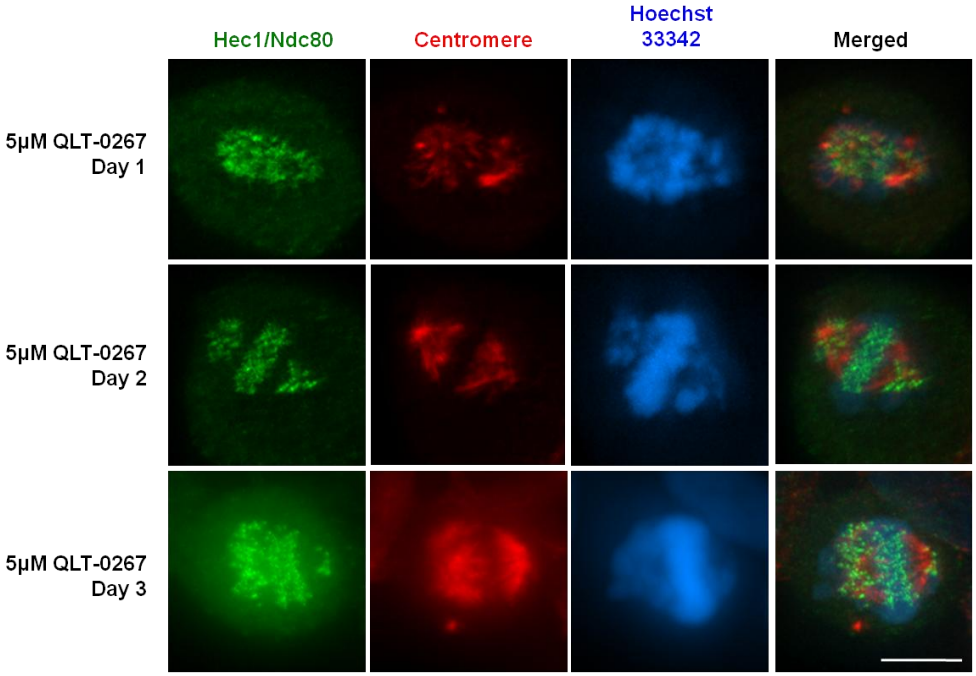

Figure 3.2 (A-B) Inhibition of ILK's kinase activity does not affect kinetochore stability.

Representative images of asynchronous HeLa mitotic cells that were (A) treated with DMSO or 10 µM QLT-0267 for 6 hours, or (B) treated with 5 µM QLT-267 over 1, 2 or 3 days. Cells were then fixed and immunostained with anti-Hec1/Ndc80 and anti-centromere antibody. Inhibition of ILK activity using QLT-0267 over a period of 3 days did not appear to affect localization of the Hec1/Ndc80 protein to the kinetochore. Images are representative of 2 independent experiments. Bar = 10 µm.

In the report by Schneider *et al.*, the authors did not observe a reduction in Hec1 localization to the kinetochores after 1 day of TACC3 depletion, but the marked reduction in Hec1 signals at the kinetochores was seen after 3 days of TACC3 depletion. Therefore, to assess if a longer duration of ILK inhibition might similarly affect Hec1 localization, I exposed HeLa cells to QLT-0267 for 1, 2 or 3 days, instead of the standard 6-hour exposure that was normally used for observing spindle defects. However, since treatment with QLT-0267 was known to induce apoptosis after 18 hours of exposure (Troussard et al., 2006), the concentration of QLT-0267 used was lowered from 10 μM to 5 μM, in order to have enough surviving cells at the end of the drug treatment for observation. As seen in Figure 3.2B, longer exposure of HeLa cells to QLT-0267 also did not appear to alter Hec1 localization to the kinetochores. Since cells did not typically survive long term exposure to QLT-0267 at higher concentrations, I cannot rule out the possibility that a 3-day exposure to 10 μM of QLT-0267 might affect Hec1 localization, although this possibility would be of little significance given that cells were dead by then.

Exposure to QLT-0267 or ILK depletion had been known to only disrupt the interaction between TACC3, ch-TOG and Aurora A, but with no effect on the localization of these proteins to the centrosomes (Fielding et al., 2008b). Since the gradual deterioration of kinetochore architecture reported by Schneider *et al.* was seen with TACC3 depletion, but not in this study with ILK inhibition (and with TACC3 remaining at the centrosomes), it is possible that TACC3's regulation of kinetochore architecture does not involve its interactions with ch-TOG or Aurora A.

(C)

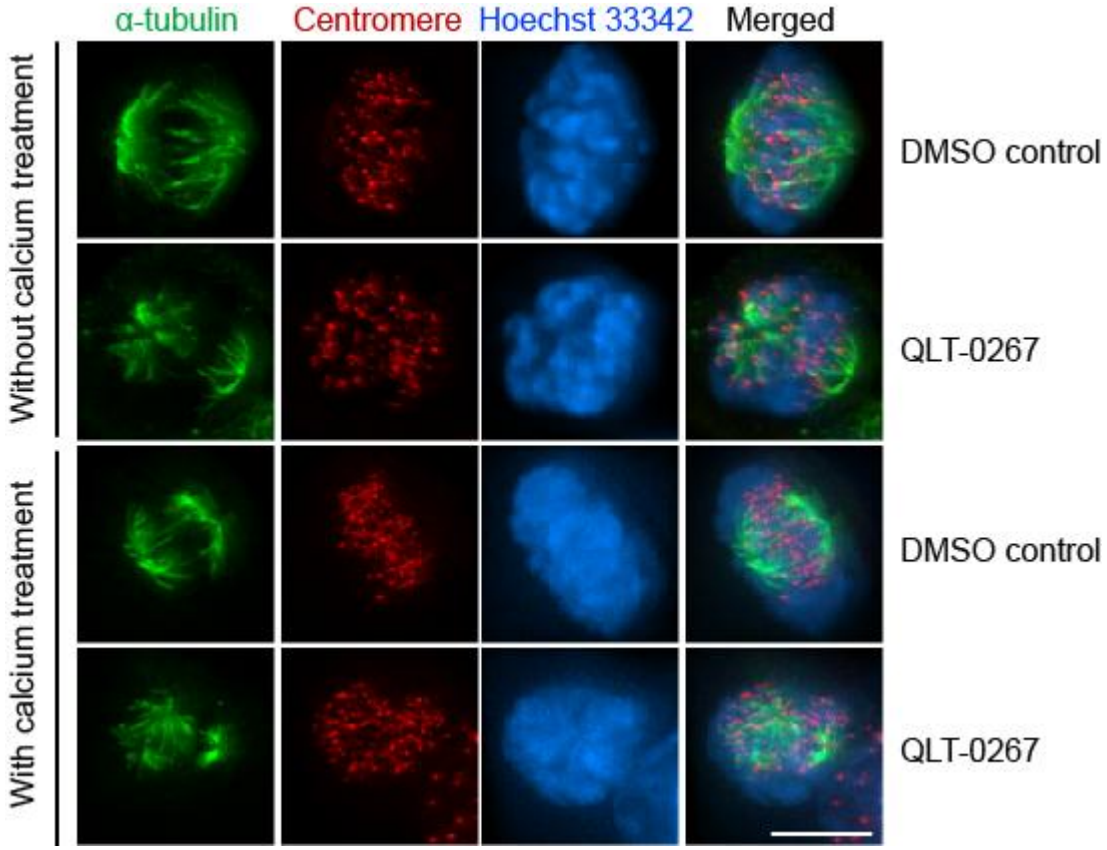

Figure 3.2 (C) Inhibition of ILK's kinase activity does not affect kinetochore-microtubule attachment.

Representative images of asynchronous HeLa mitotic cells that were treated with DMSO or 10 μM QLT-0267 for 6 hours, then fixed immediately or incubated in a calcium buffer for 2 minutes prior to fixation to depolymerize non-kinetochore microtubules. Cells were immunostained with anti-tubulin and anti-centromere antibody to visualize the mitotic spindle and centromeres, respectively. Calcium-stable spindle microtubules were still visible in QLT-0267-treated cells, indicating the presence of kinetochore-microtubules. Images are representative of 3 independent experiments. Bar = 10 μm.

Next, I wanted to determine whether the QLT-0267-induced spindle defect was a result of failed kinetochore-microtubule (kMT) attachment. To test for this, I briefly treated HeLa cells in a calcium buffer to depolymerize non-kinetochore spindle microtubules with unprotected plus ends (Weisenberg and Deery, 1981) prior to fixation. As a positive control, interphase cells were checked to ensure that non-kinetochore

microtubules were depolymerized by calcium treatment (Figure A.1). Immunofluorescence analysis revealed the presence of calcium-stable microtubules in QLT-0267-treated mitotic HeLa cells (Figure 3.2C), and the appearances of the spindles were similar between calcium-treated and non-calcium-treated cells, suggesting that cells were able to form proper kMT attachments even when ILK function was inhibited. However, the presence of kMT attachment does not provide information on the nature or stability of these attachments, and these are addressed in subsequent sections.

3.3. Inhibition of ILK's kinase activity results in higher than normal centromere tension

To further assess the stability of kMT attachment, I measured the distance between sister centromeres as a marker of inter-centromere tension generated by the spindle microtubules. HeLa cells were treated with DMSO, 1 μM nocodazole or 10 μM QLT-0267, then fixed and stained with anti-α-tubulin and anti-centromere antibody (ACA) (Figure 3.3A). Due to the rounded nature of mitotic cells, z-stacks were acquired at 0.25 μm steps to ensure that all centromeres were imaged. Each stack was visually inspected to identify pairs of sister centromeres (Figure 3.3A, arrowed) and to quantify the distance between sister centromeres (Figure 3.3B). The quantification of inter-centrosome distance in control cells was performed only in metaphase cells in which sister centromeres were clearly aligned between two spindle poles.

(A) **(B)**

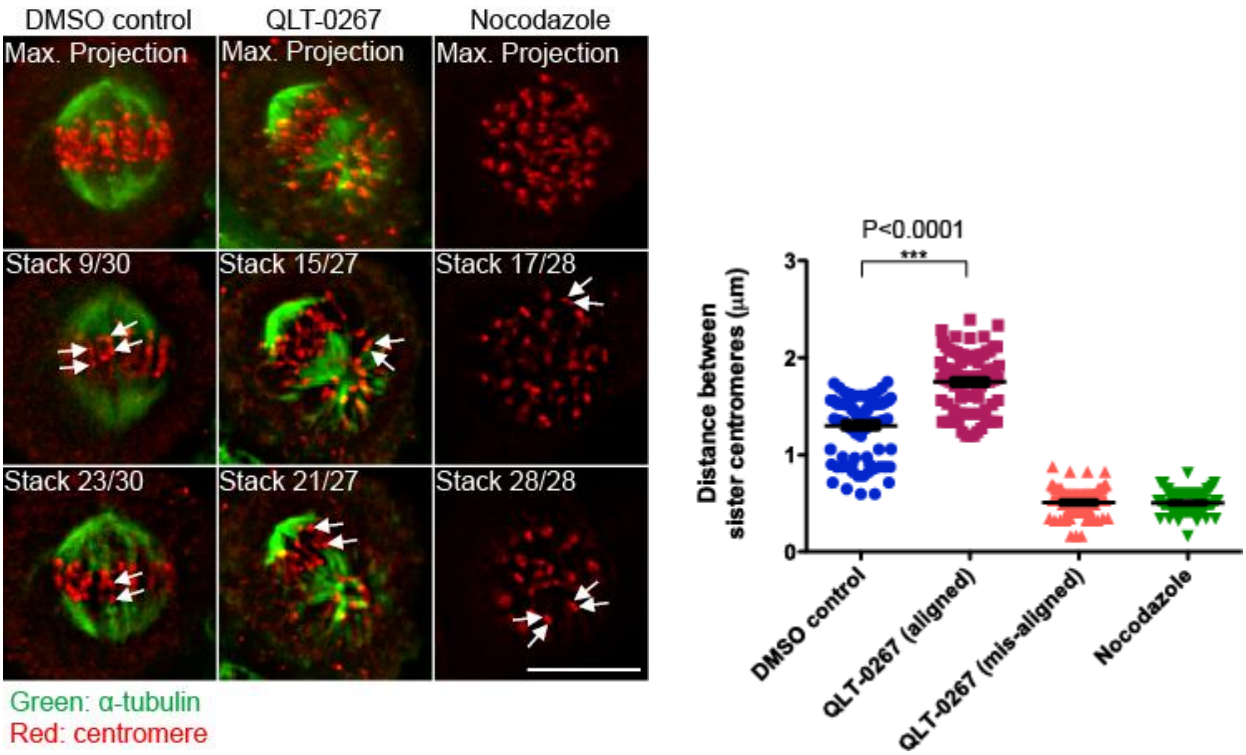

Figure 3.3 Centromere tension is higher than normal in cells treated with QLT-0267.

(A) HeLa cells were treated with DMSO (6 hours), 10 μM QLT-0267 (6 hours) or 1 μM nocodazole (16 hours) before fixation, and immunostained with anti-α-tubulin (green) and anti-centromere antibody (red). Optical sections (0.25 μm z-stacks) were obtained that would include all centromeres in a rounded mitotic cell. The images were deconvolved and pairs of sister centromeres (arrowed) were identified through visual inspection of individual optical sections. The distance between sister centromeres was measured as a marker of inter-centromere tension. Bar = 10 μm. **(B)** Quantification of distance between sister centromeres in mitotic HeLa cells treated with DMSO control, QLT0267 (aligned chromosomes between both spindle poles and mis-aligned chromosomes on the side of only one pole) and nocodazole (basal control for lack of tension between sister centromeres). Results represent mean ± S.E.M. (DMSO control N=81, QLT-0267 (aligned) N=84, QLT-0267 (mis-aligned) N=84, nocodazole N=85) from 2 independent experiments.

For QLT-0267-treated cells, a proportion of chromosomes were sometimes aligned between two spindle poles, while others were clearly found only on one side of a spindle pole (mis-aligned). The inter-centromere distance was thus measured for both

the aligned and mis-aligned chromosomes in QLT-0267-treated cells. Nocodazole is a microtubule depolymerizing agent, therefore mitotic cells treated with nocodazole would not have a mitotic spindle, and the inter-centromere distance in these cells would represent the basal distance between sister centromeres that were under no tension. During measurement of inter-centromere distance, only sister centromeres that appeared to be in focus in the same plane (z-stack) were measured, to prevent underestimation of the distance measured.

Figure 3.3B shows the graphical representation of the inter-centromere quantification. There was no significant difference between the inter-centromere distances of mis-aligned chromosomes in QLT-0267-treated cells and the unattached chromosomes in nocodazole-treated cells. Since kinetochore attachment is not an all or none phenomenon, this suggested a complete lack of tension across the mis-aligned chromosomes in QLT-0267-treated cells and they were not weakly attached to the opposite pole. Due to the limit of the widefield microscope's resolution, it was not possible to tell if these mis-aligned chromosomes were completely unattached to any microtubules or had syntelic attachments.

Higher than normal tension was also observed in the aligned chromosomes of QLT-0267-treated cells (1.93 ± 0.03 μm) compared to control cells (1.53 ± 0.01 μm). This observation was unexpected as it had been reported that small interfering RNA (siRNA) knockdown of ch-TOG in HeLa cells resulted in reduced, not increased, centromere separation (Meraldi et al., 2004). However, ILK inhibition with QLT-0267 was known to only affect ch-TOG's interaction with Aurora A and TACC3, but not the localization of all three proteins to the centrosome (Fielding et al., 2008b). This raises

the possibility that ch-TOG function in promoting kinetochore tension does not require interaction between ch-TOG, TACC3 and Aurora A at the centrosome. Ch-TOG had also been found to promote inter-centromere tension by counteracting the activity of MCAK, a microtubule-depolymerizing kinesin (Barr and Gergely, 2008). Although MCAK did not show up in a previous proteomic screen of ILK's interactome as an ILK interactor (Dobreva et al., 2008), it is entirely possible that ILK inhibition has an indirect effect on MCAK via other pathways, or is interfering with the function of other proteins that cause centromere relaxation to counteract ch-TOG's effects. A number of proteins that are regulated by ILK, such as AKT and GSK3β, also localize to the centrosome and regulate mitotic spindle organization (Fielding et al., 2008a). It is, therefore, not inconceivable that the increase in inter-centromere tension seen with ILK inhibition may also be mediated through these downstream effectors.

Since it had been reported that microtubule dynamics, rather than microtubule motors, could be primarily responsible for centromere stretching and relaxation (Kelling et al., 2003), ILK's kinase function may be involved in regulating spindle microtubule dynamics. This led me to focus on a possible role of ILK in regulating microtubule dynamics in the subsequent sections.

3.4. Inhibition of ILK's kinase activity is associated with slower microtubule regrowth and turnover

To investigate ILK's role in spindle microtubule assembly, I looked at spindle microtubule regrowth after cold depolymerization. HeLa cells were treated with DMSO or 10 μM QLT-0267 under standard conditions for 6 hours except for the last hour, when

cells were chilled on ice at 4°C to completely depolymerize all microtubules. While kinetochore-microtubules are usually cold- and calcium-stable for short periods of time, cold treatment for an hour was enough to induce disassembly of the kinetochore-microtubules (Figure 3.4A at 0min). The cells were then returned to 37°C for varying lengths of time before fixation and immunofluorescence staining to visualize spindle microtubules as the spindles re-assembled over time. Un-chilled cells were also used for measurement of microtubule length at steady state.

The lengths of the four longest microtubule bundles of each cell were measured to obtain the average microtubule bundle length. ILK inhibition clearly slowed the rate of microtubule regrowth at the centrosome (Figure 3.4A and 3.4B). After 10 minutes of regrowth, the length of microtubule bundles in control cells had regrown to that of steady state, and spindles that morphologically resembled those at steady state were seen by 20 minutes of regrowth. In contrast, QLT-0267-treated cells exhibited minimal microtubule regrowth from the centrosome at 10 minutes, while chromatin-associated microtubules were already seen. These cells took twice as long as control cells (up to 20 minutes) to reach steady state length. Quantification of microtubule bundle length revealed shorter spindle microtubules in QLT-0267-treated cells (Figure 3.4B) (6.13 μm in control and 3.74 μm in QLT-0267-treated cells).

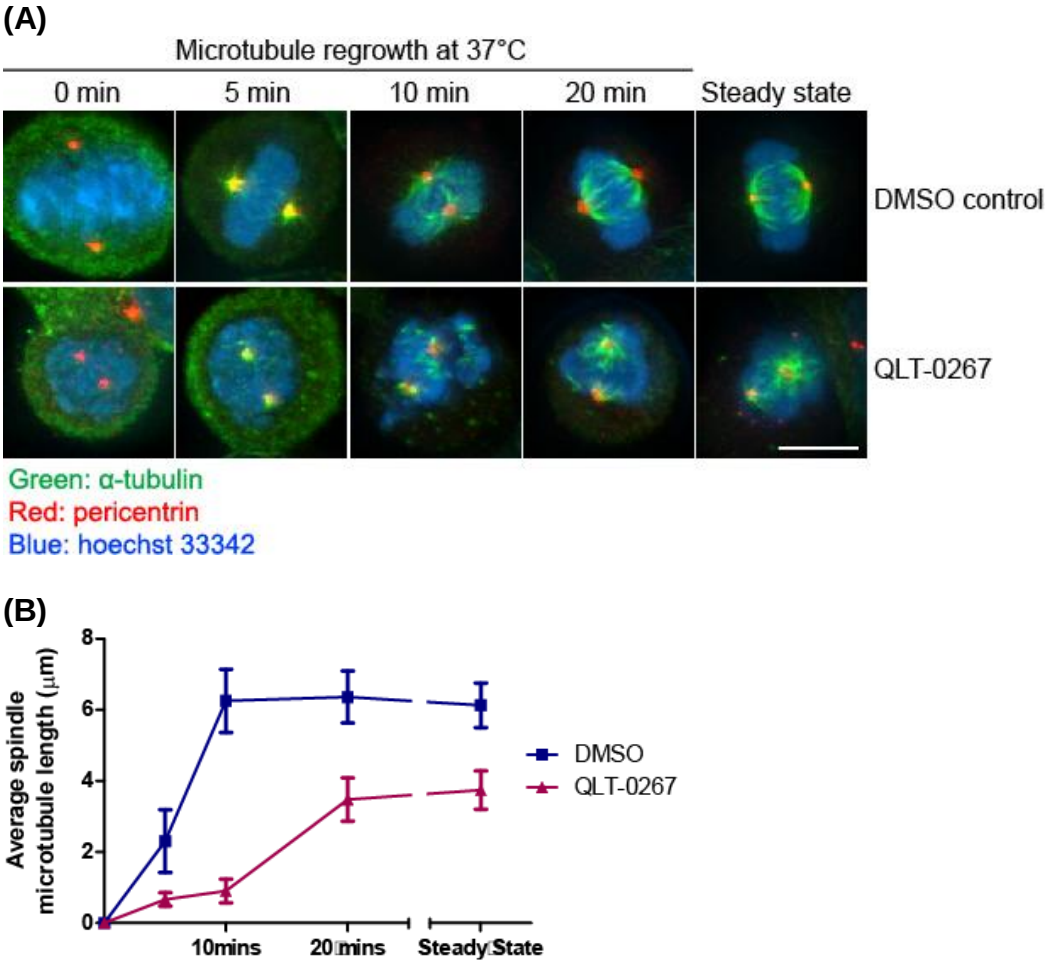

Figure 3.4 (A-B) Microtubule regrowth after depolymerization is slower in QLT-0267-treated cells.

(A) Representative immunofluorescence images of mitotic HeLa cells immunostained with anti-α-tubulin (green) and anti-centromere antibody (red). HeLa cells were treated with DMSO or 10 μM QLT-0267 for 5 hours, and then chilled at 4°C for 1 hour to depolymerize all microtubules. Following that, cells were returned to 37°C for various time-points before methanol fixation. Steady state: un-chilled cells. Bar = 10 μm. (B) Quantification of average microtubule bundle length at different time-points of microtubule regrowth. Results represent mean ± S.D., N=40 (4 longest microtubule bundles per cell, across 10 cells, per condition), and are typical of 3 independent experiments.

Since microtubule spindle reassembly was slower when ILK function was inhibited, I wondered if the spindle microtubules were also less dynamic, with slower tubulin turnover. Alpha-tubulin is acetylated over time (Webster and Borisy, 1989) and can be used as a marker for more stable, long-lived microtubules in the mitotic spindle. I quantified the levels of α-tubulin acetylation relative to total alpha-tubulin in the spindles of control cells and QLT-0267-treated HeLa cells (Figures 3.4C, 3.4D). Consistent with the view that microtubule acetylation occurs in the more stable kinetochore fibers (Wilson et al., 1994), the level of α-tubulin acetylation in control cells was relatively low in prometaphase, and became more prominent by metaphase (Figure A.2). Interestingly, in QLT-0267-treated cells, despite the absence of a metaphase plate, the intensity of alpha-tubulin acetylation was much higher than in prometaphase control cells (Figure 3.4D), and was comparable to metaphase control cells (Figure A.2), suggesting that the ILK inhibition resulted in a population of microtubules that were more stable than normal.

(C)

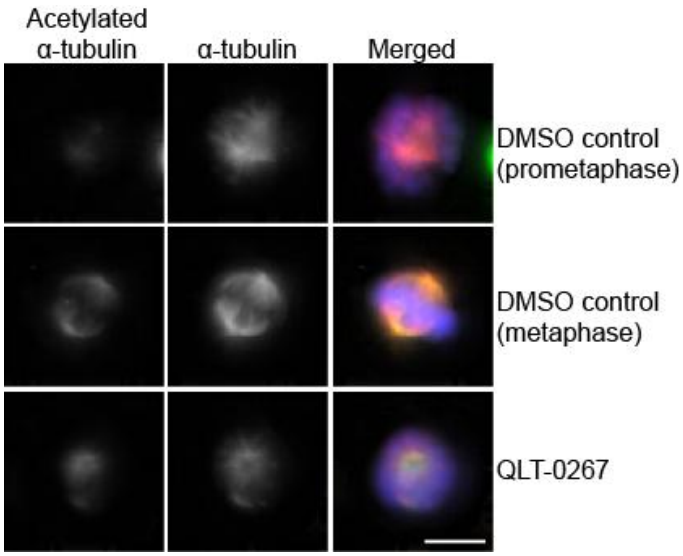

(D)

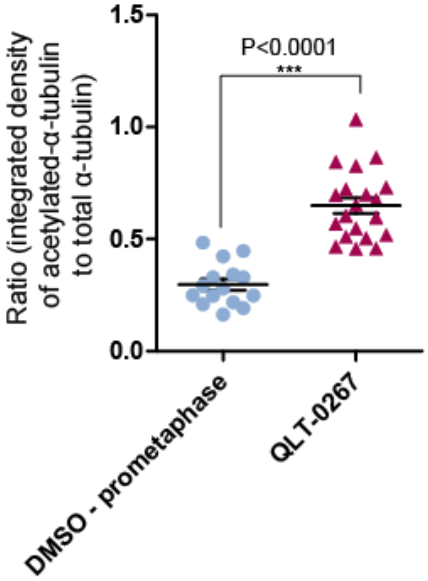

Figure 3.4 (C-D) ILK inhibition increases microtubule stability during mitosis. Representative immunofluorescence images of mitotic HeLa cells that were treated with DMSO or 10 μM QLT-0267 for 6 hours, then immunostained with anti-acetylated α-tubulin (green) and anti-α-tubulin (red). QLT-0267-treated cells showed a higher proportion of acetylated α-tubulin relative to the total amount of α-tubulin when compared to normal prometaphase cells. Bar = 10 μm. (D-E) Quantification of the integrated density of acetylated α-tubulin immunofluorescence signal relative to that of total α-tubulin. Results represent mean ± S.E.M., (N=15 for DMSO prometaphase, N=20 for QLT-0267) and are typical of 2 independent experiments.

These observations are consistent with previous reports of slower microtubule regrowth following depletion of ch-TOG (Cassimeris et al., 2009), and ch-TOG had been shown to be essential for promoting microtubule growth near the centrosome (Barr and Gergely, 2008). Shorter microtubules have also been observed with mutations of ch-TOG homologs in *C. elegans* (Zyg-9) and *Arabidopsis* (MOR1) (Matthews et al., 1998; Srayko et al., 2003; Whittington et al., 2001). In addition, ch-TOG and TACC3 depletion both appeared to increase acetylation of α-tubulin in the mitotic spindle and were believed to function together to establish a dynamic microtubule population (Barr and

Gergely, 2008). Therefore, ILK activity is probably also involved in maintaining a population of dynamic microtubules in mitosis through its influence on the interaction between ch-TOG and TACC3.

Interestingly, another ILK-regulated protein, β-catenin (Novak et al., 1998), had been reported to localize to the centrosome, where it had a role in establishing a bipolar mitotic spindle (Kaplan et al., 2004), and also in regulating microtubule regrowth (Huang et al., 2007). It is likely that ILK activity regulates microtubule assembly and turnover through its influence on the ch-TOG/Aurora-A/TACC3 complex but I cannot rule out the possibility of ILK's effects on other centrosomal proteins such as β-catenin.

3.5. Generation of stable ILK-overexpressing HeLa cell clones

Although QLT-0267 is highly selective for ILK's kinase activity, as with all small molecule inhibitors there is always the possibility of off-target effects. To address this issue, I decided to overexpress ILK in HeLa cells as a different approach to see whether overexpression of ILK and exposure to QLT-0267 would result in opposite effects in cells. Flag-ILK or Flag-vector were introduced into HeLa cells using lentiviral transduction and cells were selected with puromycin for two weeks to obtain a population of cells that were stably expressing Flag-ILK or the vector. Single cells from the bulk population were then expanded and the levels of Flag-ILK were analyzed by western blot (Figure A.3). Out of 5 clones expressing Flag-ILK, the 2 clones with the highest levels of Flag-ILK (ILK 7 and ILK 10) were selected for use, while 2 vector control clones (Vector 6 and Vector 8) were selected at random. The expression of Flag-ILK was confirmed by western blot (Figure 5A) and the levels of ILK

overexpression were estimated by quantifying the signal intensity of the bands. The ratio of Flag-ILK to endogenous ILK was 0.86 in ILK 7 and 1.75 in ILK 10. This level of overexpression was modest and suitable for further experiments because with higher levels of overexpression, there would be a concern of artifactual results due to the sheer amount of overexpressed protein that could cause unspecific protein interactions or activity.

(A)

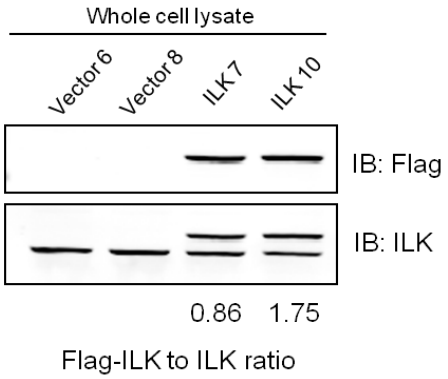

(B)

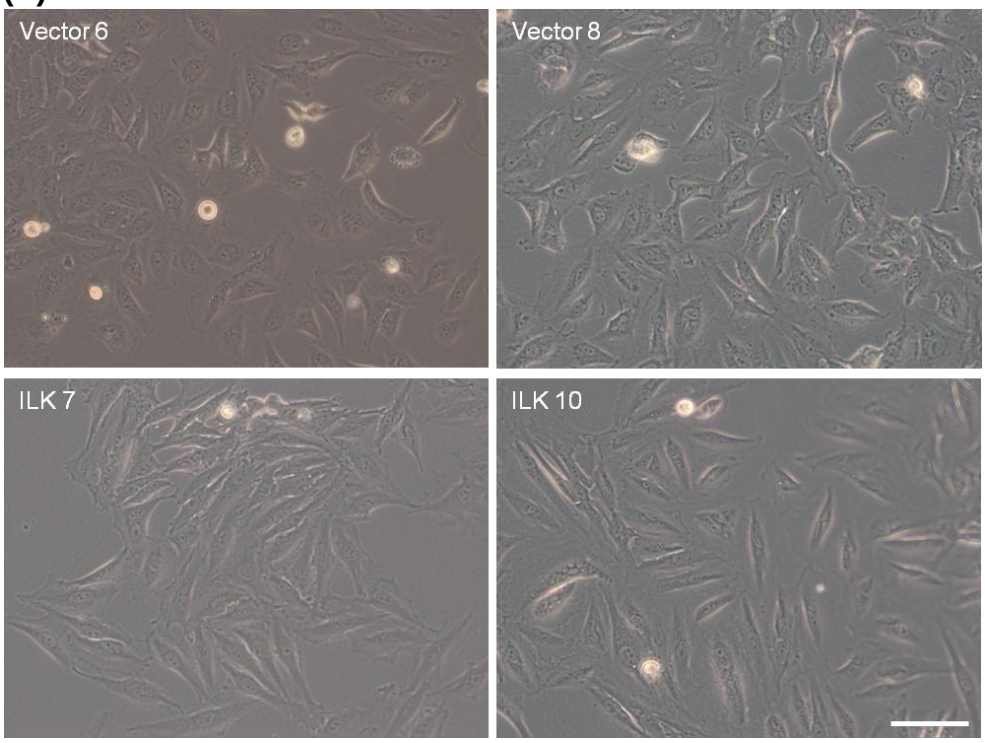

(C)

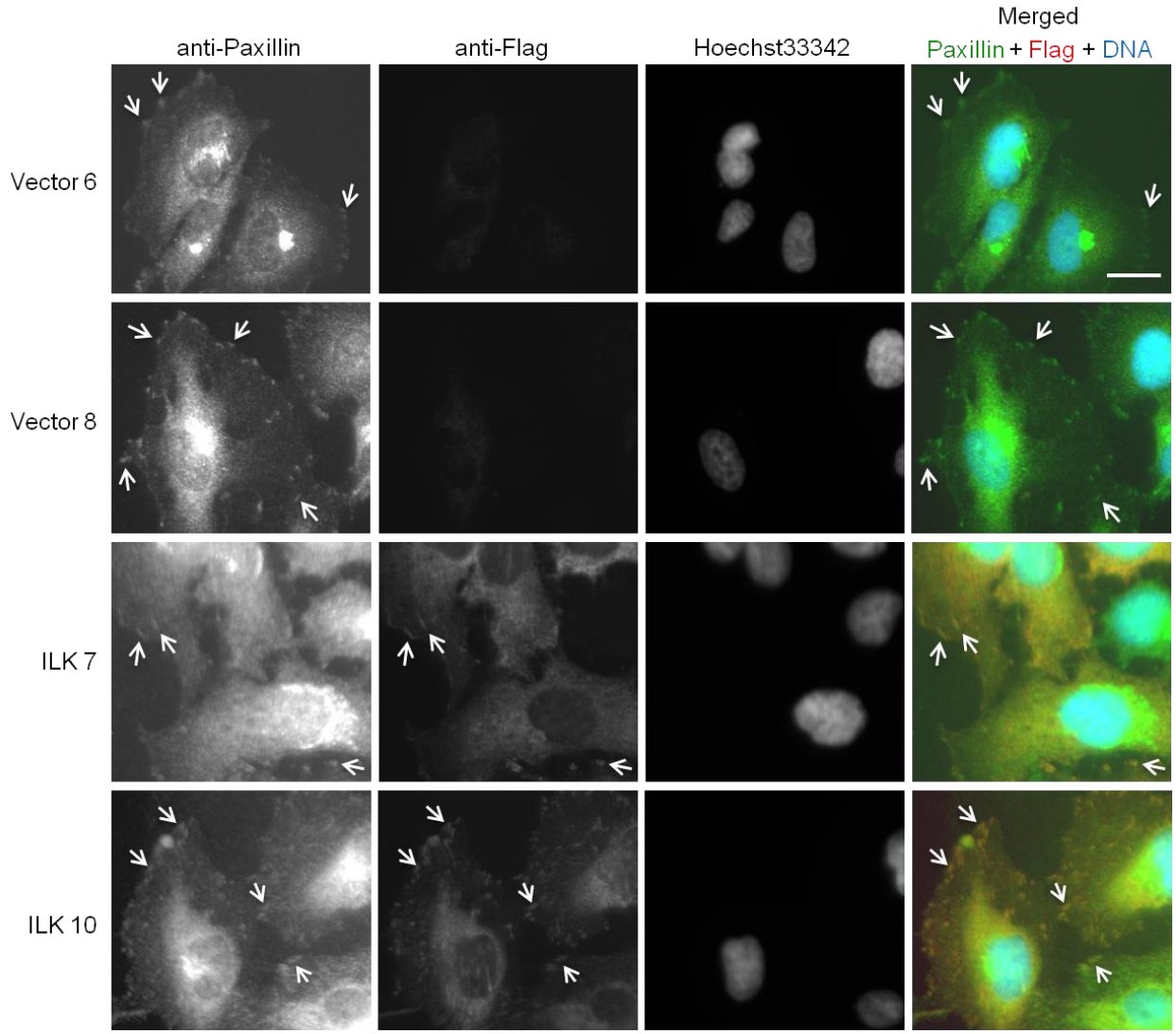
anti-Paxillin
anti-Flag
Hoechst33342
Merged
Paxillin + Flag + DNA
Vector 6
Vector 8
ILK 7
ILK 10

(D)

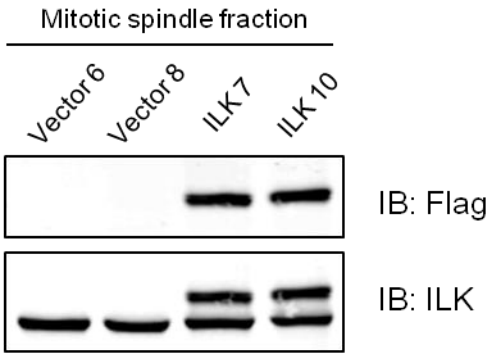
Mitotic spindle fraction
Vector 6
Vector 8
ILK 7
ILK 10
IB: Flag
IB: ILK

Figure 3.5 Generation of HeLa cell clones that stably overexpress Flag-ILK.
(A) Flag-vector or Flag-ILK was stably introduced into parental HeLa cells by lentiviral transduction. Single cell clones were expanded from the bulk culture and 4 clones were selected for further experimentation - 2 vector control clones (Vector 6 and Vector 8), and 2 Flag-ILK-expressing clones (ILK 7 and ILK 10). The expression of exogenous Flag-ILK was confirmed by western blot, with the exogenous to endogenous ILK ratio being 0.86 and 1.75 for ILK 7 and ILK 10 respectively. **(B)** Representative live cell phase images of the HeLa cell clones Vector 6, Vector 8, ILK 7 and ILK 10. Bar = 100 µm. **(C)** The clones were fixed and immunostained with anti-paxillin and anti-flag to determine the localization of Flag-ILK to the focal adhesions (arrowed). Bar = 20 µm. **(D)** Western blot analysis of mitotic spindle fractions of the HeLa clones to confirm the presence of Flag-ILK at the mitotic spindle.

The overexpression of ILK had been reported to result in epithelial-mesenchymal transition (EMT) (Novak et al., 1998; Wu et al., 1998). Phase images of the live cells showed that ILK 7 and ILK 10 cells appeared to be slightly more elongated and mesenchymal when compared to Vector 6 and Vector 8, consistent with an activation of EMT (Figure 5B). The control cells (Vector 6 and Vector 8) retained an epithelial-like morphology resembling that of the parental HeLa cells. In addition, immunofluorescence analysis was performed to assess the localization of Flag-ILK in the cells (Figure 5C).

Paxillin, a focal adhesion protein and ILK binding partner, was used as a marker for focal adhesions. Flag-ILK was observed to localize with paxillin in ILK 7 and ILK 10, whereas no Flag staining was observed in the control cells. Unfortunately, centrosomal localization could not be seen in the cells during co-staining with γ-tubulin, even after lysing the cells with detergent to remove the soluble fraction prior to fixation (data not shown). This was unsurprising due to the relatively modest Flag-ILK expression in the stable cell lines. Previous immunofluorescence staining of transiently transfected cells performed by others in the Dedhar laboratory, using the same anti-Flag antibody, showed only very weak signal at the centrosome, even though transient transfections

typically resulted in much higher levels of Flag-ILK expression (data not shown). Therefore, the localization of Flag-ILK to the centrosome was ascertained indirectly by western blot analysis of mitotic spindle fractions from the cells (Figure 5D). The same protocol for isolating mitotic spindle fractions was also utilized in a previously published report to confirm ch-TOG and RUVBL1 as binding partners of ILK at the centrosome (Fielding et al., 2008b). Figure 5D showed that Flag-ILK was present in the spindle fractions of ILK 7 and ILK 10, but not the control cells.

3.6. Overexpression of ILK is associated with faster mitotic progression

The pharmacological inhibition of ILK by QLT0267 had previously been reported to block mitotic progression and increase mitotic index (Fielding et al., 2008b). To test if these effects were ILK-specific, and whether overexpression of ILK would have an opposite effect, I monitored mitotic progression in the HeLa cell line stably overexpressing ILK (ILK 10) and the vector control (Vector 8). I chose to only use ILK 10 instead of ILK 7 for the next few experiments because of the relatively lower level of Flag-ILK expression in ILK 7, which was less than one fold over endogenous ILK, as seen in the previous section in Figure 5A. The choice of Vector 8 over Vector 6 was made at random. Live cells were imaged under phase contrast every 2 minutes for 10 hours, and the resulting series of time-lapse images were used to estimate the time taken to complete each stage of mitosis.

The classical events used to define prophase include centrosome separation, chromosome condensation and cell rounding (in adherent cells) (Gavet and Pines, 2010). Among the 3 events, cell rounding was the only one that was visible and readily

identifiable in the images. Therefore, the first observable shrinking of cells was defined as the start of mitosis (Figure 6A). The transition from prophase to prometaphase was not measured, because nuclear envelope breakdown (NEBD), which usually marks this transition (Burke and Ellenberg, 2002), could not be visualized in the images. The use of a completely rounded cell as a marker for the start of prometaphase (Bahmanyar et al., 2008) also proved to be difficult as a metaphase plate was observed in 23% of the cells before they were completely rounded up (Figure 6B). Two out of 42 ILK 10 cells would even complete mitosis without ever rounding up completely. As a result, only the combined duration of prophase and prometaphase was measured.

Cells were considered to have entered metaphase at the first frame when a metaphase plate could clearly be seen (Figure 6A). It should be noted that during the course of mitosis, the orientation of the spindle was often unstable and the metaphase plate could be seen to rotate out of view. Therefore it is possible that a metaphase plate was formed much earlier than observed, if it had occurred at an orientation that prevented visualization of the metaphase plate. This would result in an overestimation of the prophase and prometaphase duration, and an underestimation of the metaphase duration. Anaphase onset was marked by the first observation of the metaphase plate splitting into two, while the end of mitosis was estimated to occur at the first appearance of a cleavage furrow (Figure 6A).

ILK overexpression appeared to shorten the duration of mitosis in cells from 145 ± 10.9 (mean ± S.E.M.) minutes to 84.0 ± 6.24 minutes (Figure 6C). Specifically, the time taken to complete prophase and prometaphase was shorter in ILK overexpressing cells (from 83.8 ± 10.2 minutes in control cells to 51.4 ± 5.74 minutes in ILK

overexpressing cells) (Figure 6D). The time taken from metaphase to anaphase onset was also shorter, from 49.2 ± 5.36 minutes in control cells to 20.8 ± 2.11 in ILK overexpressing cells (Figure 6E).

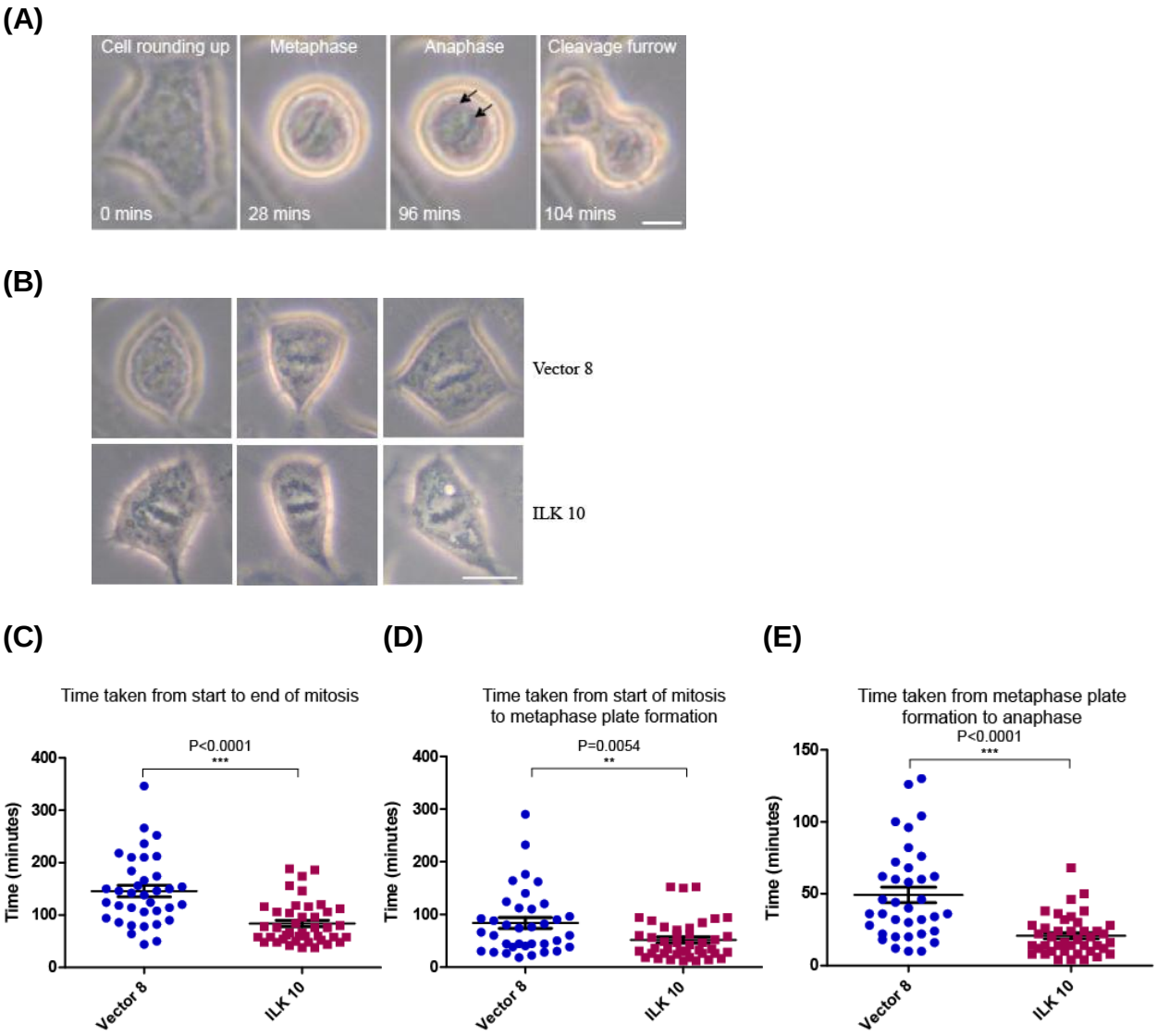

Figure 3.6 Time lapse imaging of control Vector 8 and ILK-overexpressing ILK 10 cell undergoing mitosis.

(A) Representative time lapse images of a Vector 8 cell at the various frames used for estimating the stages of mitosis - duration of prophase and prometaphase (estimated from cell rounding up to metaphase plate formation), duration of metaphase (from metaphase plate formation to onset of anaphase, and the end of mitosis (at the first appearance of a cleavage furrow). Bar = 10 µm. **(B)** Representative images of cells that reached metaphase before completely rounding up, precluding the use of a completely

rounded cell as a marker for prometaphase onset. Top panel: 3 different Vector 8 cells. Bottom panel: 3 different ILK 10 cells. Bar = 10 μm. **(C-E)** Scatter plot of the time (in minutes) taken by vector control HeLa cells (Vector 8, N=36) and ILK-overexpressing HeLa cells (ILK 10, N=42) to complete mitosis (C), prophase and prometaphase (D), and metaphase (E). Results represent mean ± S.E.M., combined from 2 independent experiments.

Due to the subjective nature of estimating mitotic stages based on cell morphology, blind scoring of the durations was performed by a second researcher (Dr. Eiko Kawamura from the Dedhar laboratory). To remove bias, the estimation of the mitosis durations was carried out by Dr. Kawamura after I had changed the filenames of the images. She had no prior knowledge of whether the cells being analyzed belonged to Vector 8 or ILK 10, and having never worked with or seen the cell lines, she was unable to recognize the ILK overexpressing cell line by morphology. The results were consistent with the first round of scoring reported here.

The observation of ILK overexpression increasing the speed of mitotic progression is consistent with the previous finding of QLT-0267 exposure blocking mitotic progression (Fielding et al., 2008b). The shorter metaphase-anaphase duration could probably be attributed to weakening of the spindle assembly checkpoint (SAC). Indeed, Aurora A kinase overexpression had been reported to induce spindle checkpoint override in HeLa cells, despite the presence of defective spindles and persistent checkpoint activation via Mad2 (Anand et al., 2003).

Another possible explanation for the shorter prophase and prometaphase duration seen in ILK 10 cells could be an increase in microtubule dynamics. While chromosome capture is no longer as simple as was proposed in the "search-and-capture" model, dynamic microtubules have been shown to be essential for efficient

capture and biorientation of chromosomes (Huang and Huffaker, 2006). Moreover, microtubule dynamics is recognized to be a vital component in all stages of mitosis (Kline-Smith and Walczak, 2004), and it is likely that ILK overexpression could have a role in enhancing microtubule dynamics.

3.7. Overexpression of ILK is associated with increased aneuploidy

In the previous section, the observation of ILK overexpresing cells progressing faster through metaphase raised the possibility that ILK overexpression may influence the spindle assembly checkpoint (SAC). The visualization of a metaphase plate did not necessarily mean that all chromosomes had aligned at the metaphase plate. A small number of chromosomes that remained unattached, but were not visible in the images, would keep the spindle assembly checkpoint activated and delay anaphase onset. With the shorter metaphase duration, ILK-overexpressing cells could be completing kinetochore attachments at a faster rate (possibly due to increased microtubule dynamics), and/or overriding the SAC to enter anaphase with unattached or incorrectly attached chromosomes. A consequence of the latter scenario would be chromosomal aneuploidy.

To test for the presence of hyperploidy in ILK overexpressing cells, I performed cell cycle analysis on Vector 8 and ILK 10, and looked for signs of DNA aneuploidy. Appropriate gating was carried out to ensure that only single cells were included for analysis and that clumps of 2 or more cells were excluded (details are in Chapter 2). The proportion of cells in each cell cycle stage was estimated using the Dean-Jett-Fox cell cycle analysis algorithm, which is available in the FlowJo software (Figure 7A).

While there was no reproducible pattern of the cell cycle stages seen in biological duplicate profiles, the proportion of hyperploid (>4N) cells was higher in ILK 10 compared to Vector 8 (Figure 7B). A G2/M cell would have duplicated its DNA content and contained twice the diploid DNA content (4N). Any cell with >4N DNA content was considered to be hyperploid, possessing more than the normal complement of DNA.

(A)

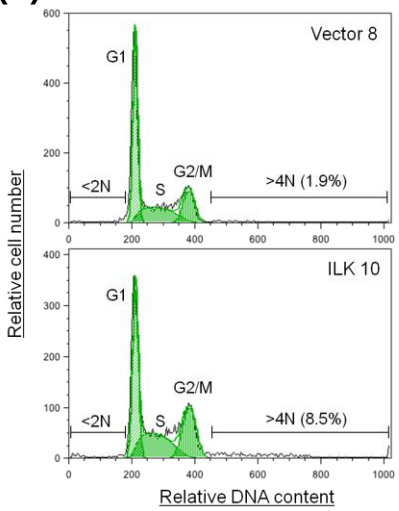

(B)

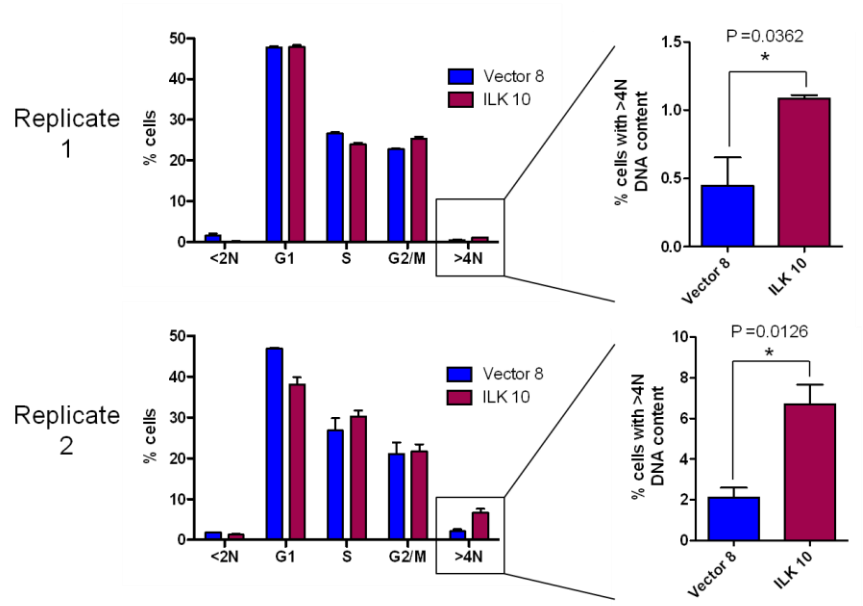

Figure 3.7 ILK overexpression is associated with increased polyploidy.
Asynchronous cultures of Vector 8 and ILK 10 cells were fixed and analyzed by FACS to determine the amount of DNA content present in the cells. **(A)** Representative cell cycle profiles of Vector 8 and ILK 10 cells. The Dean-Jett-Fox algorithm from the FlowJo software was used to estimate the proportion of cells in each cell cycle stage. N = 5,000 cells per sample. **(B)** Cell cycle profiles of Vector 8 and ILK 10 did not reveal reproducible patterns in two independent experiments (Replicate 1 and Replicate 2), except for a higher proportion of ILK 10 cells containing more than 4N DNA content (enlarged in right panels). Results represent mean ± S.E.M. of triplicate readings, N (replicate 1) = 10,000 cells at Passage 13 per sample, N (replicate 2) = 5,000 cells at Passage 9 per sample.

The results suggested that ILK overexpression might be causing an increase in aneuploidy. One possible explanation could be that ILK overexpression somehow overrode the SAC and unattached sister chromatids were left unsegregated, resulting in the observed DNA aneuploidy.

It should be noted that there was a 4- to 6-fold increase in the amount of hyperploid cells in the second experiment (replicate 2, cells at Passage 9) compared to the first experiment (replicate 1, cells at Passage 13). If ILK overexpression was resulting in aneuploidy, the proportion of hyperploid cells should increase with time and passage number. However, the biological replicates were not from the same continuous culture, i.e., replicate 1 was performed in cultures grown from an early passage cryo-stock, while replicate 2 was obtained at a later time from cultures that were grown from another cryovial of the same early passage stock. It is possible that cells from the two experiments went through chromosome misegregation errors of differing severity in the earlier passages after thawing, and these differences were accumulated and amplified over time, resulting in a different proportion of hyperploid cells. Nonetheless, the trend of increased aneuploidy in ILK 10 cells remained consistent over the two experiments.

Finally, using cell cycle analysis to detect DNA aneuploidy at the population level does not definitively prove that ILK overexpression was overriding the SAC and causing chromosome aneuploidy through misegregation errors. A more conclusive approach would be to follow single cells by first checking that spindle checkpoint proteins such as Mad2 were still active and localized to kinetochores of unattached chromosomes. It will then be interesting to see if ILK overexpressing cells would still proceed with anaphase even in the presence of unattached chromosomes that contained active checkpoint proteins. Lastly, a metaphase chromosome spread could be performed to quantify the frequency of changes to chromosome numbers in ILK overexpressing cells.

3.8. ILK regulates microtubule dynamics in living interphase HeLa cells

In the earlier experiments, I had found that inhibition of ILK's kinase activity using QLT-0267 was associated with slower microtubule regrowth and a less dynamic population of microtubules in mitotic HeLa cells. Overexpression of ILK also resulted in a faster progression through prophase and prometaphase, suggesting an enhancement of microtubule dynamics. To directly address ILK's involvement in regulating microtubule dynamics, I went on to measure the parameters of microtubule dynamic instability in live Vector 8 and ILK 10 cells.

Venus-tubulin was stably introduced into these 2 cell lines so that fluorescent microtubules could be visualized and imaged using a spinning disk confocal microscope. The level of venus-tubulin expression was matched between both cell lines by sorting cells through fluorescence-activated cell sorting (FACS) and selecting bulk cells with similar fluorescence levels. Measuring the parameters of microtubule dynamic

instability required the tracking of individual microtubule tips as they grew or shortened over time. However, the central spindle of a mitotic cell was too dense for individual microtubules to be seen, therefore microtubule tips in the lamellar region of interphase cells were tracked instead (Figure 3.8A). It should be noted that, due to the requirement of having fluorescent microtubules for visual tracking, it was possible that the parameters of microtubule dynamics measured using venus-tubulin might not reflect the true dynamics of microtubules made from endogenous tubulin.

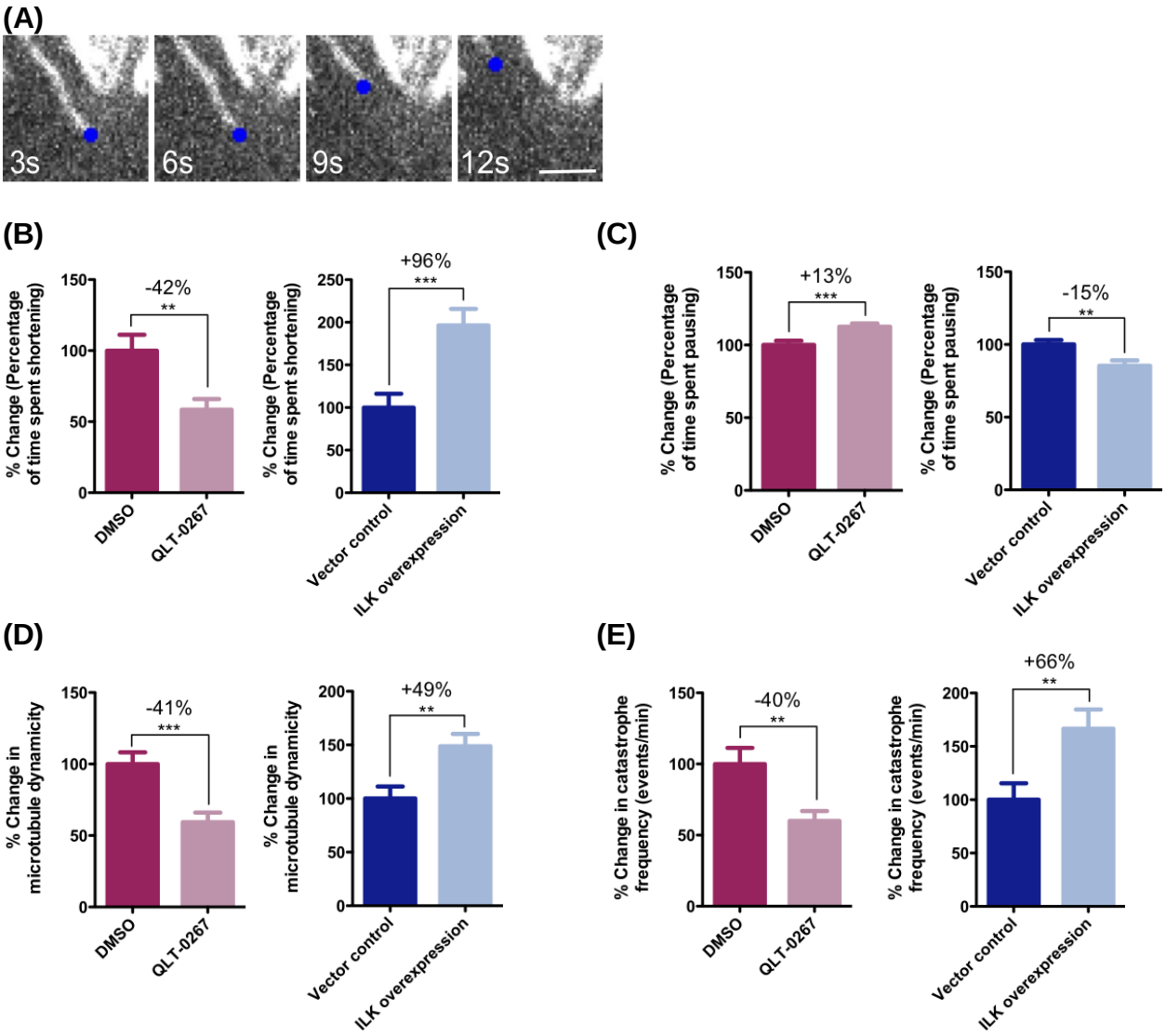

Figure 3.8 ILK regulates microtubule dynamics in living interphase HeLa cells.
(A) Representative time-lapse images of microtubule ends in a living ILK-overexpressing HeLa cell (ILK 10) that was stably expressing venus-tubulin. Images were obtained every 3 s to track the movement of microtubule tips. This series of images shows a microtubule tip near the cell cortex (tracked by a blue dot) pausing from 3 s to 6s, then shortening from 6 s to 12 s. Bar = 2 μm. (B-D) QLT-0267 suppresses, while ILK overexpression increases, microtubule dynamic instability. HeLa clones Vector 8 and ILK 10 were stably transfected with venus-tubulin. The rates and parameters of microtubule dynamic instability were measured between control (Vector 8) and ILK overexpressing (ILK 10) cells, as well as between DMSO- or QLT-0267-treated Vector 8 cells. The two controls ("DMSO" and "Vector control") were normalized to 100%. Bar graphs show mean ± S.E.M., N= 75 (DMSO), 77 (QLT0267), 54 (Vector control), 46 (ILK overexpression) from 3 independent experiments.

I investigated ILK's role in regulating microtubule dynamic instability using two approaches – testing (1) the effect of ILK inhibition by comparing DMSO and QLT0267-treated Vector 8 cells and (2) the effect of ILK overexpression by comparing untreated Vector 8 and ILK 10 cells. The living cells were imaged every 3 seconds to record the movements of the microtubules. After tracking and measuring the distance traveled by individual microtubule tips, the parameters of dynamic instability were calculated (as detailed in Chapter 2.9) and tabulated (Tables 1 and 2). Table 3 summarizes the percentage changes of parameters that showed a significant difference due to either QLT-0267 exposure or ILK overexpression.

Table 3.1: Parameters of dynamic instability in HeLa cells with DMSO or QLT-0267 treatment

Effects of 6-hr 10 µM QLT-0267 treatment on parameters of microtubule dynamic instability in HeLa cells

Parameter	DMSO	QLT-0267		Change
Number of cells	12	14		-
Number of microtubules	75	77		-
Growth rate (µm/min)	14.4 ± 0.77	12.7 ± 0.75		-
Shortening rate (µm/min)	22.0 ± 1.78	17.4 ± 1.73		-
Growth (% of lifespan)	**18.1 ± 1.59**	**12.4 ± 1.33**	**	**-32%**
Shortening (% of lifespan)	**14.2 ± 1.59**	**8.28 ± 1.90**	**	**-42%**
Pause (% of lifespan)	**72.8 ± 2.10**	**81.9 ± 1.64**	***	**+13%**
Dynamicity (µm/min)	**7.43 ± 0.60**	**4.40 ± 0.51**	***	**-41%**
Catastrophe frequency (events/min)	**2.00 ± 0.23**	**1.20 ± 0.14**	**	**-40%**
Rescue frequency (events/min)	8.81 ± 0.86	10.76 ± 0.96		-
Catastrophe frequency (events/µm)	0.54 ± 0.09	0.64 ± 0.11		-
Rescue frequency (events/µm)	**0.40 ± 0.05**	**0.65 ± 0.07**	**	**+63%**

Values are expressed as mean ± S.E.M.
** p<0.01
*** p<0.001

Table 3.2: Parameters of dynamic instability in control and ILK overexpressing HeLa cells

Effects of ILK overexpression on parameters of microtubule dynamic instability in HeLa cells

Parameter	Vector control	ILK overexpression		Change
Number of cells	11	13		-
Number of microtubules	54	46		-
Growth rate (µm/min)	14.2 ± 0.83	15.0 ± 1.10		-
Shortening rate (µm/min)	**19.5 ± 2.51**	**29.9 ± 1.95**	**	**+53%**
Growth (% of lifespan)	16.3 ± 1.75	17.6 ± 2.55		-
Shortening (% of lifespan)	**10.0 ± 1.62**	**19.6 ± 1.95**	***	**+96%**
Pause (% of lifespan)	**73.7 ± 2.26**	**62.8 ± 2.73**	**	**-15%**
Dynamicity (µm/min)	**6.02 ± 0.68**	**8.95 ± 0.69**		**+49%**
Catastrophe frequency (events/min)	**1.47 ± 0.23**	**2.44 ± 0.26**	**	**+66%**
Rescue frequency (events/min)	8.33 ± 1.17	10.6 ± 0.93		-
Catastrophe frequency (events/µm)	0.67 ± 0.15	0.77 ± 0.07		-
Rescue frequency (events/µm)	0.49 ± 0.08	0.45 ± 0.06		-

Values are expressed as mean ± S.E.M.
** p<0.01
*** p<0.001

Table 3.3: Summary of the effects of QLT-0267 treatment or ILK overexpression on parameters of dynamic instability in HeLa cells

Effects of ILK overexpression/QLT-0267 on parameters of microtubule dynamic instability in HeLa cells		
Parameter	**QLT**	**ILK o/e**
Growth rate (µm/min)		
Shortening rate (µm/min)		** +53%
Growth (% of lifespan)	** -32%	
Shortening (% of lifespan)	** -42%	*** +96%
Pause (% of lifespan)	*** +13%	** -15%
Dynamicity (µm/min)	*** -41%	** +49%
Catastrophe frequency (events/min)	** -40%	** +66%
Rescue frequency (events/min)		
Catastrophe frequency (events/µm)		
Rescue frequency (events/µm)	** +63%	
Values are expressed as percentage change over control		
** p<0.01		
*** p<0.001		

Four of the parameters (% time spent shortening, % time spent pausing, dynamicity and time-based catastrophe frequency) were significantly altered and exhibited opposite effects when ILK was inhibited or overexpressed (Figures 3.8B-E). With QLT-0267 treatment, microtubules spent 42% less time shortening and 13% more time pausing, while the opposite was observed with ILK overexpression – 96% more time spent shortening, and 15% less time pausing (Figures 3.8B, C). Microtubule dynamicity reflects the total length grown or shortened at the microtubule ends and is a measure of overall dynamic instability. This parameter was suppressed by 41% after QLT-0267 treatment, but became elevated by 49% with ILK overexpression (Figure 3.8D). Similarly, ILK inhibition reduced the time-based catastrophe frequency (the frequency of transition from growing or pausing, to shortening phases, over time) by 40%, while ILK overexpression increased the catastrophe frequency by 66%.

There were a few parameters that didn't show concordance between both approaches (compare Tables 1 and 2). For example, the distance-based rescue frequency of microtubules was significantly elevated in QLT-0267-treated cells compared to DMSO control cells, but the Student's t-test was not significant between vector control and ILK overexpressing cells. This could be due to the inherent variability in the standard method of measuring microtubule dynamic instability. The spatiotemporal nature of microtubule dynamics regulation would suggest that simply measuring the means of parameters might not provide the full and accurate picture of microtubule dynamics. Furthermore, the measured length fluctuations would also include structural changes. The ends of microtubules are seldom blunt, and elongating microtubules often have sheets and flared, or tapered ends (Arnal et al., 2000; Chretien et al., 1995; Hoog et al., 2007; Zovko et al., 2008). Due to the limits of microscopy resolution, structural changes such as sheet closure into a cylinder would be seen as growth (Chretien et al., 1995). This study therefore cannot rule out any effect of QLT-0267 or ILK overexpression on such structural changes on top of tubulin addition/loss.

Nevertheless, the method used here follows the standard method used in various published studies to facilitate data analysis and comparison with those studies (Goncalves et al., 2001; Yvon et al., 1999), and the data suggested that microtubule dynamics was suppressed by QLT-0267 and enhanced by ILK overexpression.

3.9. ILK overexpression is associated with paclitaxel resistance in HeLa cells

The findings so far suggested a role for ILK's kinase activity in regulating microtubule dynamics and mitotic progression. Overexpressing ILK in HeLa cells appeared to enhance microtubule dynamics and since ILK expression is often elevated in many cancer types (McDonald et al., 2008), I wanted to test the effect of ILK overexpression on cells' sensitivity to paclitaxel, a compound that targets microtubule dynamics. Paclitaxel and related taxanes are commonly used in the treatment of a range of epithelial cancers (Rowinsky, 1997) and these compounds arrest mitosis by stabilizing microtubules and suppressing microtubule dynamics (Jordan et al., 1993; Yvon et al., 1999).

A cell viability test was carried out using the MTT ((3-(4,5-Dimethylthiazol-2-yl)-2,5-diphenyltetrazolium bromide) assay. The control HeLa cell lines Vector 6, Vector 8, and ILK overexpressing cell lines ILK 7 and ILK 10 were exposed to a range of paclitaxel concentration over 48 hours before the percentage of viable cells was estimated using the MTT assay. An initial paclitaxel dose curve on Vector 8 was done with a 24-hour or 48-hour drug treatment (Figures A.4A and A.4B), and it appeared that a 24-hour exposure to paclitaxel was too short for drug cytotoxicity to have a significant effect on cell number. At 48 hours of paclitaxel treatment, the ILK overexpressing cell lines ILK 7 and ILK 10 were observed to be less sensitive to paclitaxel (IC_{50} 10 nM and 25 nM respectively), when compared to the controls Vector 6 (IC_{50} 6.5 nM) and Vector 8 (IC_{50} 4 nM) (Figure 3.9A).

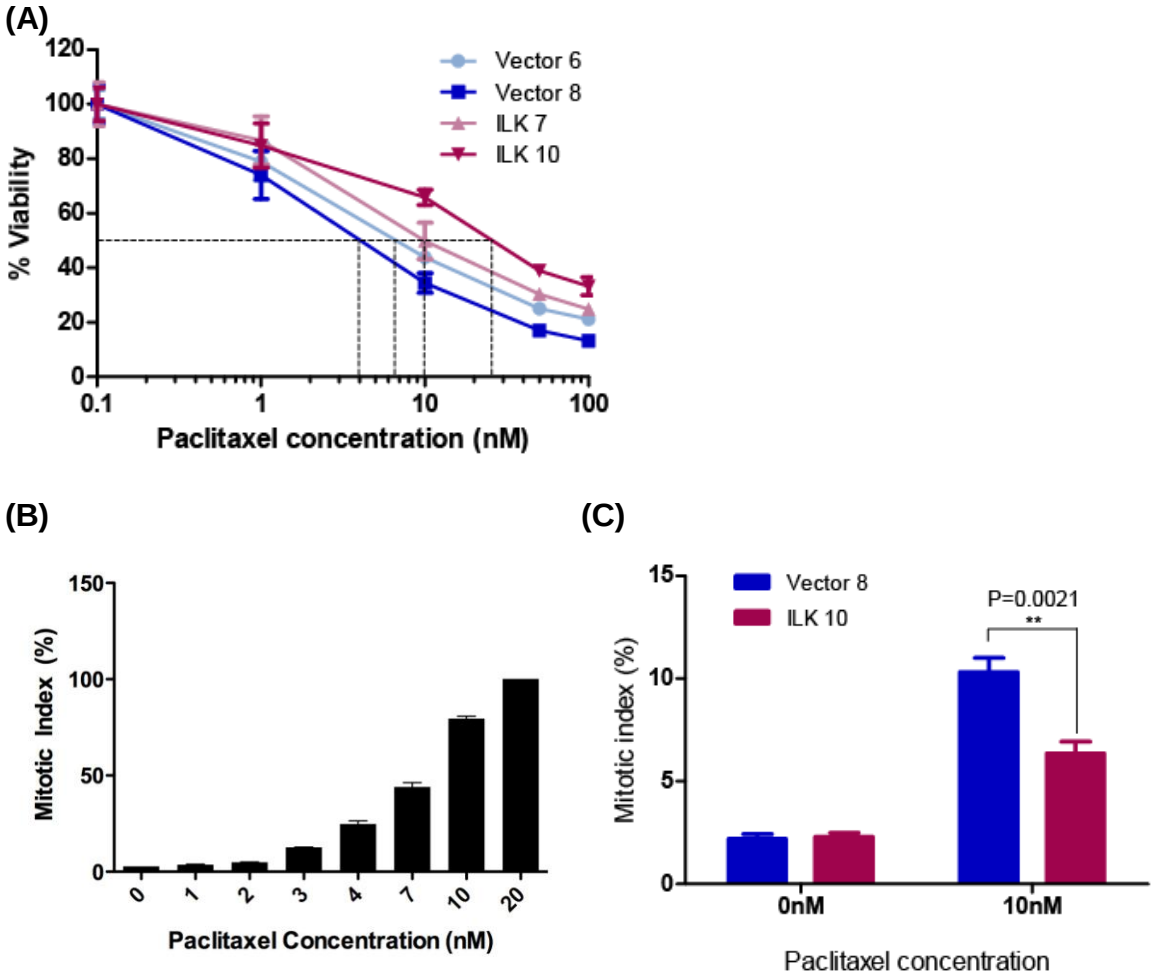

Figure 3.9 ILK overexpression is associated with paclitaxel resistance in HeLa cells.

(A) Percentage viability of HeLa clones (control: Vector 6 and Vector 8; ILK overexpressing: ILK 7 and ILK 10) after various concentrations of paclitaxel treatment for 48 hours. Results indicate mean ± S.E.M., and are representative of 3 independent experiments. Dotted lines serve as a guide to determine IC50 concentration. **(B)** Parental HeLa cells were treated with a range of paclitaxel for 20 hours before fixation and immunostaining with anti-α-tubulin to determine the mitotic index. Bar graph shows mean ± S.E.M., N>300 cells, from 1 experiment. **(C)** Mitotic index of control cells Vector 8 and ILK overexpressing cells ILK 10 after 48 hours of DMSO or 10 nM paclitaxel treatment. Bar graph shows mean ± S.E.M., N>1000 cells, from 2 independent experiments

Since the MTT assay is a measure of metabolic rate based on the reduction of MTT to formazan, the higher absorbance readings from the ILK overexpressing cell

lines may not necessarily indicate a higher number of viable cells. ILK is known to positively regulate proliferation (McDonald et al., 2008), and proliferation is intimately linked to metabolism in cancer cells (Fritz and Fajas, 2010). Therefore, there is a concern that the ILK overexpressing cell lines were actually showing a higher metabolic rate rather than a bigger number of viable cells. However, within each cell line, the absorbance readings for each paclitaxel concentration were converted to a percentage of the untreated cells (described in Section 2.5) and any difference in metabolic rates between the cell lines would not be reflected in the data. Nevertheless, the data does not exclude the possibility that the metabolic rates of the cell lines might be altered to different extents after paclitaxel exposure. An alternative approach, such as counting the viable cells in a well using the trypan blue dye exclusion test, might provide another method of estimating cell viability.

Paclitaxel is known to increase mitotic index by stabilizing microtubules, causing mitotic arrest and activating the spindle assembly checkpoint (Sudo et al., 2004). Therefore, I proceeded to assess whether ILK overexpression had any effect on the paclitaxel-induced increase in mitotic index. An initial experiment was carried out on the parental HeLa cells to check the effect of a 20-hour paclitaxel exposure to the mitotic index (Figure 3.9B). Consistent with a doubling time of around 24 hours, a 100% mitotic index was observed with 20 nM paclitaxel after a 20-hour drug treatment. The half-maximal blocking of mitosis occurred at slightly above 7 nM, which is also consistent with the 8 nM reported in the literature for HeLa cells (Jordan et al., 1993). The mitotic indices of the stable cell lines Vector 8 and ILK 10 were then determined after exposing them to 48 hours (the same duration used for the MTT assay) to 10 nM paclitaxel

(Figure 3.9C). Without paclitaxel treatment, both cell lines had comparable mitotic indices at 2.2% for Vector 8 and 2.3% for ILK 10 (Figure 3.9C), which were consistent with the mitotic index of untreated parental HeLa cells (Figure 3.9B, 0 nM). When Vector 8 cells were subjected to 10 nM paclitaxel, the mitotic index increased to 10.3%, but this increase was much more muted in ILK 10 at 6.4% (Figure 3.9C), suggesting reduced paclitaxel sensitivity in these cells.

It should be noted that despite a 48-hour treatment of 10 nM paclitaxel, the mitotic indices of Vector 8 and ILK 10 were nowhere near 100%. With the parental HeLa cells, the shorter 20-hour treatment with 10 nM paclitaxel had already resulted in an 80% mitotic index. The lower mitotic indices observed in the stable clones after a 48-hour treatment was likely due to mitotic slippage (Andreassen and Margolis, 1991; Rudner and Murray, 1996; Weaver and Cleveland, 2005). Hence, the lower mitotic index seen with ILK overexpression might be due to enhanced paclitaxel resistance by countering the drug's microtubule stabilizing effect and allowing cells to complete mitosis, or it could be due to an increased rate of mitotic slippage. A further way to resolve this uncertainty would be to perform live cell imaging to monitor the fate of mitotic cells treated with paclitaxel and see if they could successfully complete mitosis or undergo mitotic slippage.

While not completely definitive, the observations of higher IC_{50} values in the MTT assay and a lower paclitaxel-induced increase in mitotic index strongly suggest that ILK overexpression might lead to paclitaxel resistance in HeLa cells.

Chapter 4. Discussion

ILK localizes to both the focal adhesions and centrosomes in distinct multiprotein complexes. Its dual functions as a kinase and scaffolding protein had been well characterized at the focal adhesions, while its functions at the centrosomes had only been studied more recently. In this study, I sought to address the function of ILK's kinase activity at the centrosome, separate from a possible scaffolding function of the protein. To do this, I utilized pharmacological inhibition of ILK by a small molecule inhibitor, QLT-0267, to characterize the aberrant spindle phenotype that was previously observed with both ILK inhibition and knockdown (Fielding et al., 2008b). The small molecule inhibitor QLT-0267 had previously been described to be highly selective for ILK phosphotransferase activity (Younes et al., 2005), and inhibited ILK kinase activity with a half maximal inhibitory concentration (IC_{50}) of between 2-5 μM, depending on cell type (Troussard et al., 2006). This concentration correlated well with the appearance of aberrant spindles in HeLa cells, whereas at 10 μM, which is the concentration used in this study, 100% of mitotic cells exhibited spindle defects (Fielding et al., 2008b).

A drawback of using a small molecule inhibitor is that complete specificity against ILK kinase activity cannot be achieved. While our knowledge of ILK's role at the centrosomes is still incomplete, ILK's role as an adaptor protein at the focal adhesions suggested the possibility of a similar adaptor role at the centrosomes, and precluded the use of siRNA as an experimental approach. Any effect seen with ILK knockdown could be attributed to the lack of kinase activity, but could also be due to the loss of adaptor function. To circumvent this drawback, I complemented the use of QLT-0267 with

overexpression of ILK in HeLa cells when measuring microtubule dynamics. The level of expression of exogenous flag-tagged ILK was less than two times that of endogenous ILK to prevent excessive protein overexpression that could result in unspecific protein interactions or activity.

This study has demonstrated that while ILK inhibition with QLT-0267 resulted in a highly disorganized mitotic spindle and misaligned chromosomes, the microtubules were not dramatically destabilized, as evidenced by the presence of calcium-stable microtubules. Unexpectedly, higher than normal inter-centromere tension was observed in QLT-0267-treated HeLa cells. This result suggested an alteration in spindle microtubule dynamics, because microtubule dynamics, rather than microtubule motors, is thought to be the primary mechanism by which a cell controls centromere stretching and relaxation (Kelling et al., 2003). QLT-0267 treatment also resulted in other effects on microtubule dynamics of the mitotic spindle in HeLa cells, including a slower rate of microtubule regrowth after cold depolymerization, and higher levels of acetylated α-tubulin that suggested the presence of a population of more stable microtubules. As mentioned in the results chapter (Chapter 3), slower microtubule regrowth had previously been observed with ch-TOG and TACC3 depletion (Cassimeris et al., 2009; Gergely et al., 2003), and increased acetylated α-tubulin levels had also been reported with ch-TOG depletion (Barr and Gergely, 2008). Both ch-TOG and TACC3 are well known for their roles in controlling global microtubule dynamics in early mitosis (Barr and Gergely, 2008), and phosphorylation of TACC3 in the Aurora-A/ch-TOG/TACC3 complex is required for their proper function in mitotic spindle assembly (Barr and Gergely, 2007). Since treatment of cells with QLT-0267 disrupts the complex formation

of Aurora A-ch-TOG/TACC3 (Fielding et al., 2008b) and decreases the Aurora A-dependent phosphorylation of TACC3 at Ser 558 (Fielding et al., 2011), it is therefore likely that the suppression of spindle microtubule dynamics seen in this study was mediated through ch-TOG and TACC3.

To further confirm the possible role of ILK's kinase activity in regulating mitotic spindle dynamics, future work could include repeating these experiments using a kinase-deficient form of ILK by making a lysine to alanine mutation at K220, the residue that is required for ILK's maximal catalytic activity (Maydan et al., 2010). In addition, rescue experiments could also be performed with ch-TOG and TACC3 depletion/overexpression to provide additional evidence that the observations made in this study were indeed mediated through ch-TOG and TACC3. In this study, the regulation of microtubule dynamics by ILK in mitosis was further confirmed by following ILK overexpressing cells through mitotic progression. Given the importance of microtubule dynamics in all stages of mitosis (Kline-Smith et al., 2005), the faster mitotic progression observed in ILK overexpressing cells suggested an enhancement of microtubule dynamics. Of course, the data could not rule out the possibility of a weakened spindle assembly checkpoint (SAC), or other mechanisms by which cells could bypass the SAC, such as an increase in Aurora A level and activity (Anand et al., 2003).

In interphase HeLa cells, QLT-0267 also suppressed microtubule dynamics, as demonstrated by less time spent shortening and more time spent pausing. The time-based catastrophe frequency was also decreased by QLT-0267, as was the overall dynamicity. These four parameters were altered in the opposite manner in ILK

overexpressing HeLa cells, suggesting that QLT-0267's effects on microtubule dynamics could be mediated through inhibition of ILK's kinase activity. However, since microtubule dynamics regulation is cell cycle dependent (Rusan et al., 2001; Zhai et al., 1996), the changes in microtubule dynamics seen in interphase cells here might not necessarily reflect the effects of QLT-0267 treatment or ILK overexpression on mitotic cells. Moreover, unlike in mitotic cells, it is less clear whether the effects seen in interphase cells were mediated by ch-TOG.

Even though ch-TOG is currently viewed as one of the predominant regulators of microtubule dynamics in mitosis, there is conflicting data on its role in interphase microtubule dynamics. In the budding yeast, depletion of Stu2p (a homolog of ch-TOG) decreased catastrophe frequency and dynamicity *in vivo*, as was observed with QLT-0267 treatment (Kosco et al., 2001). On the other hand, siRNA knockdown of ch-TOG in HeLa cells increased the time-based catastrophe frequency of microtubules (van der Vaart et al., 2011), which would be inconsistent with ch-TOG acting downstream of ILK, since ILK overexpression also increased the time-based catastrophe frequency. Yet another study in human leukemia cells showed that overexpression of ch-TOG resulted in destabilization of interphase microtubules (Holmfeldt et al., 2004). There is also the possibility that ILK might also regulate microtubule dynamics through its interaction with RUVBL1. ILK and RUVBL1 are mutually required for their localization to the centrosomes (Fielding et al., 2008b), and RUVBL1 has been implicated in spindle assembly (Ducat et al., 2008; Gartner et al., 2003), but unfortunately, this aspect of RUVBL1's wide range of functions has not been well studied.

The targeting of microtubule dynamics is a common strategy in chemotherapy, and paclitaxel-mediated suppression of microtubule dynamics has been well studied both in isolated microtubules and living cells (Jordan et al., 1993; Yvon et al., 1999). The effects of QLT0267 on microtubule dynamic instability seen here were similar to those reported for paclitaxel – reduced dynamicity and an increase in distance-based rescue frequency (Jordan et al., 1993; Yvon et al., 1999). Paclitaxel is also known to reduce the rate of microtubule shortening and microtubule dynamicity (Jordan et al., 1993; Yvon et al., 1999), and both parameters were enhanced with ILK overexpression. This raised the question of whether ILK overexpression might influence microtubule dynamics in a way that would counter paclitaxel's effects and alter drug sensitivity. Increased microtubule dynamics have been associated with paclitaxel resistance, with microtubules in paclitaxel-resistant cell lines exhibiting increased shortening rates, lower percentage time pausing, and higher microtubule dynamicity (Goncalves et al., 2001), all of which were observed in the ILK-overexpressing cells. Indeed, the ILK overexpressing HeLa cells in this study showed increased MTT assay readout and a muted increase in mitotic index after long-term paclitaxel treatment, suggesting reduced sensitivity to the drug.

Enhancement of microtubule dynamics thus appears to be one of the mechanisms by which ILK overexpression induces paclitaxel resistance, and this has important clinical implications because elevated ILK levels have been found in many cancer types (McDonald et al., 2008). We would then expect inhibition of ILK activity by QLT-0267 to complement paclitaxel treatment, but one study that looked at cell viability after combination therapy with paclitaxel and QLT-0267 on breast cancer cell lines had

found the two drugs to be antagonistic, while treatment with QLT0267 and docetaxel (a synthetic analogue of paclitaxel) proved to be synergistic (Kalra et al., 2009). Given the multiple functions of ILK, it is certainly possible that the perturbation of other important ILK-regulated signaling pathways by QLT-0267 had come into play. Nevertheless, it will be useful to look for any correlation between ILK expression and paclitaxel resistance in clinical samples, and to consider alternative drug therapies that take into consideration ILK's enhancement of microtubule dynamics.

It should be noted that the data presented in this thesis do not rule out other possible mechanisms of ILK-mediated paclitaxel resistance. Again, the possibility of a weakened SAC, as suggested by the shorter metaphase-anaphase duration in ILK overexpressing mitotic HeLa cells, could contribute to cells overcoming paclitaxel-induced mitotic arrest. Furthermore, the activation of survival pathways such as PI3k/AKT has been known to confer resistance to paclitaxel (Hu et al., 2002), and ILK regulates cell survival through phosphorylation and activation of AKT (Delcommenne et al., 1998).

Chapter 5. Conclusions and future research directions

In summary, the work in this thesis suggested a role for ILK's kinase activity in regulating microtubule dynamics in interphase and mitotic HeLa cells. The defective spindle phenotype observed with QLT-0267 treatment could be attributed to a suppression of spindle microtubule dynamics that interfered with spindle assembly. A second finding was that overexpression of ILK could mediate paclitaxel resistance, possibly through the enhancement of microtubule dynamics. Finally, this study presented a novel mechanism of action for the small molecule inhibitor, QLT-0267, through the suppression of microtubule dynamics in HeLa cells.

Many questions remain unanswered regarding ILK's role and function at the centrosomes, one of them being whether ILK overexpression might interfere with the spindle assembly checkpoint (SAC). Aurora A overexpression had previously been shown to perturb the function of Bub1 (a SAC protein), resulting in a weakened SAC and paclitaxel resistance (Anand et al., 2003). Since ILK kinase activity regulates the interactions of Aurora A during mitosis, and both proteins are known to be overexpressed in epithelial cancers (Gritsko et al., 2003; Negritescu et al., 1976), it will be particularly interesting to see if ILK overexpression will have the same wide-ranging implications on mitosis as Aurora A.

The observation of a shorter metaphase-anaphase duration in ILK overexpressing HeLa cells hint at a possible weakening of the SAC. One way to investigate this possibility is to assess the expression and phosphorylation levels of SAC proteins in ILK overexpressing cells compared to control cells.

Immunofluorescence can also be performed to quantify the percentage of cells undergoing anaphase despite having unaligned chromosomes, and to check whether SAC proteins such as Mad2 and Bub1 are still present on the unaligned kinetochores. An alternative approach to look at whether paclitaxel resistance could be mediated by a weakened checkpoint will be to overexpress SAC proteins, and assessing whether drug resistance can be reversed.

The regulation of microtubule dynamics by ILK could be mediated through ch-TOG, but also through binding with RUVBL1. Currently, the functional implication of the interaction between RUVBL1 and ILK is unknown and represents an area of study that might yield valuable new insights. Another promising avenue to pursue will be to investigate the signaling/interaction network of ILK at the centrosomes. Many known interactors of ILK at the focal adhesions, such as β-catenin, Akt/PKB and GSK3β have been shown to also localize to and function at the centrosomes (Kaplan et al., 2004; Wakefield et al., 2003) and are therefore candidate downstream effectors of ILK at this subcellular localization. An initial phosphoprotein screen had already been performed to identify a list of putative downstream effectors of ILK at the centrosomes (unpublished data from the Dedhar laboratory). These proteins have wide-ranging functions that include histone phosphorylation and binding of insulin receptor substrates. In particular, TPX2 and zyxin are interesting because TPX2 is known to activate Aurora A (Giubettini et al., 2011; Kufer et al., 2003), and zyxin is a focal adhesion and centrosomal protein like ILK that regulates mitosis (Hirota et al., 2000). Furthermore, it is unclear how ILK function at the centrosome is regulated, and a bioinformatic search of potential kinases that can phosphorylate ILK will be a good way to start.

A recent study made the interesting observation that ILK could regulate the local microtubule dynamics required for plasma membrane targeting of caveolae in mouse keratinocytes (Wickstrom et al., 2010a). ILK was found to recruit the scaffold protein IQGAP1 and its downstream effector mDIA1 to nascent, cortical adhesion sites, thereby inducing local stabilization of microtubules which is required for the proper trafficking of caveolin-1-containing vesicles. The same study by Wickstrom *et al.* also measured a few parameters of microtubule dynamics in interphase mice keratinocytes after *Ilk* gene deletion (these mice were named ILK-K5 in their published paper). Surprisingly, the results were the opposite of those observed in this thesis. In particular, the time-based catastrophe frequency was enhanced in ILK-K5 cells, while the same was observed in ILK overexpressing HeLa cells. This difference suggests that ILK's regulation of microtubule dynamics may be dependent on cell type and function. For example, caveolae are only abundant in specific cell types such as the smooth muscle cells, fibroblasts, endothelial cells and adipocytes (Parton and Simons, 2007), and cells that do not utilize as much caveolae may have markedly different regulation of microtubule dynamics at the cell periphery.

This study leads to the question of how the two pools of ILK (at the focal adhesions and centrosomes) cooperate to regulate global and local microtubule dynamics, and it will be very interesting to investigate the role of ILK in organizing interphase microtubules and membrane trafficking, especially between different cell types (including normal and cancer cells).

Finally, in addition to regulating spindle dynamics and centrosome clustering (Fielding et al., 2011), ILK may have a much more complex role in mitosis. As cells

round up in mitosis, they disassemble most of their extracellular matrix (ECM) contacts, remaining attached only by actin-rich retraction fibers (Mitchison, 1992). Integrins are also important for the process of spindle positioning during mitosis (Thery et al., 2005; Toyoshima and Nishida, 2007). With its dual localization at the centrosomes and focal adhesions, as well as roles in regulating the actin and microtubule cytoskeletons, ILK is an ideal candidate to co-ordinate the disassembly of focal adhesions followed by cytoskeletal reorganization at the onset of mitosis and spindle positioning.

Our knowledge of the full extent of ILK's role at the centrosomes is still limited, but there are hints that its centrosomal functions may be as wide-ranging as the ones that have already been well characterized at the focal adhesions. Taken together with the potential new roles, ILK is likely to be near the top of a network that controls an impressive and diverse array of cellular processes and function, and validates the idea of ILK as an attractive therapeutic target in cancer therapy.

References

Alvarez, M., K. Paull, A. Monks, C. Hose, J.S. Lee, J. Weinstein, M. Grever, S. Bates, and T. Fojo. 1995. Generation of a drug resistance profile by quantitation of mdr-1/P-glycoprotein in the cell lines of the National Cancer Institute Anticancer Drug Screen. *The Journal of clinical investigation*. 95:2205-2214.

Anand, S., S. Penrhyn-Lowe, and A.R. Venkitaraman. 2003. AURORA-A amplification overrides the mitotic spindle assembly checkpoint, inducing resistance to Taxol. *Cancer Cell*. 3:51-62.

Andersen, S.S. 2000. Spindle assembly and the art of regulating microtubule dynamics by MAPs and Stathmin/Op18. *Trends Cell Biol*. 10:261-267.

Andreassen, P.R., and R.L. Margolis. 1991. Induction of partial mitosis in BHK cells by 2-aminopurine. *Journal of cell science*. 100 (Pt 2):299-310.

Arnal, I., E. Karsenti, and A.A. Hyman. 2000. Structural transitions at microtubule ends correlate with their dynamic properties in Xenopus egg extracts. *The Journal of cell biology*. 149:767-774.

Bahmanyar, S., D.D. Kaplan, J.G. Deluca, T.H. Giddings, Jr., E.T. O'Toole, M. Winey, E.D. Salmon, P.J. Casey, W.J. Nelson, and A.I. Barth. 2008. beta-Catenin is a Nek2 substrate involved in centrosome separation. *Genes Dev*. 22:91-105.

Balachandran, R., M.J. Welsh, and B.W. Day. 2003. Altered levels and regulation of stathmin in paclitaxel-resistant ovarian cancer cells. *Oncogene*. 22:8924-8930.

Banerjee, A. 2002. Increased levels of tyrosinated alpha-, beta(III)-, and beta(IV)-tubulin isotypes in paclitaxel-resistant MCF-7 breast cancer cells. *Biochemical and biophysical research communications*. 293:598-601.

Bantscheff, M., D. Eberhard, Y. Abraham, S. Bastuck, M. Boesche, S. Hobson, T. Mathieson, J. Perrin, M. Raida, C. Rau, V. Reader, G. Sweetman, A. Bauer, T. Bouwmeester, C. Hopf, U. Kruse, G. Neubauer, N. Ramsden, J. Rick, B. Kuster, and G. Drewes. 2007. Quantitative chemical proteomics reveals mechanisms of action of clinical ABL kinase inhibitors. *Nat Biotechnol*. 25:1035-1044.

Barr, A.R., and F. Gergely. 2007. Aurora-A: the maker and breaker of spindle poles. *Journal of cell science*. 120:2987-2996.

Barr, A.R., and F. Gergely. 2008. MCAK-independent functions of ch-Tog/XMAP215 in microtubule plus-end dynamics. *Molecular and cellular biology*. 28:7199-7211.

Barros, T.P., K. Kinoshita, A.A. Hyman, and J.W. Raff. 2005. Aurora A activates D-TACC-Msps complexes exclusively at centrosomes to stabilize centrosomal microtubules. *The Journal of cell biology*. 170:1039-1046.

Bauer, A., S. Chauvet, O. Huber, F. Usseglio, U. Rothbacher, D. Aragnol, R. Kemler, and J. Pradel. 2000. Pontin52 and reptin52 function as antagonistic regulators of beta-catenin signalling activity. *The EMBO journal*. 19:6121-6130.

Bauer, A., O. Huber, and R. Kemler. 1998. Pontin52, an interaction partner of beta-catenin, binds to the TATA box binding protein. *Proceedings of the National Academy of Sciences of the United States of America*. 95:14787-14792.

Bhalla, K.N. 2003. Microtubule-targeted anticancer agents and apoptosis. *Oncogene*. 22:9075-9086.

Billger, M.A., G. Bhattacharjee, and R.C. Williams, Jr. 1996. Dynamic instability of microtubules assembled from microtubule-associated protein-free tubulin: neither variability of growth and shortening rates nor "rescue" requires microtubule-associated proteins. *Biochemistry*. 35:13656-13663.

Blagosklonny, M.V. 2007. Mitotic arrest and cell fate: why and how mitotic inhibition of transcription drives mutually exclusive events. *Cell Cycle*. 6:70-74.

Boudeau, J., D. Miranda-Saavedra, G.J. Barton, and D.R. Alessi. 2006. Emerging roles of pseudokinases. *Trends Cell Biol*. 16:443-452.

Boveri, T. 1914. Zur Frage der Entstehung maligner Tumoren. Gustav Fischer Verlag, Jena, Germany.

Brinkley, B.R., and J. Cartwright, Jr. 1975. Cold-labile and cold-stable microtubules in the mitotic spindle of mammalian cells. *Ann N Y Acad Sci*. 253:428-439.

Brouhard, G.J., J.H. Stear, T.L. Noetzel, J. Al-Bassam, K. Kinoshita, S.C. Harrison, J. Howard, and A.A. Hyman. 2008. XMAP215 is a processive microtubule polymerase. *Cell*. 132:79-88.

Buffin, E., D. Emre, and R.E. Karess. 2007. Flies without a spindle checkpoint. *Nat Cell Biol*. 9:565-572.

Burke, B., and J. Ellenberg. 2002. Remodelling the walls of the nucleus. *Nature reviews. Molecular cell biology*. 3:487-497.

Cahill, D.P., C. Lengauer, J. Yu, G.J. Riggins, J.K. Willson, S.D. Markowitz, K.W. Kinzler, and B. Vogelstein. 1998. Mutations of mitotic checkpoint genes in human cancers. *Nature*. 392:300-303.

Cassimeris, L. 1999. Accessory protein regulation of microtubule dynamics throughout the cell cycle. *Curr Opin Cell Biol*. 11:134-141.

Cassimeris, L., B. Becker, and B. Carney. 2009. TOGp regulates microtubule assembly and density during mitosis and contributes to chromosome directional instability. *Cell Motil Cytoskeleton*. 66:535-545.

Cheeseman, I.M., J.S. Chappie, E.M. Wilson-Kubalek, and A. Desai. 2006. The conserved KMN network constitutes the core microtubule-binding site of the kinetochore. *Cell*. 127:983-997.

Chretien, D., S.D. Fuller, and E. Karsenti. 1995. Structure of growing microtubule ends: two-dimensional sheets close into tubes at variable rates. *The Journal of cell biology*. 129:1311-1328.

Chun, A.C., and D.Y. Jin. 2003. Transcriptional regulation of mitotic checkpoint gene MAD1 by p53. *The Journal of biological chemistry*. 278:37439-37450.

Ciferri, C., A. Musacchio, and A. Petrovic. 2007. The Ndc80 complex: hub of kinetochore activity. *FEBS Lett*. 581:2862-2869.

Cullen, C.F., and H. Ohkura. 2001. Msps protein is localized to acentrosomal poles to ensure bipolarity of Drosophila meiotic spindles. *Nature cell biology*. 3:637-642.

Dai, W., Q. Wang, T. Liu, M. Swamy, Y. Fang, S. Xie, R. Mahmood, Y.M. Yang, M. Xu, and C.V. Rao. 2004. Slippage of mitotic arrest and enhanced tumor development in mice with BubR1 haploinsufficiency. *Cancer research*. 64:440-445.

Delcommenne, M., C. Tan, V. Gray, L. Rue, J. Woodgett, and S. Dedhar. 1998. Phosphoinositide-3-OH kinase-dependent regulation of glycogen synthase kinase 3 and protein kinase B/AKT by the integrin-linked kinase. *Proceedings of*

the National Academy of Sciences of the United States of America. 95:11211-11216.

Derry, W.B., L. Wilson, I.A. Khan, R.F. Luduena, and M.A. Jordan. 1997. Taxol differentially modulates the dynamics of microtubules assembled from unfractionated and purified beta-tubulin isotypes. *Biochemistry*. 36:3554-3562.

Desai, A., and T.J. Mitchison. 1997. Microtubule polymerization dynamics. *Annu Rev Cell Dev Biol*. 13:83-117.

Diaz, J.F., J.M. Valpuesta, P. Chacon, G. Diakun, and J.M. Andreu. 1998. Changes in microtubule protofilament number induced by Taxol binding to an easily accessible site. Internal microtubule dynamics. *The Journal of biological chemistry*. 273:33803-33810.

Dobles, M., V. Liberal, M.L. Scott, R. Benezra, and P.K. Sorger. 2000. Chromosome missegregation and apoptosis in mice lacking the mitotic checkpoint protein Mad2. *Cell*. 101:635-645.

Dobreva, I., A. Fielding, L.J. Foster, and S. Dedhar. 2008. Mapping the integrin-linked kinase interactome using SILAC. *J Proteome Res*. 7:1740-1749.

Ducat, D., S. Kawaguchi, H. Liu, J.R. Yates, 3rd, and Y. Zheng. 2008. Regulation of microtubule assembly and organization in mitosis by the AAA+ ATPase Pontin. *Molecular biology of the cell*. 19:3097-3110.

Ferlini, C., G. Raspaglio, S. Mozzetti, L. Cicchillitti, F. Filippetti, D. Gallo, C. Fattorusso, G. Campiani, and G. Scambia. 2005. The seco-taxane IDN5390 is able to target class III beta-tubulin and to overcome paclitaxel resistance. *Cancer research*. 65:2397-2405.

Fielding, A.B., I. Dobreva, and S. Dedhar. 2008a. Beyond focal adhesions: integrin-linked kinase associates with tubulin and regulates mitotic spindle organization. *Cell Cycle*. 7:1899-1906.

Fielding, A.B., I. Dobreva, P.C. McDonald, L.J. Foster, and S. Dedhar. 2008b. Integrin-linked kinase localizes to the centrosome and regulates mitotic spindle organization. *J Cell Biol*. 180:681-689.

Fielding, A.B., S. Lim, K. Montgomery, I. Dobreva, and S. Dedhar. 2011. A critical role of integrin-linked kinase, ch-TOG and TACC3 in centrosome clustering in cancer cells. *Oncogene*. 30:521-534.

Foster, L.J., A. Rudich, I. Talior, N. Patel, X. Huang, L.M. Furtado, P.J. Bilan, M. Mann, and A. Klip. 2006. Insulin-dependent interactions of proteins with GLUT4 revealed through stable isotope labeling by amino acids in cell culture (SILAC). *J Proteome Res*. 5:64-75.

Fritz, V., and L. Fajas. 2010. Metabolism and proliferation share common regulatory pathways in cancer cells. *Oncogene*. 29:4369-4377.

Fukuda, K., J.D. Knight, G. Piszczek, R. Kothary, and J. Qin. 2011. Biochemical, proteomic, structural, and thermodynamic characterizations of integrin-linked kinase (ILK): cross-validation of the pseudokinase. *J Biol Chem*. 286:21886-21895.

Galletti, E., M. Magnani, M.L. Renzulli, and M. Botta. 2007. Paclitaxel and docetaxel resistance: molecular mechanisms and development of new generation taxanes. *ChemMedChem*. 2:920-942.

Gard, D.L., and M.W. Kirschner. 1987. A microtubule-associated protein from Xenopus eggs that specifically promotes assembly at the plus-end. *The Journal of cell biology*. 105:2203-2215.

Gartner, W., J. Rossbacher, B. Zierhut, T. Daneva, W. Base, M. Weissel, W. Waldhausl, M.S. Pasternack, and L. Wagner. 2003. The ATP-dependent helicase RUVBL1/TIP49a associates with tubulin during mitosis. *Cell Motil Cytoskeleton*. 56:79-93.

Gavet, O., and J. Pines. 2010. Progressive activation of CyclinB1-Cdk1 coordinates entry to mitosis. *Dev Cell*. 18:533-543.

Gergely, F., V.M. Draviam, and J.W. Raff. 2003. The ch-TOG/XMAP215 protein is essential for spindle pole organization in human somatic cells. *Genes Dev*. 17:336-341.

Gergely, F., C. Karlsson, I. Still, J. Cowell, J. Kilmartin, and J.W. Raff. 2000. The TACC domain identifies a family of centrosomal proteins that can interact with microtubules. *Proceedings of the National Academy of Sciences of the United States of America*. 97:14352-14357.

Giet, R., D. McLean, S. Descamps, M.J. Lee, J.W. Raff, C. Prigent, and D.M. Glover. 2002. Drosophila Aurora A kinase is required to localize D-TACC to centrosomes and to regulate astral microtubules. *The Journal of cell biology*. 156:437-451.

Giubettini, M., I.A. Asteriti, J. Scrofani, M. De Luca, C. Lindon, P. Lavia, and G. Guarguaglini. 2011. Control of Aurora-A stability through interaction with TPX2. *Journal of cell science*. 124:113-122.

Goncalves, A., D. Braguer, K. Kamath, L. Martello, C. Briand, S. Horwitz, L. Wilson, and M.A. Jordan. 2001. Resistance to Taxol in lung cancer cells associated with increased microtubule dynamics. *Proceedings of the National Academy of Sciences of the United States of America*. 98:11737-11742.

Gritsko, T.M., D. Coppola, J.E. Paciga, L. Yang, M. Sun, S.A. Shelley, J.V. Fiorica, S.V. Nicosia, and J.Q. Cheng. 2003. Activation and overexpression of centrosome kinase BTAK/Aurora-A in human ovarian cancer. *Clin Cancer Res*. 9:1420-1426.

Gruss, O.J., and I. Vernos. 2004. The mechanism of spindle assembly: functions of Ran and its target TPX2. *J Cell Biol*. 166:949-955.

Haber, M., C.A. Burkhart, D.L. Regl, J. Madafiglio, M.D. Norris, and S.B. Horwitz. 1995. Altered expression of M beta 2, the class II beta-tubulin isotype, in a murine J774.2 cell line with a high level of taxol resistance. *The Journal of biological chemistry*. 270:31269-31275.

Hanahan, D., and R.A. Weinberg. 2011. Hallmarks of cancer: the next generation. *Cell*. 144:646-674.

Hannigan, G., A.A. Troussard, and S. Dedhar. 2005. Integrin-linked kinase: a cancer therapeutic target unique among its ILK. *Nat Rev Cancer*. 5:51-63.

Hannigan, G.E., J. Bayani, R. Weksberg, B. Beatty, A. Pandita, S. Dedhar, and J. Squire. 1997. Mapping of the gene encoding the integrin-linked kinase, ILK, to human chromosome 11p15.5-p15.4. *Genomics*. 42:177-179.

Hannigan, G.E., J.G. Coles, and S. Dedhar. 2007. Integrin-linked kinase at the heart of cardiac contractility, repair, and disease. *Circulation research*. 100:1408-1414.

Hannigan, G.E., C. Leung-Hagesteijn, L. Fitz-Gibbon, M.G. Coppolino, G. Radeva, J. Filmus, J.C. Bell, and S. Dedhar. 1996. Regulation of cell adhesion and

anchorage-dependent growth by a new beta 1-integrin-linked protein kinase. *Nature*. 379:91-96.

Hannigan, G.E., P.C. McDonald, M.P. Walsh, and S. Dedhar. 2011. Integrin-linked kinase: not so 'pseudo' after all. *Oncogene*. 30:4375-4385.

Hari, M., H. Yang, C. Zeng, M. Canizales, and F. Cabral. 2003. Expression of class III beta-tubulin reduces microtubule assembly and confers resistance to paclitaxel. *Cell Motil Cytoskeleton*. 56:45-56.

Hauf, S., R.W. Cole, S. LaTerra, C. Zimmer, G. Schnapp, R. Walter, A. Heckel, J. van Meel, C.L. Rieder, and J.M. Peters. 2003. The small molecule Hesperadin reveals a role for Aurora B in correcting kinetochore-microtubule attachment and in maintaining the spindle assembly checkpoint. *The Journal of cell biology*. 161:281-294.

Hayden, J.H., S.S. Bowser, and C.L. Rieder. 1990. Kinetochores capture astral microtubules during chromosome attachment to the mitotic spindle: direct visualization in live newt lung cells. *The Journal of cell biology*. 111:1039-1045.

Heim, S.a.M., F. 1995. Cancer cytogenetics. Wiley-Liss Inc., New York.

Hirota, T., T. Morisaki, Y. Nishiyama, T. Marumoto, K. Tada, T. Hara, N. Masuko, M. Inagaki, K. Hatakeyama, and H. Saya. 2000. Zyxin, a regulator of actin filament assembly, targets the mitotic apparatus by interacting with h-warts/LATS1 tumor suppressor. *The Journal of cell biology*. 149:1073-1086.

Holmfeldt, P., S. Stenmark, and M. Gullberg. 2004. Differential functional interplay of TOGp/XMAP215 and the KinI kinesin MCAK during interphase and mitosis. *The EMBO journal*. 23:627-637.

Hoog, J.L., C. Schwartz, A.T. Noon, E.T. O'Toole, D.N. Mastronarde, J.R. McIntosh, and C. Antony. 2007. Organization of interphase microtubules in fission yeast analyzed by electron tomography. *Dev Cell*. 12:349-361.

Horwitz, S.B. 1994. How to make taxol from scratch. *Nature*. 367:593-594.

Hoyt, M.A., L. Totis, and B.T. Roberts. 1991. S. cerevisiae genes required for cell cycle arrest in response to loss of microtubule function. *Cell*. 66:507-517.

Hu, L., J. Hofmann, Y. Lu, G.B. Mills, and R.B. Jaffe. 2002. Inhibition of phosphatidylinositol 3'-kinase increases efficacy of paclitaxel in in vitro and in vivo ovarian cancer models. *Cancer research*. 62:1087-1092.

Huang, B., and T.C. Huffaker. 2006. Dynamic microtubules are essential for efficient chromosome capture and biorientation in S. cerevisiae. *The Journal of cell biology*. 175:17-23.

Huang, P., T. Senga, and M. Hamaguchi. 2007. A novel role of phospho-beta-catenin in microtubule regrowth at centrosome. *Oncogene*. 26:4357-4371.

Hwang, L.H., L.F. Lau, D.L. Smith, C.A. Mistrot, K.G. Hardwick, E.S. Hwang, A. Amon, and A.W. Murray. 1998. Budding yeast Cdc20: a target of the spindle checkpoint. *Science*. 279:1041-1044.

Hyman, A.A., D. Chretien, I. Arnal, and R.H. Wade. 1995. Structural changes accompanying GTP hydrolysis in microtubules: information from a slowly hydrolyzable analogue guanylyl-(alpha,beta)-methylene-diphosphonate. *The Journal of cell biology*. 128:117-125.

Iwanaga, Y., and K.T. Jeang. 2002. Expression of mitotic spindle checkpoint protein hsMAD1 correlates with cellular proliferation and is activated by a gain-of-function p53 mutant. *Cancer research*. 62:2618-2624.

Jin, L., Y. Tabe, S. Konoplev, Y. Xu, C.E. Leysath, H. Lu, S. Kimura, A. Ohsaka, M.B. Rios, L. Calvert, H. Kantarjian, M. Andreeff, and M. Konopleva. 2008. CXCR4 up-regulation by imatinib induces chronic myelogenous leukemia (CML) cell migration to bone marrow stroma and promotes survival of quiescent CML cells. *Mol Cancer Ther*. 7:48-58.

Jordan, M.A., R.J. Toso, D. Thrower, and L. Wilson. 1993. Mechanism of mitotic block and inhibition of cell proliferation by taxol at low concentrations. *Proc Natl Acad Sci U S A*. 90:9552-9556.

Jordan, M.A., K. Wendell, S. Gardiner, W.B. Derry, H. Copp, and L. Wilson. 1996. Mitotic block induced in HeLa cells by low concentrations of paclitaxel (Taxol) results in abnormal mitotic exit and apoptotic cell death. *Cancer research*. 56:816-825.

Joshi, H.C. 1998. Microtubule dynamics in living cells. *Curr Opin Cell Biol*. 10:35-44.

Kalitsis, P., E. Earle, K.J. Fowler, and K.H. Choo. 2000. Bub3 gene disruption in mice reveals essential mitotic spindle checkpoint function during early embryogenesis. *Genes Dev*. 14:2277-2282.

Kalra, J., M. Anantha, C. Warburton, D. Waterhouse, H. Yan, Y.J. Yang, D. Strut, M. Osooly, D. Masin, and M.B. Bally. 2011. Validating the use of a luciferase labeled breast cancer cell line, MDA435LCC6, as a means to monitor tumor progression and to assess the therapeutic activity of an established anticancer drug, docetaxel (Dt) alone or in combination with the ILK inhibitor, QLT0267. *Cancer Biol Ther*. 11:826-838.

Kalra, J., C. Warburton, K. Fang, L. Edwards, T. Daynard, D. Waterhouse, W. Dragowska, B.W. Sutherland, S. Dedhar, K. Gelmon, and M. Bally. 2009. QLT0267, a small molecule inhibitor targeting integrin-linked kinase (ILK), and docetaxel can combine to produce synergistic interactions linked to enhanced cytotoxicity, reductions in P-AKT levels, altered F-actin architecture and improved treatment outcomes in an orthotopic breast cancer model. *Breast Cancer Res*. 11:R25.

Kamath, K., E. Oroudjev, and M.A. Jordan. 2010. Determination of microtubule dynamic instability in living cells. *Methods in cell biology*. 97:1-14.

Kaplan, D.D., T.E. Meigs, P. Kelly, and P.J. Casey. 2004. Identification of a role for beta-catenin in the establishment of a bipolar mitotic spindle. *J Biol Chem*. 279:10829-10832.

Karsenti, E., J. Newport, R. Hubble, and M. Kirschner. 1984. Interconversion of metaphase and interphase microtubule arrays, as studied by the injection of centrosomes and nuclei into Xenopus eggs. *The Journal of cell biology*. 98:1730-1745.

Kelling, J., K. Sullivan, L. Wilson, and M.A. Jordan. 2003. Suppression of centromere dynamics by Taxol in living osteosarcoma cells. *Cancer Res*. 63:2794-2801.

Khodjakov, A., and J. Pines. 2010. Centromere tension: a divisive issue. *Nat Cell Biol*. 12:919-923.

Kinoshita, K., T.L. Noetzel, L. Pelletier, K. Mechtler, D.N. Drechsel, A. Schwager, M. Lee, J.W. Raff, and A.A. Hyman. 2005. Aurora A phosphorylation of TACC3/maskin is required for centrosome-dependent microtubule assembly in mitosis. *The Journal of cell biology*. 170:1047-1055.

Kirschner, M., and T. Mitchison. 1986. Beyond self-assembly: from microtubules to morphogenesis. *Cell*. 45:329-342.

Kline-Smith, S.L., S. Sandall, and A. Desai. 2005. Kinetochore-spindle microtubule interactions during mitosis. *Curr Opin Cell Biol*. 17:35-46.

Kline-Smith, S.L., and C.E. Walczak. 2004. Mitotic spindle assembly and chromosome segregation: refocusing on microtubule dynamics. *Molecular cell*. 15:317-327.

Kops, G.J., D.R. Foltz, and D.W. Cleveland. 2004. Lethality to human cancer cells through massive chromosome loss by inhibition of the mitotic checkpoint. *Proc Natl Acad Sci U S A*. 101:8699-8704.

Kops, G.J., B.A. Weaver, and D.W. Cleveland. 2005. On the road to cancer: aneuploidy and the mitotic checkpoint. *Nature reviews. Cancer*. 5:773-785.

Kosco, K.A., C.G. Pearson, P.S. Maddox, P.J. Wang, I.R. Adams, E.D. Salmon, K. Bloom, and T.C. Huffaker. 2001. Control of microtubule dynamics by Stu2p is essential for spindle orientation and metaphase chromosome alignment in yeast. *Molecular biology of the cell*. 12:2870-2880.

Koul, D., R. Shen, S. Bergh, Y. Lu, J.F. de Groot, T.J. Liu, G.B. Mills, and W.K. Yung. 2005. Targeting integrin-linked kinase inhibits Akt signaling pathways and decreases tumor progression of human glioblastoma. *Mol Cancer Ther*. 4:1681-1688.

Krishna, R., and L.D. Mayer. 2000. Multidrug resistance (MDR) in cancer. Mechanisms, reversal using modulators of MDR and the role of MDR modulators in influencing the pharmacokinetics of anticancer drugs. *Eur J Pharm Sci*. 11:265-283.

Kufer, T.A., E.A. Nigg, and H.H. Sillje. 2003. Regulation of Aurora-A kinase on the mitotic spindle. *Chromosoma*. 112:159-163.

Kumar, A.S., I. Naruszewicz, P. Wang, C. Leung-Hagesteijn, and G.E. Hannigan. 2004. ILKAP regulates ILK signaling and inhibits anchorage-independent growth. *Oncogene*. 23:3454-3461.

Kwon, M., S.A. Godinho, N.S. Chandhok, N.J. Ganem, A. Azioune, M. Thery, and D. Pellman. 2008. Mechanisms to suppress multipolar divisions in cancer cells with extra centrosomes. *Genes Dev*. 22:2189-2203.

Lampson, M.A., K. Renduchitala, A. Khodjakov, and T.M. Kapoor. 2004. Correcting improper chromosome-spindle attachments during cell division. *Nature cell biology*. 6:232-237.

Larsson, N., B. Segerman, H.M. Gradin, E. Wandzioch, L. Cassimeris, and M. Gullberg. 1999. Mutations of oncoprotein 18/stathmin identify tubulin-directed regulatory activities distinct from tubulin association. *Molecular and cellular biology*. 19:2242-2250.

Lee, M.J., F. Gergely, K. Jeffers, S.Y. Peak-Chew, and J.W. Raff. 2001. Msps/XMAP215 interacts with the centrosomal protein D-TACC to regulate microtubule behaviour. *Nature cell biology*. 3:643-649.

Legate, K.R., E. Montanez, O. Kudlacek, and R. Fassler. 2006. ILK, PINCH and parvin: the tIPP of integrin signalling. *Nat Rev Mol Cell Biol*. 7:20-31.

Lengauer, C., K.W. Kinzler, and B. Vogelstein. 1997. Genetic instability in colorectal cancers. *Nature*. 386:623-627.

LeRoy, P.J., J.J. Hunter, K.M. Hoar, K.E. Burke, V. Shinde, J. Ruan, D. Bowman, K. Galvin, and J.A. Ecsedy. 2007. Localization of human TACC3 to mitotic spindles is mediated by phosphorylation on Ser558 by Aurora A: a novel pharmacodynamic method for measuring Aurora A activity. *Cancer research*. 67:5362-5370.

Leung-Hagesteijn, C., A. Mahendra, I. Naruszewicz, and G.E. Hannigan. 2001. Modulation of integrin signal transduction by ILKAP, a protein phosphatase 2C associating with the integrin-linked kinase, ILK1. *The EMBO journal*. 20:2160-2170.

Li, R., and A.W. Murray. 1991. Feedback control of mitosis in budding yeast. *Cell*. 66:519-531.

Ligon, L.A., S.S. Shelly, M. Tokito, and E.L. Holzbaur. 2003. The microtubule plus-end proteins EB1 and dynactin have differential effects on microtubule polymerization. *Molecular biology of the cell*. 14:1405-1417.

Liu, D., and M.A. Lampson. 2009. Regulation of kinetochore-microtubule attachments by Aurora B kinase. *Biochemical Society transactions*. 37:976-980.

Liu, J., P.C. Costello, N.A. Pham, M. Pintillie, M. Jabali, J. Sanghera, M.S. Tsao, and M.R. Johnston. 2006. Integrin-linked kinase inhibitor KP-392 demonstrates clinical benefits in an orthotopic human non-small cell lung cancer model. *J Thorac Oncol*. 1:771-779.

Long, B.H., and C.R. Fairchild. 1994. Paclitaxel inhibits progression of mitotic cells to G1 phase by interference with spindle formation without affecting other microtubule functions during anaphase and telephase. *Cancer research*. 54:4355-4361.

Lowe, J., H. Li, K.H. Downing, and E. Nogales. 2001. Refined structure of alpha beta-tubulin at 3.5 A resolution. *J Mol Biol*. 313:1045-1057.

Luduena, R.F. 1998. Multiple forms of tubulin: different gene products and covalent modifications. *Int Rev Cytol*. 178:207-275.

Luqmani, Y.A. 2005. Mechanisms of drug resistance in cancer chemotherapy. *Med Princ Pract*. 14 Suppl 1:35-48.

Mandelkow, E.M., E. Mandelkow, and R.A. Milligan. 1991. Microtubule dynamics and microtubule caps: a time-resolved cryo-electron microscopy study. *The Journal of cell biology*. 114:977-991.

Maney, T., M. Wagenbach, and L. Wordeman. 2001. Molecular dissection of the microtubule depolymerizing activity of mitotic centromere-associated kinesin. *The Journal of biological chemistry*. 276:34753-34758.

Marumoto, T., D. Zhang, and H. Saya. 2005. Aurora-A - a guardian of poles. *Nat Rev Cancer*. 5:42-50.

Matthews, L.R., P. Carter, D. Thierry-Mieg, and K. Kemphues. 1998. ZYG-9, a Caenorhabditis elegans protein required for microtubule organization and function, is a component of meiotic and mitotic spindle poles. *The Journal of cell biology*. 141:1159-1168.

Maydan, M., P.C. McDonald, J. Sanghera, J. Yan, C. Rallis, S. Pinchin, G.E. Hannigan, L.J. Foster, D. Ish-Horowicz, M.P. Walsh, and S. Dedhar. 2010. Integrin-linked

kinase is a functional Mn2+-dependent protein kinase that regulates glycogen synthase kinase-3beta (GSK-3beta) phosphorylation. *PLoS One*. 5:e12356.

McDonald, P.C., A.B. Fielding, and S. Dedhar. 2008. Integrin-linked kinase--essential roles in physiology and cancer biology. *J Cell Sci*. 121:3121-3132.

Meraldi, P., V.M. Draviam, and P.K. Sorger. 2004. Timing and checkpoints in the regulation of mitotic progression. *Dev Cell*. 7:45-60.

Michel, L.S., V. Liberal, A. Chatterjee, R. Kirchwegger, B. Pasche, W. Gerald, M. Dobles, P.K. Sorger, V.V. Murty, and R. Benezra. 2001. MAD2 haplo-insufficiency causes premature anaphase and chromosome instability in mammalian cells. *Nature*. 409:355-359.

Mills, J., M. Digicaylioglu, A.T. Legg, C.E. Young, S.S. Young, A.M. Barr, L. Fletcher, T.P. O'Connor, and S. Dedhar. 2003. Role of integrin-linked kinase in nerve growth factor-stimulated neurite outgrowth. *The Journal of neuroscience : the official journal of the Society for Neuroscience*. 23:1638-1648.

Mitchison, T.J. 1992. Actin based motility on retraction fibers in mitotic PtK2 cells. *Cell Motil Cytoskeleton*. 22:135-151.

Muller-Reichert, T., D. Chretien, F. Severin, and A.A. Hyman. 1998. Structural changes at microtubule ends accompanying GTP hydrolysis: information from a slowly hydrolyzable analogue of GTP, guanylyl (alpha,beta)methylenediphosphonate. *Proceedings of the National Academy of Sciences of the United States of America*. 95:3661-3666.

Muranyi, A.L., S. Dedhar, and D.E. Hogge. 2009. Combined inhibition of integrin linked kinase and FMS-like tyrosine kinase 3 is cytotoxic to acute myeloid leukemia progenitor cells. *Experimental hematology*. 37:450-460.

Musacchio, A., and K.G. Hardwick. 2002. The spindle checkpoint: structural insights into dynamic signalling. *Nature reviews. Molecular cell biology*. 3:731-741.

Musacchio, A., and E.D. Salmon. 2007. The spindle-assembly checkpoint in space and time. *Nature reviews. Molecular cell biology*. 8:379-393.

Negritescu, S., E. Mihalas, M. Sterescu, and C. Ioan. 1976. [Thin-layer chromatographic separation of reaction products formed during nitration in nitrazepam synthesis]. *Pharmazie*. 31:823.

Nezi, L., and A. Musacchio. 2009. Sister chromatid tension and the spindle assembly checkpoint. *Curr Opin Cell Biol*. 21:785-795.

Nikolopoulos, S.N., and C.E. Turner. 2001. Integrin-linked kinase (ILK) binding to paxillin LD1 motif regulates ILK localization to focal adhesions. *The Journal of biological chemistry*. 276:23499-23505.

Nikolopoulos, S.N., and C.E. Turner. 2002. Molecular dissection of actopaxin-integrin-linked kinase-Paxillin interactions and their role in subcellular localization. *The Journal of biological chemistry*. 277:1568-1575.

Nogales, E. 2001. Structural insight into microtubule function. *Annu Rev Biophys Biomol Struct*. 30:397-420.

Nogales, E., S.G. Wolf, I.A. Khan, R.F. Luduena, and K.H. Downing. 1995. Structure of tubulin at 6.5 A and location of the taxol-binding site. *Nature*. 375:424-427.

Novak, A., S.C. Hsu, C. Leung-Hagesteijn, G. Radeva, J. Papkoff, R. Montesano, C. Roskelley, R. Grosschedl, and S. Dedhar. 1998. Cell adhesion and the integrin-linked kinase regulate the LEF-1 and beta-catenin signaling pathways.

Proceedings of the National Academy of Sciences of the United States of America. 95:4374-4379.

Oloumi, A., S. Syam, and S. Dedhar. 2006. Modulation of Wnt3a-mediated nuclear beta-catenin accumulation and activation by integrin-linked kinase in mammalian cells. *Oncogene*. 25:7747-7757.

Ong, S.E., B. Blagoev, I. Kratchmarova, D.B. Kristensen, H. Steen, A. Pandey, and M. Mann. 2002. Stable isotope labeling by amino acids in cell culture, SILAC, as a simple and accurate approach to expression proteomics. *Mol Cell Proteomics*. 1:376-386.

Orr, G.A., P. Verdier-Pinard, H. McDaid, and S.B. Horwitz. 2003. Mechanisms of Taxol resistance related to microtubules. *Oncogene*. 22:7280-7295.

Ouyang, B., J.A. Knauf, K. Ain, B. Nacev, and J.A. Fagin. 2002. Mechanisms of aneuploidy in thyroid cancer cell lines and tissues: evidence for mitotic checkpoint dysfunction without mutations in BUB1 and BUBR1. *Clin Endocrinol (Oxf)*. 56:341-350.

Panda, D., H.P. Miller, A. Banerjee, R.F. Luduena, and L. Wilson. 1994. Microtubule dynamics in vitro are regulated by the tubulin isotype composition. *Proceedings of the National Academy of Sciences of the United States of America*. 91:11358-11362.

Parness, J., and S.B. Horwitz. 1981. Taxol binds to polymerized tubulin in vitro. *The Journal of cell biology*. 91:479-487.

Parton, R.G., and K. Simons. 2007. The multiple faces of caveolae. *Nature reviews. Molecular cell biology*. 8:185-194.

Persad, S., S. Attwell, V. Gray, M. Delcommenne, A. Troussard, J. Sanghera, and S. Dedhar. 2000. Inhibition of integrin-linked kinase (ILK) suppresses activation of protein kinase B/Akt and induces cell cycle arrest and apoptosis of PTEN-mutant prostate cancer cells. *Proceedings of the National Academy of Sciences of the United States of America*. 97:3207-3212.

Peset, I., J. Seiler, T. Sardon, L.A. Bejarano, S. Rybina, and I. Vernos. 2005. Function and regulation of Maskin, a TACC family protein, in microtubule growth during mitosis. *The Journal of cell biology*. 170:1057-1066.

Pihan, G.A., J. Wallace, Y. Zhou, and S.J. Doxsey. 2003. Centrosome abnormalities and chromosome instability occur together in pre-invasive carcinomas. *Cancer research*. 63:1398-1404.

Prescott, D.M. 1964. Cellular sites of RNA synthesis. *Prog Nucleic Acid Res Mol Biol*. 3:33-57.

Rieder, C.L., A. Schultz, R. Cole, and G. Sluder. 1994. Anaphase onset in vertebrate somatic cells is controlled by a checkpoint that monitors sister kinetochore attachment to the spindle. *J Cell Biol*. 127:1301-1310.

Riffell, J.L., C. Zimmerman, A. Khong, L.M. McHardy, and M. Roberge. 2009. Effects of chemical manipulation of mitotic arrest and slippage on cancer cell survival and proliferation. *Cell Cycle*. 8:3025-3038.

Rowinsky, E.K. 1997. The development and clinical utility of the taxane class of antimicrotubule chemotherapy agents. *Annu Rev Med*. 48:353-374.

Rudner, A.D., and A.W. Murray. 1996. The spindle assembly checkpoint. *Curr Opin Cell Biol*. 8:773-780.

Rusan, N.M., C.J. Fagerstrom, A.M. Yvon, and P. Wadsworth. 2001. Cell cycle-dependent changes in microtubule dynamics in living cells expressing green fluorescent protein-alpha tubulin. *Molecular biology of the cell*. 12:971-980.

Schiff, P.B., J. Fant, and S.B. Horwitz. 1979. Promotion of microtubule assembly in vitro by taxol. *Nature*. 277:665-667.

Schneider, L., F. Essmann, A. Kletke, P. Rio, H. Hanenberg, W. Wetzel, K. Schulze-Osthoff, B. Nurnberg, and R.P. Piekorz. 2007. The transforming acidic coiled coil 3 protein is essential for spindle-dependent chromosome alignment and mitotic survival. *The Journal of biological chemistry*. 282:29273-29283.

Schondorf, T., A. Scharl, C.M. Kurbacher, O. Bien, M. Becker, R. Neumann, H. Kolhagen, J. Rustemeyer, P. Mallmann, and U.J. Gohring. 1999. Amplification of the mdr1-gene is uncommon in recurrent ovarian carcinomas. *Cancer Lett*. 146:195-199.

Spittle, C., S. Charrasse, C. Larroque, and L. Cassimeris. 2000. The interaction of TOGp with microtubules and tubulin. *The Journal of biological chemistry*. 275:20748-20753.

Srayko, M., S. Quintin, A. Schwager, and A.A. Hyman. 2003. Caenorhabditis elegans TAC-1 and ZYG-9 form a complex that is essential for long astral and spindle microtubules. *Curr Biol*. 13:1506-1511.

Sudakin, V., G.K. Chan, and T.J. Yen. 2001. Checkpoint inhibition of the APC/C in HeLa cells is mediated by a complex of BUBR1, BUB3, CDC20, and MAD2. *The Journal of cell biology*. 154:925-936.

Sudo, T., M. Nitta, H. Saya, and N.T. Ueno. 2004. Dependence of paclitaxel sensitivity on a functional spindle assembly checkpoint. *Cancer research*. 64:2502-2508.

Tanaka, K., N. Mukae, H. Dewar, M. van Breugel, E.K. James, A.R. Prescott, C. Antony, and T.U. Tanaka. 2005. Molecular mechanisms of kinetochore capture by spindle microtubules. *Nature*. 434:987-994.

Taylor, S.S., M.I. Scott, and A.J. Holland. 2004. The spindle checkpoint: a quality control mechanism which ensures accurate chromosome segregation. *Chromosome Res*. 12:599-616.

Thery, M., V. Racine, A. Pepin, M. Piel, Y. Chen, J.B. Sibarita, and M. Bornens. 2005. The extracellular matrix guides the orientation of the cell division axis. *Nature cell biology*. 7:947-953.

Tighe, A., V.L. Johnson, M. Albertella, and S.S. Taylor. 2001. Aneuploid colon cancer cells have a robust spindle checkpoint. *EMBO Rep*. 2:609-614.

Toso, R.J., M.A. Jordan, K.W. Farrell, B. Matsumoto, and L. Wilson. 1993. Kinetic stabilization of microtubule dynamic instability in vitro by vinblastine. *Biochemistry*. 32:1285-1293.

Tournebize, R., A. Popov, K. Kinoshita, A.J. Ashford, S. Rybina, A. Pozniakovsky, T.U. Mayer, C.E. Walczak, E. Karsenti, and A.A. Hyman. 2000. Control of microtubule dynamics by the antagonistic activities of XMAP215 and XKCM1 in Xenopus egg extracts. *Nature cell biology*. 2:13-19.

Toyoshima, F., and E. Nishida. 2007. Integrin-mediated adhesion orients the spindle parallel to the substratum in an EB1- and myosin X-dependent manner. *The EMBO journal*. 26:1487-1498.

Troussard, A.A., P.C. McDonald, E.D. Wederell, N.M. Mawji, N.R. Filipenko, K.A. Gelmon, J.E. Kucab, S.E. Dunn, J.T. Emerman, M.B. Bally, and S. Dedhar. 2006. Preferential dependence of breast cancer cells versus normal cells on integrin-linked kinase for protein kinase B/Akt activation and cell survival. *Cancer research*. 66:393-403.

van der Vaart, B., C. Manatschal, I. Grigoriev, V. Olieric, S.M. Gouveia, S. Bjelic, J. Demmers, I. Vorobjev, C.C. Hoogenraad, M.O. Steinmetz, and A. Akhmanova. 2011. SLAIN2 links microtubule plus end-tracking proteins and controls microtubule growth in interphase. *The Journal of cell biology*. 193:1083-1099.

Vasquez, R.J., D.L. Gard, and L. Cassimeris. 1994. XMAP from Xenopus eggs promotes rapid plus end assembly of microtubules and rapid microtubule polymer turnover. *The Journal of cell biology*. 127:985-993.

Wakefield, J.G., D.J. Stephens, and J.M. Tavare. 2003. A role for glycogen synthase kinase-3 in mitotic spindle dynamics and chromosome alignment. *Journal of cell science*. 116:637-646.

Wallin, M., and E. Stromberg. 1995. Cold-stable and cold-adapted microtubules. *Int Rev Cytol*. 157:1-31.

Wang, X., D.Y. Jin, Y.C. Wong, A.L. Cheung, A.C. Chun, A.K. Lo, Y. Liu, and S.W. Tsao. 2000. Correlation of defective mitotic checkpoint with aberrantly reduced expression of MAD2 protein in nasopharyngeal carcinoma cells. *Carcinogenesis*. 21:2293-2297.

Wani, M.C., H.L. Taylor, M.E. Wall, P. Coggon, and A.T. McPhail. 1971. Plant antitumor agents. VI. The isolation and structure of taxol, a novel antileukemic and antitumor agent from Taxus brevifolia. *J Am Chem Soc*. 93:2325-2327.

Weaver, B.A., and D.W. Cleveland. 2005. Decoding the links between mitosis, cancer, and chemotherapy: The mitotic checkpoint, adaptation, and cell death. *Cancer Cell*. 8:7-12.

Webster, D.R., and G.G. Borisy. 1989. Microtubules are acetylated in domains that turn over slowly. *J Cell Sci*. 92 (Pt 1):57-65.

Weisenberg, R.C., and W.J. Deery. 1981. The mechanism of calcium-induced microtubule disassembly. *Biochem Biophys Res Commun*. 102:924-931.

Whittington, A.T., O. Vugrek, K.J. Wei, N.G. Hasenbein, K. Sugimoto, M.C. Rashbrooke, and G.O. Wasteneys. 2001. MOR1 is essential for organizing cortical microtubules in plants. *Nature*. 411:610-613.

Wickstrom, S.A., A. Lange, M.W. Hess, J. Polleux, J.P. Spatz, M. Kruger, K. Pfaller, A. Lambacher, W. Bloch, M. Mann, L.A. Huber, and R. Fassler. 2010a. Integrin-linked kinase controls microtubule dynamics required for plasma membrane targeting of caveolae. *Dev Cell*. 19:574-588.

Wickstrom, S.A., A. Lange, E. Montanez, and R. Fassler. 2010b. The ILK/PINCH/parvin complex: the kinase is dead, long live the pseudokinase! *The EMBO journal*. 29:281-291.

Wilson, P.J., A. Forer, and C. Leggiadro. 1994. Evidence that kinetochore microtubules in crane-fly spermatocytes disassemble during anaphase primarily at the poleward end. *J Cell Sci*. 107 (Pt 11):3015-3027.

Witt, P.L., H. Ris, and G.G. Borisy. 1980. Origin of kinetochore microtubules in Chinese hamster ovary cells. *Chromosoma*. 81:483-505.

Wollman, R., E.N. Cytrynbaum, J.T. Jones, T. Meyer, J.M. Scholey, and A. Mogilner. 2005. Efficient chromosome capture requires a bias in the 'search-and-capture' process during mitotic-spindle assembly. *Curr Biol*. 15:828-832.

Wu, C., S.Y. Keightley, C. Leung-Hagesteijn, G. Radeva, M. Coppolino, S. Goicoechea, J.A. McDonald, and S. Dedhar. 1998. Integrin-linked protein kinase regulates fibronectin matrix assembly, E-cadherin expression, and tumorigenicity. *The Journal of biological chemistry*. 273:528-536.

Younes, M.N., S. Kim, O.G. Yigitbasi, M. Mandal, S.A. Jasser, Y. Dakak Yazici, B.A. Schiff, A. El-Naggar, B.N. Bekele, G.B. Mills, and J.N. Myers. 2005. Integrin-linked kinase is a potential therapeutic target for anaplastic thyroid cancer. *Mol Cancer Ther*. 4:1146-1156.

Younes, M.N., O.G. Yigitbasi, Y.D. Yazici, S.A. Jasser, C.D. Bucana, A.K. El-Naggar, G.B. Mills, and J.N. Myers. 2007. Effects of the integrin-linked kinase inhibitor QLT0267 on squamous cell carcinoma of the head and neck. *Arch Otolaryngol Head Neck Surg*. 133:15-23.

Yvon, A.M., P. Wadsworth, and M.A. Jordan. 1999. Taxol suppresses dynamics of individual microtubules in living human tumor cells. *Mol Biol Cell*. 10:947-959.

Zhai, Y., P.J. Kronebusch, P.M. Simon, and G.G. Borisy. 1996. Microtubule dynamics at the G2/M transition: abrupt breakdown of cytoplasmic microtubules at nuclear envelope breakdown and implications for spindle morphogenesis. *The Journal of cell biology*. 135:201-214.

Zhang, Y., L. Guo, K. Chen, and C. Wu. 2002. A critical role of the PINCH-integrin-linked kinase interaction in the regulation of cell shape change and migration. *The Journal of biological chemistry*. 277:318-326.

Zovko, S., J.P. Abrahams, A.J. Koster, N. Galjart, and A.M. Mommaas. 2008. Microtubule plus-end conformations and dynamics in the periphery of interphase mouse fibroblasts. *Molecular biology of the cell*. 19:3138-3146.

Zyss, D., and F. Gergely. 2009. Centrosome function in cancer: guilty or innocent? *Trends Cell Biol*. 19:334-346.

Appendix A

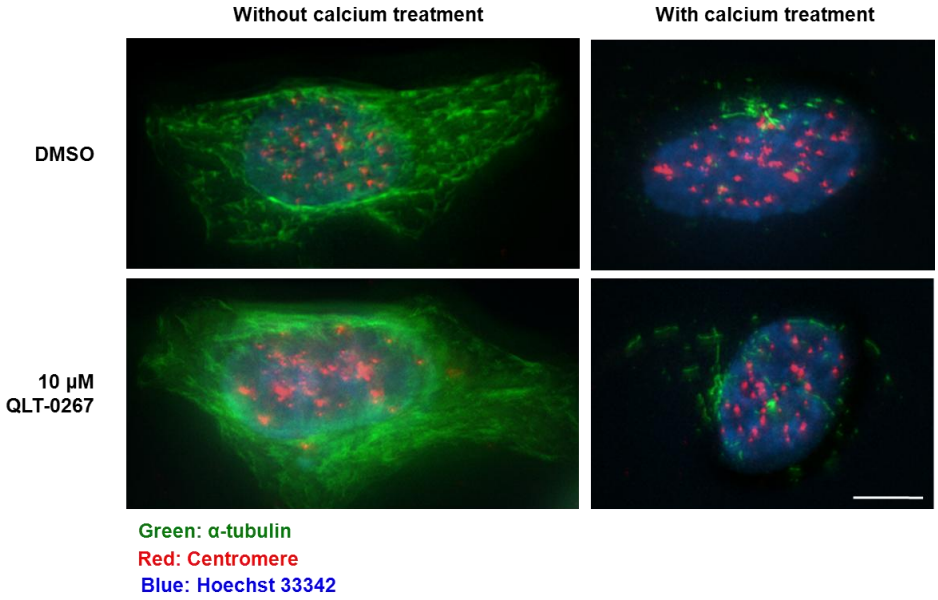

Figure A.1 Positive control for calcium-induced depolymerization of non-kinetochore microtubules

Representative images of interphase HeLa cells as a positive control for calcium-induced depolymerization of non-kinetochore microtubules. HeLa cells were treated with DMSO or 10 μM QLT-0267 for 6 hours, and then treated with or without calcium prior to fixation and immunofluorescence staining. Bar = 10 μm.

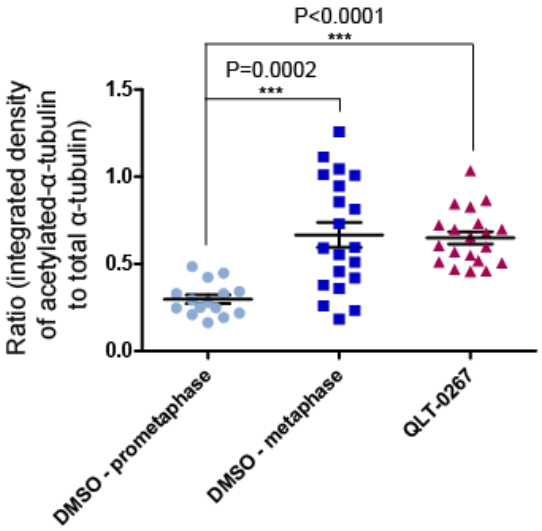

Figure A.2 Quantification of the integrated density of acetylated α-tubulin immunofluorescence signal relative to that of total α-tubulin

QLT-0267-treated cells typically had a prometaphase-like appearance but showed an acetylation level closer to that of control metaphase cells than control prometaphase cells. Results represent mean ± S.E.M., (N= 15 for DMSO prometaphase, 20 for DMSO metaphase, 20 for QLT-0267) and are typical of 2 independent experiments.

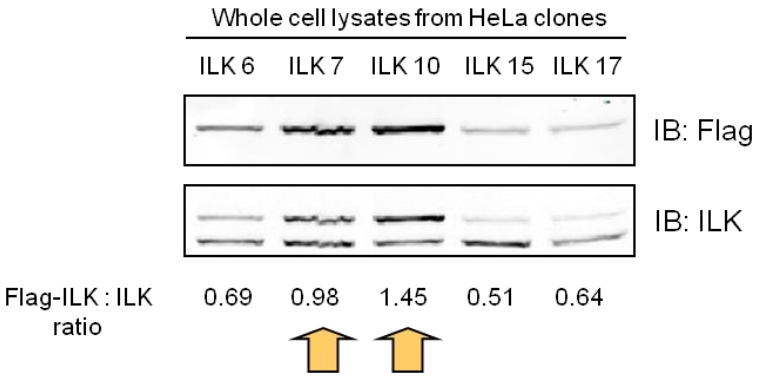

Figure A.3 Western blot to check expression levels stable HeLa clones expressing Flag-ILK

(A)

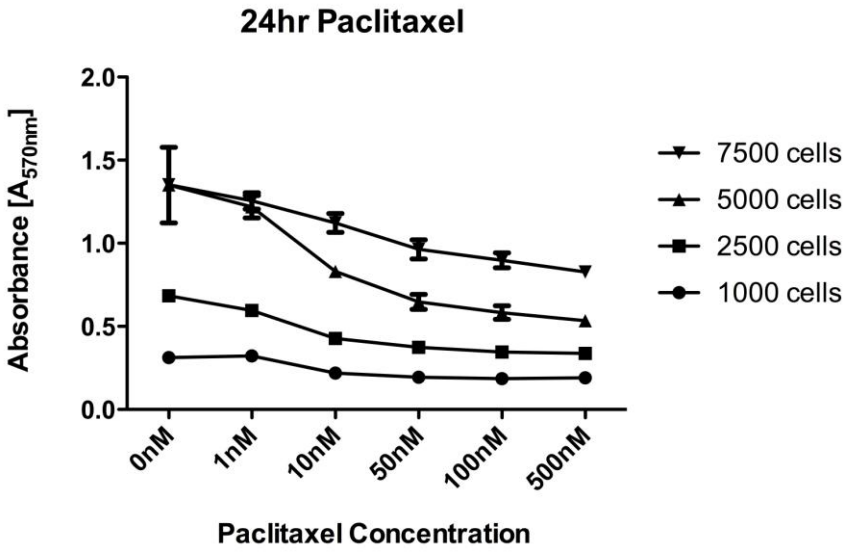

(B)

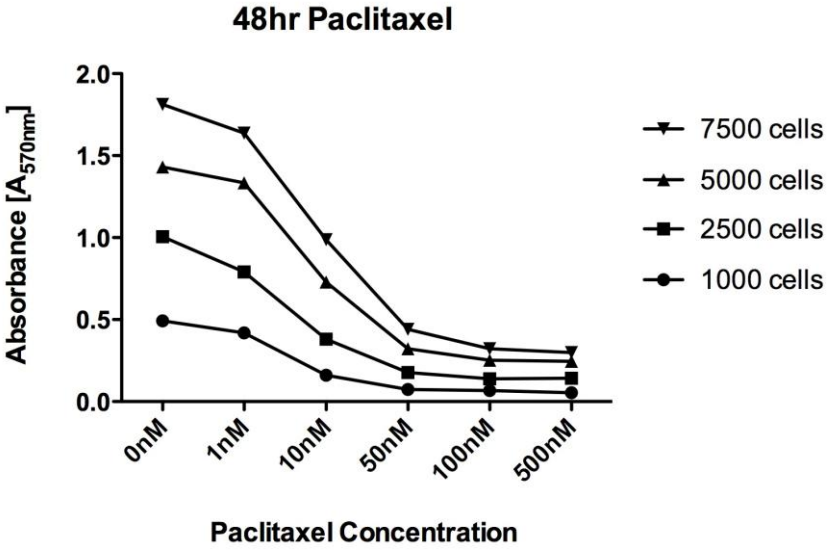

Figure A.4 Spectrophotometric absorbance readings of Vector 8 cells

Spectrophotometric absorbance readings of Vector 8 cells at various cell numbers and paclitaxel concentration after (**A)** 24 hours or **(B)** 48 hours of paclitaxel treatment. The amount of absorbance at the wavelength of 570 nm corresponds to the amount of intracellular purple formazan and is a measure of the number of cells present in the sample.